FACTORS INFLUENCING THE ABUNDANCE, COMPOSITION AND DIVERSITY OF DEEP-WATER BENTHIC MEGAFAUNAL COMMUNITIES

by

Myriam Lacharité

Submitted in partial fulfilment of the requirements
for the degree of Doctor of Philosophy

at

Dalhousie University
Halifax, Nova Scotia
August 2016

The ocean is just a murky mist that keeps me from seeing the bottom.
To be honest, I wish the whole thing'd just dry up.

- DR. MAURICE EWING

TABLE OF CONTENTS

LIST OF TABLES

LIST OF FIGURES

ABSTRACT

This thesis examines the role of the physical environment in influencing the abundance, composition and diversity of epibenthic megafaunal communities – i.e. organisms > 2-3 cm living on the seafloor – in deep waters on continental margins (>100 m). In particular, I examine the role of fine-scale substrate features (e.g. presence of cobbles, boulders), the shape of the seafloor at local scales (100 m – kilometers), and oceanographic properties (temperature, currents, water column structure) at broader spatial scales (1 – 100s km). Factors were assessed at varying spatial scales (< 1 m to 100s of km), and in various deep-water habitats on continental shelves (~75 – 530 m depth), in a submarine canyon (~650 – 850 m depth), and at the base of the continental slope (~1000 – 3000 m depth). Sampling tools for biological communities included a 4-year field experiment, optical imagery from high-definition video and photographic cameras, and epibenthic trawling surveys. At fine spatial scales (< 1 m), recruitment of 2 species of deep-water corals in a submarine canyon was influenced by substrate type, with a preference for hard substrate (Chapter 2). I suggested that recruitment is also dependent on reproductive mode in corals, which differed between species, and local hydrodynamics. To further examine the role of substrate at fine spatial scales, I developed an approach using optical imagery to estimate substrate complexity based on principles of computer vision (Chapter 3). At local scales (10 m – 1 km), using the approach I developed in Chapter 3, I determined the influence of variability in substrate types on epibenthic megafaunal community composition and diversity (Chapters 4 and 5). In contrast, megafaunal abundance was correlated with variability in geomorphometry and oceanographic properties (Chapter 5). At mesoscales (10 – 100s km), on a dynamic continental shelf influenced by a strong oceanographic front, community composition was best explained by oceanographic properties, especially spatial patterns in temperature (Chapter 6). This thesis provided new approaches (Chapters 3 and 6) to study deep benthic ecosystems, and described scale-specific species-environment relationships (Chapters 2, 4, 5 and 6) necessary to design sampling surveys in unexplored environments and establish conservation strategies.

LIST OF ABBREVIATIONS AND SYMBOLS USED

Abbreviation /symbol	*Definition*	*Units*
AA	Annual amplitude	
ANOVA	Analysis of variance	
BC	Browns Channel (Gulf of Maine)	m
BPI	Bathymetric Position Index	
CCGS	Canadian Coast Guard Ship	
CHONe	Canadian Healthy Oceans Network	
CGS M	Alexander Graham Bell Canada Graduate Scholarships (Master's level)	
CI	Confusion Index	
CIELab	Commission Internationale de l'Éclairage – Luminosity,a,b	
CTD	Conductivity – temperature - depth	
DBM	Digital Bathymetric Model	
DFO	Department of Fisheries and Oceans	
ER	Expected species richness	# species
ESSIM	Eastern Scotian Shelf Integrated Management Plan	
FVCOM	Finite-Volume Community Ocean Model	
GB	Georges Basin (Gulf of Maine)	
GDM	Generalized dissimilarity modelling	
GHz	Gigahertz	s^{-1}
GPS	Geographic Positioning System	
H'	Shannon-Wiener Diversity Index	
HD	High-Definition	
HSD	Tukey's Honestly Significant Difference	
IC	Image Complexity	
ICC	Intraclass Correlation Coefficient	
J'	Pielou's evenness	
JB	Jordan Basin (Gulf of Maine)	ϕ scale
K-S	Kolmogorov-Smirnov test	
LBP	Linear Binary Patterns	
MaxEC	Maximum epifaunal cover	%
MeanEC	Mean epifaunal cover	%
MGS	Mean particle grain size	
MS	Marginally significant	
N^2	Brunt-Väisälä buoyancy frequency	s^{-2}
nMDS	Non-metric multidimensional scaling	
NEC	Northeast Channel	
NPP	Net surface primary production	
NSERC	Natural Sciences and Engineering Research Council	

Abbreviation /symbol	*Definition*	*Units*
NW	Northwest	
OBIA	Object-based image analysis	
OBIS	Ocean Biogeographic Information System	
PC	Principal Component	
PCA	Principal Component Analysis	
PGS D	Postgraduate Scholarships Doctoral	
POC	Particulate organic carbon	
POME	Prediction and Observation of the marine environment	
PSU	Practical Salinity Unit	
R^2	Coefficient of determination	
RAM	Random Access Memory	
RGB	Red-Green-Blue colour space	
Ri	Richardson Number	
ROMS	Regional Ocean Modelling System	
ROPOS	Remotely-Operated Platform for Ocean Sciences	
ROV	Remotely-Operated Vehicle	
SAC	Sample Autocorrelation Coefficient	
SD	Standard deviation	
SE	Standard error of the mean	
SR	Sewell Ridge (Gulf of Maine)	
T	Temperature	°C
USBL	Ultra-Short Baseline	
UTM	Universal Transverse Mercator	
ϕ	phi scale of particle grain size	
ρ	Spearman's correlation coefficient	
r	Pearson's correlation coefficient	

ACKNOWLEDGEMENTS

Firstly, I'd like to thank my supervisor Dr. Anna Metaxas for her mentorship, her openness to new ideas, and for letting me stray off to various parts of the world. I am grateful to my committee members, Drs. Keith Louden and Jonathan Grant, for their suggestions, support and seeing me through the various hoops necessary to complete my degree, and Dr. Peter Lawton, who provided helpful advice, support and guidance.

Financial support for this research was provided by the Natural Sciences and Engineering Research Council (NSERC) grants to Anna Metaxas (Discovery and the Strategic Network for the Canadian Healthy Oceans Network – CHONe). I was also supported by NSERC (CGS M and PGS D), Dalhousie University (Graduate Scholarships and President's Award), the Killam Memorial Trust, and the Canada-Norway exchange programme 'Prediction and Observation of the Marine Environment' (POME).

Many people have contributed over the years to the completion of this thesis. Aboard research cruises, I am especially indebted to the professionalism of the ROPOS crew, who without fail stayed on track, Kelly Bentham for the amazing quality of the DFO Campod imagery, and the ship crew of the *CCGS Hudson*. Special thanks to Jessie Short who provided invaluable help at sea. Thanks to the undergraduate research assistants who assisted with data processing on shore: Jessica Bryk, Danika Wong, and Liz Nagel. Thanks to Swaantje Bennecke for crossing the Atlantic Ocean and showing a keen interest in deep-water corals, even in the absence of *Lophelia pertusa*. I am very thankful for the many opportunities provided by CHONe, allowing me to interact with researchers across Canada and beyond. Thanks to the welcoming Norwegians: Jarle Berntsen, Hein Rune Skjoldal, Vidar Lien, and especially Lis Lindal Jørgensen, for her kind hospitality in Tromsø.

Even more people have provided invaluable moral support and friendship, without which the path to become a doctor would have been gloomier. Thanks to my colleagues for introducing me to the various sub-disciplines of oceanography, either at

Dalhousie or beyond. Thanks to all lab members – Michelle Lloyd, Remi Daigle, Danielle Denley, Erika Simonson, Kevin Sorochan, and Emily Higgins – to bear with me, the ‘deep-sea person’. Thanks to all the good friends, for their individuality, quirkiness, and humanity: Jonathan Lacasse, Angela Fuentes-Pardo, Diksha Bista, Christoph Renkl, Francisco Javier Bravo Avendaño, Angela Kuhn, Alana Westwood, Laurie Baker, and Jenna Hare.

Many thanks to my family, my parents, Louise and Denis, and sister, Véronique, for their unwavering support in good times and bad. Lastly, I am grateful to my partner Nadine for her support and kindness during the last crucial miles of this long run.

CHAPTER 1

INTRODUCTION

Deep-water benthic ecosystems are found at depths > ~100-200 m, below the euphotic zone, and are most commonly referred to as 'offshore waters', the 'neritic' and 'oceanic' zones, and the 'deep sea', although the latter term is used in reference to ecosystems seaward of the continental break. Groupings of benthic organisms inhabiting these ecosystems reflect sampling and processing techniques, with 'megafauna' describing a group of organisms that is not adequately sampled by grab or core samplers, and by convention, larger than 2-3 cm or 'readily visible in seafloor photographs' (Wolff 1977, Gage and Tyler 1991). The ecological role of megafauna is not fully understood. Most studies highlight their role as habitat provider for other species (e.g. Smith et al. 1986; Galluci et al. 2008; Biongiorni et al. 2010; Buhl-Mortensen et al. 2010), and an important component of community respiration at depths (Piepenburg et al. 1995, Piepenburg and Schmid 1996). Echinoderms (e.g. ophiuroidea and holothuroidea) are a major component of deep-water benthic megafauna, but many other faunal groups are also present, occasionally at high density, such as cnidarians - for example, cold-water corals (Roberts et al. 2006) - and beds of poriferans (e.g. Kiltgaard and Tendal 2004).

The distribution of deep-water benthic fauna was initially thought to be mostly driven by interspecific interactions, such as niche differentiation (Sanders 1968) and predation (Dayton and Hessler 1972), and by reproductive strategies distinct from those of their shallow-water counterparts (Grassle and Sanders 1973). These hypotheses

assumed a stable physical environment in the deep ocean, with limited spatial and temporal environmental variability. Subsequent hypotheses incorporated the potential role of the physical environment in shaping benthic faunal communities, such as in the importance of micro-habitat specialization in the sediment (Jumars 1975). Strong vertical zonation in communities was attributed to the food supply regime from the surface ocean, which was considered from then on the most limiting factor on benthic megafauna (Grassle et al. 1975; Gardiner and Haedrich 1978; Kitchell et al. 1978). Much focus was therefore placed on scavengers and deposit-feeders (Wolf 1977), and the relationship with food supply was made apparent with the rapid response of mobile megafauna to pulses of organic matter input to the seafloor (e.g. Smith et al. 1994).

With further deep-water exploration, heterogeneity in benthic ecosystems became apparent, and thus additional environmental factors were proposed to contribute to the distribution of deep-water benthic megafauna. Most of the deep seafloor is covered with fine-grain sediment (mud and sand), but more diverse substrate types, in particular the sporadic presence of hard substrate (e.g. coarse sediment, bedrock, carbonate mounds), revealed different megafaunal communities (e.g. Schneider et al. 1987, reviewed in Young 2009), some of which are dependent on the presence of hard substrate, such as certain species of cold-water corals (Mortensen and Buhl-Mortensen 2004; Watanabe et al. 2009). Vertical zonation in communities was also attributed to hydrographic conditions, especially along deep continental margins, where gradients in oxygen (Levin et al. 1991; Rogers 2000), and temperature due to varying water masses (e.g. Currie & Sorokin 2014) occur. The influence of the geomorphology of the seafloor (e.g. steep

bathymetric features) on the distribution of megafauna was first proposed for seamounts (Genin et al. 1986), but abundant megafauna in steep benthic environments have also been reported on deep continental margins (e.g. Rice et al. 1990; Genin et al. 1992; Dolan et al. 2008). This suggests that geomorphology is an important factor in influencing patterns in megafauna in deep waters, mostly through its relationship with enhanced current speeds, which affects the delivery of particles, and the potential for re-suspension, and reduces sedimentation, thus exposing hard substrate.

Uncertainty remains in determining the spatial scales at which environmental factors influence patterns of deep-water benthic fauna. In the case of oceanographic properties, temporal variability of conditions and the three-dimensionality of the water column add complexity to these relationships. For example, strong advection influences re-suspension, the movement of larval stages, and the delivery of food particles. On continental shelves, the latter can lead to the decoupling of surface primary productivity with the sedimentation of organic matter (Dunton et al. 2005), which is contrary to the widely-held view of this coupling in influencing benthic biomass (Wei et al. 2010; Jones et al. 2014). At a larger scale, circulation patterns influence the dispersal kernel of benthic fauna, and hence the distribution of individual species and communities (e.g Miller et al. 2010; Yearsley and Sigwart 2011). 'Connectivity' aims to resolve how these different scales overlap. Similarly, describing the spatial structure of geological features is challenging since substrate types can vary at multiple scales, from forming relatively homogeneous 'patches' on the seafloor to the presence of sporadic features (e.g. large boulders, bedrock outcrops) in an otherwise homogeneous environment. At a larger scale,

the distribution of geomorphic features – such as submarine canyons, seamounts, and cold seeps – is irregular in space (Harris and Whiteway 2007), and thus influences the heterogeneity of seascapes at regional to global scales.

Determining the scales(s) at which environmental drivers influence benthic fauna is inevitably tied to the size of organisms and their biological traits. For example, while macrofaunal diversity is influenced by small-scale habitat variability (such as sediment diversity) (Etter and Grassle 1992), megafaunal diversity is influenced by the presence of a wider range of particle grain size (e.g. Jones et al. 2013). Ontogenetic habitat shifts in megafaunal communities could occur, but are poorly studied in the deep ocean, despite their acknowledged importance in shallow waters, in particular for the role of the environment in post-settlement/recruitment and juvenile mortality (Gosselin and Qian 1997; Hunt and Scheibling 1997). The physiology and reproductive biology of organisms also influence the temporal scale at which the role of environmental factors should be assessed. Deep-sea megafauna has been reported to live hundreds (Mortensen and Buhl-Mortensen 2005) to thousands (Roark et al. 2009) of years, and reproductive strategies may act on a similar time scale (Robison et al. 2014). Benthic megafauna could thus be seen as 'environmental integrators' and the influence of environmental conditions on their distribution may be best determined on a similarly long time scale.

Scientific sampling of the seafloor in deep waters is logistically difficult and often performed sporadically in particular areas of interest. For benthic communities, the use of different sampling tools yields complimentary, but not interchangeable metrics of

diversity and abundance, and trade-offs must be considered given the survey objectives (Williams et al. 2015). The collection of megabenthic specimens with direct sampling methods (e.g. with epibenthic sleds) facilitates taxonomic identification, and allows genetic and stable isotopes analyses. In contrast, benthic environments with complex geomorphology (e.g. submarine canyons, carbonate mounds) can be sampled more effectively using high-definition video and photographic cameras with minimal disturbance to the seafloor, which is a key requirement for vulnerable species. Imagery also conveys details on the fine-scale features of the proximate environment of benthic organisms influencing their distribution. Additional remote sensing tools are increasingly being used to determine the features of the physical environment of deep-water benthic habitats, such as acoustic imagery (Browns et al. 2011) and, given the scarcity of empirical observations, modelled oceanographic data (e.g. Mohn et al. 2014; Navas et al. 2014).

Overall, the paucity of information on the biological communities inhabiting the deep seafloor relative to shallow-water ecosystems makes it challenging to study the biotic and abiotic factors influencing their distribution. This highlights both the importance of using statistical modelling to infer processes based on patterns, and also the added incentive to maximize the amount of information (biological and physical) extracted from sampling surveys, while potentially relying extensively on remote sensing tools. An additional challenge lies in the diversity of habitats with distinct environmental features found in the deep ocean. The ‘deep sea’ is in reality composed of (among others) deep basins and trenches on continental shelves, submarine canyons, hydrothermal vents,

cold seeps, the continental slope and the continental rise, and the abyssal plains that underlie most of the world's oceans, and the factors influencing megafauna, in addition to the role of scale, may differ among these environments.

1.1 Objectives

This thesis aims to increase our understanding of the factors influencing the abundance, composition, and diversity of deep-water benthic megafaunal communities, with a particular focus on communities inhabiting heterogeneous environments. Broadly, the chapters of this thesis address the different drivers influencing these communities, the scale(s) at which these operate and/or are strongest, using existing and developing new tools to evaluate the physical features of the environment in the deep ocean. In this thesis, I mostly focus on abiotic drivers of megafauna (e.g. substrate complexity, geomorphology – **Chapters 2-6**), except in **Chapter 2**, which also includes biological traits. The role of different scales is assessed in **Chapters 2-5** by addressing fine-scale features (< 1 – 10 m), and their heterogeneity in space (**Chapter 4** and **Chapter 5**). Local scales (10s m – kms) are incorporated in **Chapter 5** in a multiscale approach, and the role of mesoscale features (10- 100s km) is assessed in **Chapter 6**. Temporal variability over a 10-year period is considered in **Chapter 5** and **Chapter 6**. Lastly, different sampling tools are used in this thesis: a 4-year field experiment is used in **Chapter 2**, optical imagery (high-definition video and photographic surveys) in **Chapters 3-5**, with **Chapter 3** describing a novel application of these data, and modelled oceanographic data in **Chapters 5** and **6**, with a novel approach to use these data developed in **Chapter 6**.

This thesis contains 7 chapters (including this Introduction); **Chapters 2-6** address the research objectives, and are developed as standalone manuscripts for publication in the primary literature. **Chapters 2** and **3** have been published (Lacharité and Metaxas 2013, Lacharité et al. 2015), **Chapter 6** has been accepted for publication pending revisions, and **Chapter 4** has been submitted for publication. In **Chapter 2**, I examine the influence of fine-scale complexity of the recipient substrate on recruitment of 2 species of deep-water corals, *Primnoa resedaeformis* and *Paragorgia arborea* in a submarine canyon. In **Chapter 3**, I develop an approach based on computer vision to estimate fine-scale substrate complexity and identify epibenthic megafauna when using optical imagery. In **Chapter 4**, I apply the approach developed in **Chapter 3** to determine the influence of substrate complexity (and spatial variability of substrate complexity along transects) on epibenthic megafaunal communities on the continental slope (~1000 – 3000 m depth) seaward of a submarine canyon on the continental margin off the Gulf of Maine (northwest Atlantic). In **Chapter 5**, I determine the influence of physical drivers on epibenthic megafaunal communities using a multiscale approach, from fine-scale substrate complexity (< 1 m), to geomorphometric features (100 m – kms), to broader-scale oceanographic properties (1-10 km) in the deep waters of the eastern Gulf of Maine. In **Chapter 6**, I determine the influence of mesoscale oceanographic properties (10-100s km) on the composition of epibenthic megafaunal communities in a region with a complex oceanography, the western Barents Sea (sub-Arctic Ocean). In **Chapter 7**, I provide broad conclusions stemming from the work presented in this thesis.

A large portion of this thesis (**Chapters 2-5**) is part of a project within the Canadian Healthy Oceans Network (CHONe; 2008-13) under the theme of Marine Biodiversity. This project (Project 1.1.2 'Atlantic Corridor Biodiversity') aimed in part to quantify patterns and processes of benthic communities along cross-shelf gradients in depth, seafloor structure and oceanographic properties (eastern Gulf of Maine, from land-sea margin to abyssal depths). **Chapter 6** is the outcome of a Canada-Norway exchange programme (Prediction and Observation of the Marine Environment - 'POME'), where I developed a collaboration with researchers at the Institute of Marine Research (Bergen and Tromsø, Norway) to examine the role of oceanographic properties on epibenthic communities in the western Barents Sea.

CHAPTER 2

EARLY LIFE HISTORY OF DEEP-WATER GORGONIAN CORALS MAY LIMIT THEIR ABUNDANCE[1]

2.1 Abstract

Deep-water gorgonian corals are long-lived organisms found worldwide off continental margins and seamounts, usually occurring at depths of ~200-1,000 m. Most corals undergo sexual reproduction by releasing a planktonic larval stage that disperses; however, recruitment rates and the environmental and biological factors influencing recruitment in deep-sea species are poorly known. Here, we present results from a 4-year field experiment conducted in the Gulf of Maine (northwest Atlantic) at depths > 650 m that document recruitment for 2 species of deep-water gorgonian corals, *Primnoa resedaeformis* and *Paragorgia arborea*. The abundance of *P. resedaeformis* recruits was high, and influenced by the structural complexity of the recipient habitat, but very few recruits of *P. arborea* were found. We suggest that divergent reproductive modes (*P. resedaeformis* as a broadcast spawner and *P. arborea* as a brooder) may explain this pattern. Despite the high recruitment of *P. resedaeformis*, severe mortality early on in the benthic stage of this species may limit the abundance of adult colonies. Most recruits of this species (~80%) were at the primary polyp stage, and less than 1% of recruits were at stage of 4 polyps or more. We propose that biological disturbance, possibly by the

[1] Lacharité, M., and A.Metaxas. 2013. Early life history of deep-water gorgonian corals may limit their abundance. PLoS ONE **8(6)**: e65394.

My coauthor Dr. Anna Metaxas supervised the study design and analyses, and edited the manuscript.

presence of suspension-feeding brittle stars, and limited food supply in the deep sea may cause this mortality. Our findings reinforce the vulnerability of these corals to anthropogenic disturbances, such as trawling with mobile gear, and the importance of incorporating knowledge on processes during the early life history stages in conservation decisions.

2.2 Introduction

Deep-water gorgonian corals (Octocorallia: Alcyonacea; "sea fans") are increasingly being recognized as important foundation species of deep-sea benthic ecosystems, particularly on seamounts and continental margins (Roberts et al. 2006). With their typical arborescent shape, these organisms form structures, which foster biodiversity, either as substrate for epifaunal communities (Buhl-Mortensen and Mortensen 2004; Buhl-Mortensen and Mortensen 2005; Etnoyer and Morgan 2005), or by creating shelter for bottom-dwelling fish from strong currents and predators (Auster 2005; Du Preez and Tunnicliffe 2011). The protruding shape of the corals, however, along with slow growth and high longevity (Andrews et al. 2002; Mortensen and Buhl-Mortensen 2005), make them vulnerable to destructive fishing practices, such as trawling with mobile gear (Krieger 2001; Heifetz et al. 2009; Murillo et al. 2011). Most deep-water gorgonians require hard substrate for settlement and, as suspension-feeders, strong currents for the delivery of food. Hence, they typically are found on steep topographic features on shelf breaks and the upper continental slope (Mortensen and Buhl-Mortensen 2004; Gass and Willison 2005; Bryan and Metaxas 2006; Wareham and Edinger 2007;

Tong et al. 2012), where strong bottom currents prevent the accumulation of fine-grained sediment and increase the encounter rate with food particles (Genin et al. 1986).

The reproductive ecology of deep-water corals (including gorgonians) remains largely undescribed. Corals undergo sexual reproduction to disperse to new habitats. Colonies are either male or female (gonochorism), or both (hermaphroditism), and produce planula larvae through 2 reproductive modes: fertilization inside or on the surface of the female colony (brooding) or external fertilization where gametes from both male and females colonies are released in the water column (broadcast spawning) (Richmond 1997). In octocorals (including shallow-water species), gonochorism dominates, but broadcast spawning and brooding are equally present among species (Kahng et al. 2011). Planula larvae subsequently disperse as plankton before eventually settling on a suitable substrate (settlement) and metamorphosing into a benthic stage. Measures of recruitment reflect our ability to detect the primary polyp stage after a certain period of time. Physical factors influencing recruitment (or post-settlement mortality) have not been assessed for deep-water gorgonian corals. For sessile organisms, these factors include predation, disturbance (physical or biological) and space and/or resource competition (Hunt and Scheibling 1997). Once settled, corals undergo asexual reproduction when additional polyps bud from the primary polyp to form a juvenile colony.

Despite its importance in determining population dynamics, our knowledge of the magnitude, frequency and environmental factors influencing recruitment of deep-sea (> 200 m) benthic invertebrates is incomplete. The presumed environmental stability of

deep-sea ecosystems, in particular on the abyssal plains, led to the hypothesis that most deep-sea organisms grow slowly, mature late and live to a greater age, while investing relatively less energy into reproduction than their shallow-water counterparts (Sanders 1979). Consequently, the recruitment rate is expected to be low, given the investment in growth and maintenance, rather than in the colonization of new habitats (Grassle 1977; Young 2003). However, fast recruitment rates have been recorded on artificial food patches (Snelgrove et al. 1994), and in unstable and transient deep-sea environments, such as hydrothermal vents (Mullineaux et al. 1998; Kelly et al. 2007) and whale falls (Smith and Baco 2003), where colonization rates tend to vary spatially and temporally. Continental margins, the transitional habitats between the shallow continental shelves and deep abyssal plains, are now considered to harbour dynamic, heterogeneous ecosystems increasingly affected by anthropogenic disturbances (Levin and Sibuet 2012). Knowledge is lacking on the reproductive strategies of organisms of the diverse epibenthic megafauna inhabiting continental margins, in particular cnidarians and poriferans.

To our knowledge, in-situ measures of recruitment of deep-water corals are not available in waters deeper than 200 m, where these organisms are most commonly found (Roberts et al. 2006). At these depths, recruitment has been inferred only sporadically by analysing size-frequency distributions of adult colonies. Off the Hawaiian Archipelago (375-450 m), slow recruitment, slow growth, and high mortality during the early benthic life stages have been suggested to limit the population of the gorgonian *Corallium secundum* (pink coral) (Grigg 1988), while the periodicity of recruitment events of the solitary scleractinian *Desmophyllum dianthus* is estimated at 25 years off the Tasmanian

coast (Australia; 1,000 – 2,100 m) and adjacent seamounts (Thresher et al. 2011). At depths < 200 m, size-frequency distributions indicated that the cosmopolitan scleractinian *Lophelia pertusa* recruited annually on oil platforms in the North Sea, and the magnitude of these recruitment pulses decreased with increasing distance from the potential source population located 10s of km's away, off the northern coast of Scotland (Gass and Roberts 2006).

In Atlantic Canada, fishermen have long associated gorgonians, referred to as the 'trees', with highly productive fishing grounds (Breeze et al. 1997), in different locations along the continental margin, including the deep Northeast Channel, which separates Georges Bank and the Scotian Shelf in the Gulf of Maine. Northeast Channel harbours the highest known density in Atlantic Canada of intact colonies of 2 species of large gorgonians: the seacorn coral *Primnoa resedaeformis*, and the bubblegum coral *Paragorgia arborea* (Gass and Willison 2005). A coral conservation area (424 km^2) was established by Fisheries and Oceans Canada in 2002 at the shelf-edge of Northeast Channel, extending to a depth of 1,200 m to prevent further damage. In the Northeast Channel Coral Conservation Area, *P. resedaeformis* and *P. arborea* have aggregated distributions (Mortensen and Buhl-Mortensen 2004; Watanabe et al. 2009), and given the recurrent observations of uncolonized substrate within these regions, the availability of suitable substrate is not thought to limit their distribution (Mortensen and Buhl-Mortensen 2004; Watanabe et al. 2009). Few small colonies (< 10 cm) have been observed, leading to the hypothesis that reproductive processes may be limiting these populations (Watanabe et al. 2009).

The preferred substrate of *P. resedaeformis* and *P. arborea* is a mixture of cobbles, pebbles and boulders (Mortensen and Buhl-Mortensen 2004; Watanabe et al. 2009). Such hard substrate is necessary for their settlement, even in areas of moderate relief (Tong et al. 2012), underscoring the potential influence of microhabitat complexity (three-dimensional) on post-settlement processes. Habitat complexity increases the surface area available for settlement and provides shelter from physical and biological disturbances (Kovalenko et al. 2011). As trawling with mobile gear has been shown to alter benthic habitat complexity (Watling and Norse 2008), this characteristic of the recipient habitat could be critical in the potential of deep-water corals to recover from anthropogenic disturbance.

Here, we report results of a 4-year field experiment in the Northeast Channel Coral Conservation Area where we determined: 1) the magnitude of recruitment, and 2) the role of substrate complexity in recruitment for the deep-water gorgonian corals *P. resedaeformis* and *P. arborea*. We found that recruitment was high for *P. resedaeformis*, but limited for *P. arborea*. We suggest that this difference possibly indicates divergent reproductive modes in these species. For *P. resedaeformis*, the 3-dimensional structural complexity of the recipient environment influenced recruitment. However, despite high larval supply and recruitment, we suggest that mortality occurring after settlement is particularly significant in determining the recruitment rate in this species, and hence the abundance of larger, adult colonies.

2.3 Materials & Methods

2.3.1 Study area & sites

The Northeast Channel, separating Georges Bank and the Scotian Shelf, is the only deep passage connecting the northwest Atlantic with the Gulf of Maine proper (Ramp et al. 1985). Water circulation in the channel is dominated by tides, with an inflow alternating between Warm Slope Water and Labrador Slope Water along the northeastern side, and outflow of Maine Intermediate Water along the southwestern side (Ramp et al. 1985). At the shelf edge, where the channel is 20-30 km wide, the seafloor plunges from a depth of 210-370 m into 3 steep-walled submarine canyons to a maximum depth of ~ 1,000 m (Ramp et al. 1985; ESSIM Planning Office 2006). The detailed water circulation within these canyons is unknown. The field experiment was conducted at 3 locations in the Middle Canyon of Northeast Channel Coral Conservation Area. Two locations were on opposite walls of the canyon separated by a distance of ~2 km (north wall – depth: 658 m; south wall – depth: 671 m), while the third location was on the floor of the canyon (floor – depth: 863 m). Permission to perform this field experiment was granted by Fisheries and Oceans Canada.

The surficial geology of the Northeast Channel and adjacent upper continental slope is a relic of the glacial history of the region, being mostly comprised of ice-contact sediment such as pebbles, cobbles and boulders in a matrix of coarse sand patches (Edinger et al. 2011). The seafloor is swept by strong currents, which prevent the accumulation of fine-grained sediment (Genin et al. 1986; Edinger et al. 2011). Large gorgonian corals are often observed on the tops and sides of boulders (Mortensen and

Buhl-Mortensen 2004; Watanabe et al. 2009; Edinger et al. 2011). On the north and south walls sites of the Middle Canyon, we observed a similar surficial geology, while on the floor of the canyon, the seafloor was mostly comprised of sand and sparse cobbles and pebbles, but a large boulder (> 3 m in width) was present within 5 m of the larval settlement collectors (see Experimental design below).

The local abundance of coral colonies differed between the canyon locations where the experiment was conducted. On the north wall of the canyon, we observed multiple thickets of large, dense *P. resedaeformis* colonies within 10 m of the collectors (the closest colony was approximately 1 m away from the collectors). We did not observe colonies of *P. arborea* within meters of the collectors, but colonies were present within 100 m. On the south wall of the canyon, a single thicket of *P. resedaeformis* and a *P. arborea* colony were observed within 10 m of the collectors. At the floor of the canyon, a large colony of *P. arborea* (> 1.5 m in height and width) and few smaller colonies of the same species were present within 5 m of the collectors, and more were present within 10s of meters. Colonies of *P. resedaeformis* were not observed at this location.

Three video transects were performed in the area when the arrays of larval settlement collectors were deployed (Watanabe et al. 2009) (Fig. 2.1). A summary of the mean and maximum abundance of *P. resedaeformis* and *P. arborea* is presented in Table 2.1. In all transects, the density of *P. resedaeformis* decreased with increasing depth. On average, less than 1 colony/10 m^2 was observed at depths greater than 750 m. No relationship was observed between the density of *P. arborea* colonies and depth, although higher densities tended to be observed at greater depths than *P. resedeaformis* (Watanabe

et al. 2009). This pattern has also been reported on the continental margins of Newfoundland (Wareham and Edinger 2007) and Norway (Tong et al. 2012).

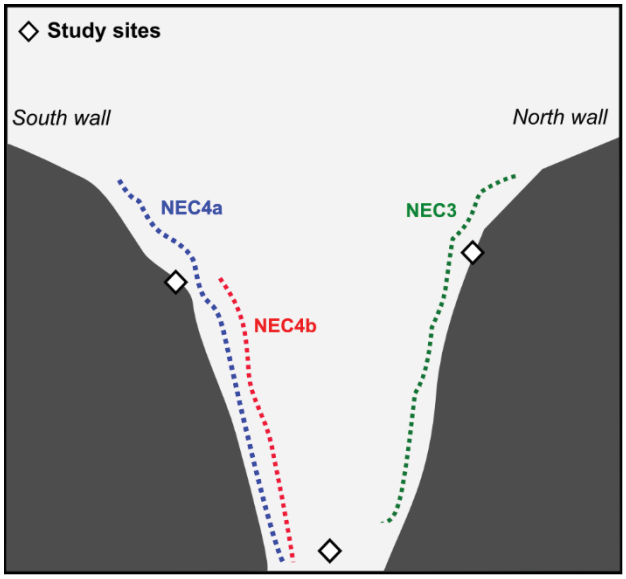

Figure 2.1: Study sites (this study) and locations of abundance transects (Watanabe et al. 2009). Experimental study sites in the Middle Canyon of the Northeast Channel Coral Conservation Area (Gulf of Maine). The sites are shown relative to 3 upslope transects ('NEC3', 'NEC4a', 'NEC4b') performed in the area in 2006 (Watanabe et al. 2009). Diagram is not to scale.

Table 2.1: Summary of mean and maximum abundance of *P. resedaeformis* and *P. arborea* along 3 transects in the Middle Canyon of the Northeast Channel Coral Conservation Area (Watanabe et al. 2009).

	Canyon location (Transect)	Mean abundance ± SD, n (10 m^{-2})	Maximum abundance (10 m^{-2})	Depth interval of maximum abundance (m)
P. resedaeformis	North wall (NEC3)	2.37 ± 5.52, 263	37.7	500-525
	South wall (NEC4a)	1.30 ± 1.54, 280	18.3	600-625
	South wall (NEC4b)	3.08 ± 4.26, 146	8.96	675-700
P. arborea	North wall (NEC3)	0.09 ± 0.54, 263	5.88	725.750
	South wall (NEC4a)	0.44 ± 1.63, 280	15.0	825-850
	South wall (NEC4b)	1.08 ± 1.54, 146	10.0	850-875

2.3.2 Experimental design

Recruitment was measured between July 2006 and August 2010. Because of the longevity of deep-water corals (spanning 10s to 100s of years), and unknown periodicity of reproductive dynamics, this deployment period was assumed to be sufficient to capture and integrate early life history processes. Sixteen larval settlement collectors were attached to a single galvanized steel frame for ease of deployment with a 20-cm steel threaded rod covered with a plastic tube (Fig. 2.2). Collectors included either 1) a basalt rock (~7 x 10 x 2 cm) supported by a plastic ring (n = 10), or 2) mesh pads (~7.5 x 10 x 1.5 cm, 'Scotch-Brite' pads, mesh openings: ~3.5 mm^2) (n = 6). More basalt rocks than mesh pads were included because 1) hard substrate is most prevalent in this area, and 2) it is the preferred substrate of the species of interest. Each settlement plate was placed in a

plastic container pierced with holes on the underside to allow water flow, which is critical for the recruitment of suspension-feeders. The experimental array of larval settlement

Figure 2.2: Array of larval settlement collectors at deployment in 2006 (South wall: 671 m). Collectors included either a basalt rock (~7 x 10 x 2 cm) supported by a plastic ring (n = 10), or mesh pads (~7.5 x 10 x 1.5 cm, blue 'Scotch-Brite' pads, mesh openings: ~3.5 mm^2) (n = 6).

collectors may have influenced the small-scale flow velocity, but we considered that its structure reasonably mimicked the surrounding seafloor habitat in the Middle Canyon. The individual collectors were randomly positioned on the frame, and separated by a few centimeters, therefore representing independent samples, particularly for sedentary colonists. The total surface area available for recruitment on the collectors was 547 cm^2 for those composed of basalt rocks (top planar surface area: 70 cm^2) and 322 cm^2 for those composed of mesh pads (top planar surface area: 79 cm^2). Only the top planar

surface of the mesh pads was considered suitable for settlement since deep-water gorgonian corals are suspension-feeders that require access to water flow. Arrays of collectors were deployed and recovered at each location in a polycarbonate lidded box (~80 x 60 x 35 cm) with the remotely-operated vehicle ROPOS. To avoid dislodgement of organisms during ascent, a piece of open cell foam (~ 5 cm in thickness) was attached to the underside of the box lid. All components of the collectors and the corresponding section of the foam were preserved in 95% ethanol at sea.

2.3.3 Sample processing

Coral recruits were identified morphologically based on high-resolution pictures of adult colonies. We used available genetic information to confirm the identity of *P. resedaeformis*, but genetic identification of *P. arborea* was inconclusive given the few recruits we retrieved (see Results). Therefore, we used distinct morphological features to distinguish *P. arborea* recruits from those of *P. resedaeformis* recruits. We recorded the abundance of recruits on the basalt rocks and mesh pads, the plastic tube around the rod, the plastic container, and the plastic ring. For the basalt rocks, the position of the corals (top vs. underside/sides) was recorded. Corals retrieved from foam sections were considered to have dislodged from the top of the settlement plates. Recruits of *P. resedaeformis* were attached to the substrate with a thin basal foot (Fig. 2.3A - inset). Because of their elongated shape (growing as 'small trees'), we measured the height with an ocular micrometer mounted on a dissecting microscope (Nikon SMZ1500) from the tip of the foot to the tallest end, and recorded the amount of polyps. Recruits were not measured if the basal foot had been truncated during manipulations. For *P. arborea*, due

to its morphology (Fig. 2.3B – inset), we only recorded the number of polyps, as heights measurements were impractical.

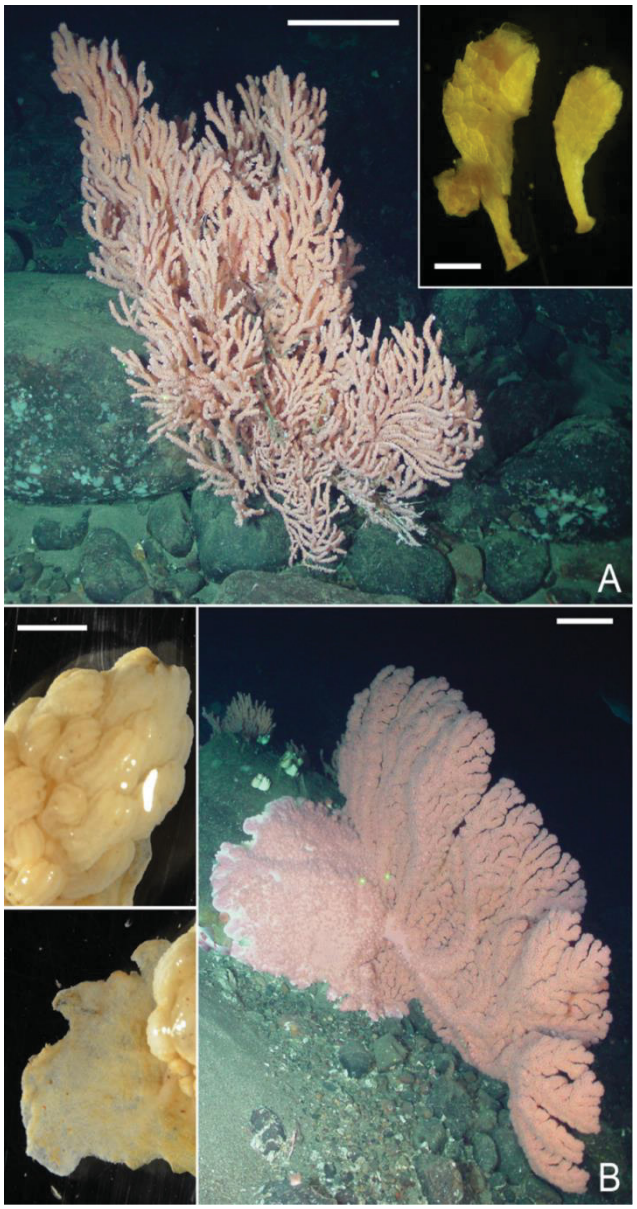

Figure 2.3: Recruits and adult colonies of deep-water gorgonian coral in Northeast Channel. Scale bars for adult colonies represent 20 cm. (A) *P. resedaeformis*. Depth: 288 m. Scale bar in inset represents 1 mm. (B) *P. arborea*. Depth: 314 m. Scale bar in inset represents 5 mm.

2.3.4 Statistical analyses

To determine whether the abundance of *P. resedaeformis* recruits (per 100 cm^2) differed among canyon locations (north wall, south wall, floor) and types of surfaces on top of the collectors (basalt rocks vs. mesh pads), we performed a 2-way ANOVA with unequal replication with canyon location (3 levels) and surface type (2 levels) as fixed factors. For canyon locations, differences detected with ANOVA were further tested with Tukey's Honestly Significant Difference (HSD) post-hoc tests. To determine whether 3-dimensional structural complexity of the collectors influenced the abundance of recruits (per 100 cm^2), we divided the collectors into 2 microhabitats: 1) flat surface on top of the collectors, 2) other components of the collectors (plastic container, plastic ring, plastic tube and sides/undersides of basalt rocks). We performed paired *t*-tests between these microhabitats at each canyon location and for each type of collector. The abundance of recruits (per 100 cm^2) was square-root transformed to meet assumptions of normality and homoscedacity. To compare the height-frequency distributions of recruits between and within (between types of collectors) locations, we performed 2-sample Kolmogorov-Smirnov (K-S) tests. These tests are robust against deviations from normality and unequal sample size. Statistical analyses were performed in the R programming environment, version 2.14.1.

2.4 Results

We collected recruits at the stages of both primary polyp only and juvenile colonies (2 polyps or more) of the deep-water gorgonian corals *P. resedaeformis* (Fig. 2.3A) and *P. arborea* (Fig. 2.3B) on all components of both types (basalt rocks and mesh

pads) of collectors. Recruits of both species were collected at each location (north wall, south wall and floor of the canyon), but those of *P. resedaeformis* were far more abundant (Table 2.2). We retrieved 2 *P. arborea* recruits at the deepest location (floor: 863 m), one of which was composed of more than 20 polyps, the largest recruit retrieved in our study (Fig. 2.3B – inset). Based on similar morphological features, 2 more recruits were identified as *P. arborea*, one at each location on the north and south walls. The relatively low abundance of *P. arborea* restricted further analyses on this species.

Table 2.2: Total abundance of recruits of the deep-water gorgonian corals *P. resedaeformis* and *P. arborea* retrieved from arrays of larval settlement collectors deployed in the Middle Canyon of the Northeast Channel Coral Conservation Area from 2006 to 2010.

Canyon location	Depth (m)	*P. resedaeformis*	*P. arborea*
North wall	658	1289	1
South wall	671	792	1
Floor	863	97	2

Total abundance of *P. resedaeformis* recruits (standardized per 100 cm^2) on the collectors (all components combined) differed among canyon locations, but did not differ between surface types (Fig. 2.4A) (2-way ANOVA with unequal replication; Location: $F_{2,42} = 117.09$, $P < 0.001$, Surface type: $F_{1,42} = 0.08$, $P = 0.78$, Location x Surface Type: $F_{2,42} = 1.08$, $P = 0.35$). Total abundance of recruits differed among all 3 canyon locations (Tukey's HSD, $P < 0.001$), being highest on the north wall (17.22 ± SD: 5.26 recruits/100

cm^2), intermediate on the south wall (10.95 ± SD: 3.97 recruits/100 cm^2), and lowest at the floor of the canyon (1.28 ± 0.62 recruits/100 cm^2).

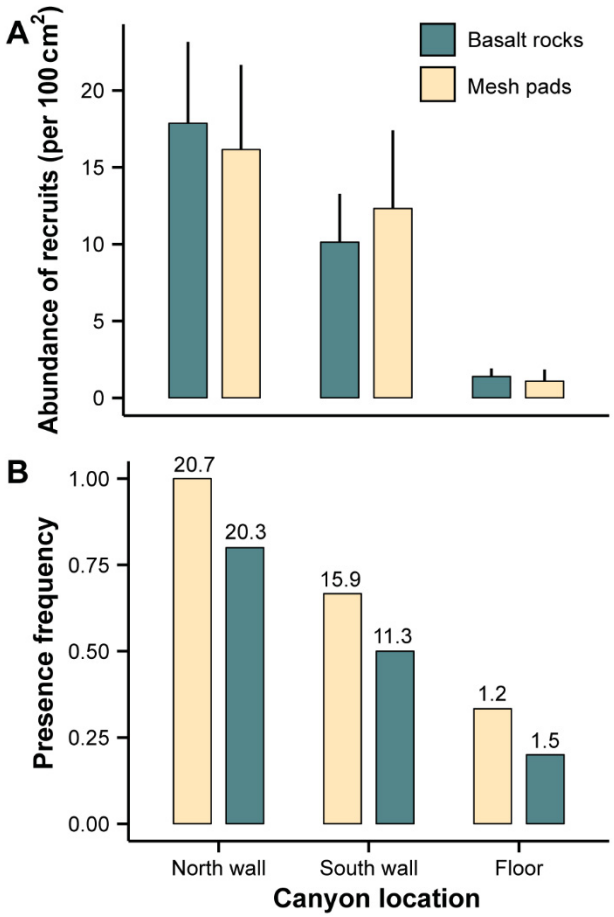

Figure 2.4: Recruitment of *P. resedaeformis* on arrays of larval settlement collectors. Arrays were deployed at 3 locations (north wall: 658 m, south wall: 671 m, floor: 863 m). Settlement collectors included either a basalt rock (n = 10 per location) or mesh pads (n = 6 per location). (A) Mean abundance (+SD) of recruits on all components of the settlement collectors combined. (B) Frequency of presence of recruits on the top flat surfaces of the larval settlement collectors. Mean abundance of recruits (per 100 cm^2) on the other components of the settlement collectors (i.e. excluding the top flat surfaces) is indicated at each location and for each surface type.

We found few *P. resedaeformis* recruits on the flat top surfaces of the basalt rocks and mesh pads (no recruitment on 21 of the 48 collectors, maximum: 6 recruits). Most recruits (~98% on average) were retrieved on the other components of the collectors (plastic container, plastic ring, plastic tube and sides/undersides of basalt rocks). The frequency of presence of recruits (at least one) on the top surfaces of each type of collector was more closely related to their abundance on the other components of the collectors than surface type on which they settled (Fig. 2.4B). The density of *P. resedaeformis* recruits was significantly greater on all other components of the collectors than on their flat surfaces at both walls of the canyon (paired *t*-tests; north wall – basalt rocks: $t_9 = 10.32$, $P < 0.001$; mesh pads: $t_5 = 6.19$, $P = 0.002$; south wall - basalt rocks: $t_9 = 8.90$, $P < 0.001$; mesh pads: $t_5 = 4.75$, $P = 0.005$), and for basalt rocks at the deepest location (floor: $t_9 = 3.30$, $P = 0.009$).

The height of *P. resedaeformis* primary polyps ranged from 0.85 mm to 9.30 mm (mean ± SD: 3.03 mm ± 0.99 mm; n = 1262), while the height of juvenile colonies ranged from 2.35 mm to 11.90 mm (4.78 mm ± 1.36 mm; n = 378). Relative height-frequency distributions of the *P. resedaeformis* recruits were unimodal and right-skewed at the south wall and north wall sites (Fig. 2.5), suggesting continuous recruitment. We compared the height-frequency distributions of recruits between the north and south walls, and between surface types within each location. Low recruitment restricted us from including the deepest location (floor) in this analysis. For both surface types, recruits were taller on the south wall (2-sample K-S test; basalt rocks: D = 0.20, $P < 0.001$; mesh

pads: D = 0.22, $P < 0.001$) than the north, and within each of these locations, recruits were taller on basalt rocks than mesh pads (2-sample K-S test; south wall: D = 0.15, $P = 0.005$; north wall: D = 0.16, $P < 0.001$).

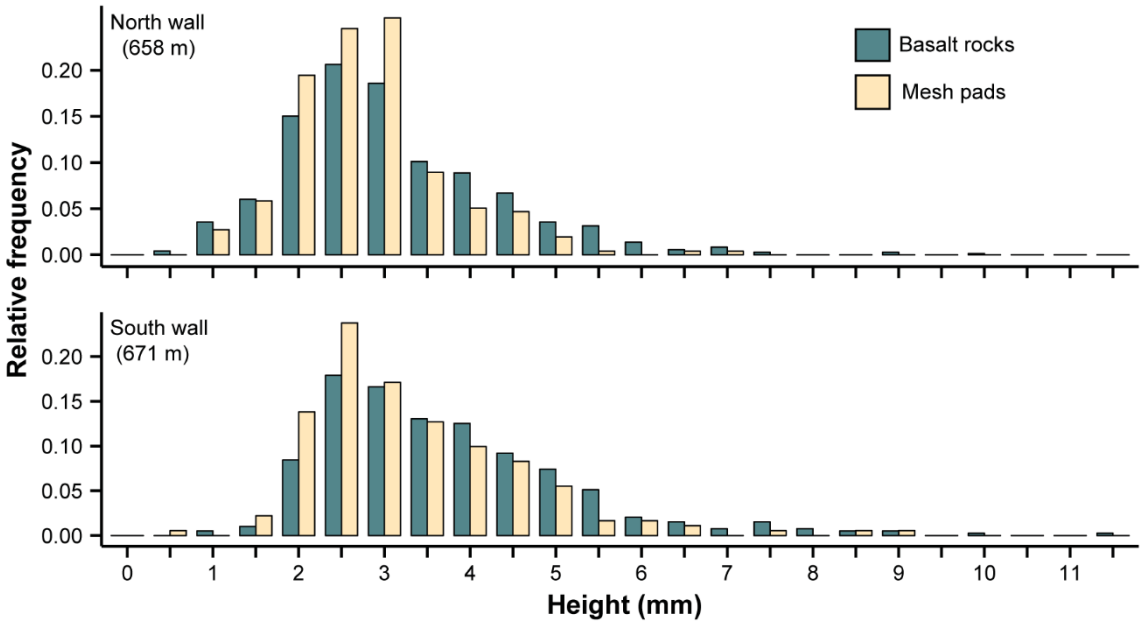

Figure 2.5: Relative height-frequency distributions of pooled *P. resedaeformis* recruits. Recruits were retrieved on larval settlement collectors with basalt rocks (north wall: n = 732; south wall: n = 391) and mesh pads (north wall: n = 257, south wall: n = 181). Heights indicate the lower ends of 0.5 mm-bins.

We consider each additional polyp on *P. resedaeformis* recruits as an important transition in the early development stages. The mean relative frequency of recruits decreased with increasing number of polyps, a pattern that was consistent on both walls and at the floor of the canyon, and on both surface types (Fig. 2.6). The majority of

recruits were at the primary polyp stage (mean relative frequencies ranging from 70% to 86%), and on average, fewer than 10% of the recruits were found with 3 polyps or more. Recruits reached a maximum size of 5 polyps, found on the south and north walls of the canyon, and in both cases, represented fewer than 0.5% of the recruits from these locations.

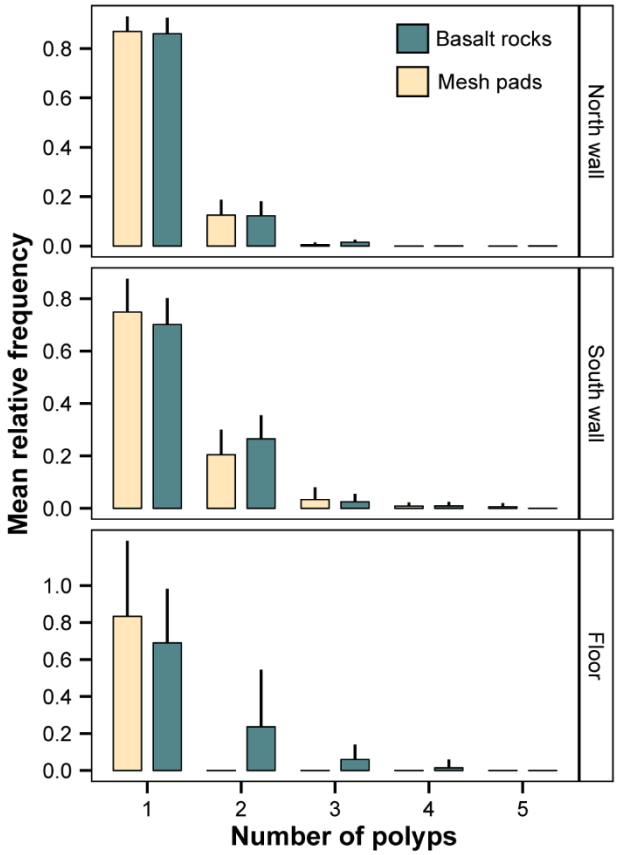

Figure 2.6: Mean relative frequency (+SD) of *P. resedaeformis* recruits on settlement collectors. Collectors were either composed of basalt rocks (n = 10) or mesh pads (n = 6) on arrays deployed at 3 locations (north wall: 658 m, south wall: 671 m, floor: 863 m). The number of polyps reflects early life stages of the recruits: 'one polyp' is the primary polyp, and '2 or more polyps' are juvenile colonies.

2.5 Discussion

In our study, recruitment on the collectors was high for *P. resedaeformis* (most likely reflecting significant larval supply for this species), but limited for *P. arborea*. Such differences could possibly be explained by divergent reproductive modes between the 2 species. Recruitment of corals depends on local larval availability, which itself is linked to the density of adults, their reproductive output (fecundity), and the dispersal potential of larvae (Hughes et al. 2000).

Broadcast spawning is present in deep-water reef-building (scleractinian) corals (Waller 2005), but studies on deep-water soft corals have generally reported gonochoric brooding as the main reproductive strategy (Cordes et al. 2001; Orejas et al. 2002; Orejas et al. 2007; Sun et al. 2010). A recent study based on fecundity analyses proposed that *P. resedaeformis* may be one of the few deep-water soft coral species to be a gonochoric broadcast spawner (Mercier and Hamel 2011). In our study, the abundance of *P. resedaeformis* recruits was higher on the north (depth: 658 m) and south (depth: 671 m) walls than on the floor (depth: 863 m) of the canyon, which reflected both the local abundance of colonies and general bathymetric range of this species. In the Middle Canyon of the Northeast Channel, the abundance of *P. resedeaformis* colonies peaks at depths between ~ 500 and 650 m, decreasing at greater depths, and being virtually absent at depths greater than 750-800 m (Watanabe et al. 2009). In this area, the distribution of colonies is clustered and dense thickets are frequently observed (Watanabe et al. 2009). On the north wall, the maximum density observed was of 37.7 colonies/10 m^2 (at depths of 500-525 m), while on the south wall, the maximum density reached 18.3 colonies/10

m^2 (at depths of 600-625 m) (Watanabe et al. 2009). *P. resedaeformis* recruits were overall more abundant, but shorter on the north wall, while they were less abundant, but taller on the south wall. This suggests asynchrony in recruitment dynamics among these locations, despite being at similar depths, and the potential importance of local conditions in influencing recruitment. However, recruits of *P. resedaeformis* were retrieved at the floor of the Middle Canyon, indicating a potential for this species to supply larvae beyond its reported range. In shallow waters, it is typically assumed that reef-building broadcast spawners disperse over wider areas than brooding species (Nishikawa et al. 2003), but this relationship remains unclear (Ayre and Hughes 2000). The positively-buoyant eggs of spawners, followed by a generally longer larval pre-competency period than brooders, allow them to use wide-reaching ocean currents for dispersal (Harrison and Wallace 1990). The deep flow in Northeast Channel is dominated by tides (Ramp et al. 1985), but local water circulation in the Middle Canyon is unknown. In general, submarine canyons have been reported to funnel water from the continental shelf to the deep sea known as 'dense shelf water cascading' (Canals et al. 2006). Our results suggest that larvae of *P. resedaeformis* may be utilizing these currents, but the lack of suitable substrate (mostly comprised of coarse sand on the floor of the canyon, which is not the preferred substrate of this species (Mortensen and Buhl-Mortensen 2004; Watanabe et al. 2009; Edinger et al. 2011; Tong et al. 2012)) may prevent recruitment at great depths.

On the north and south walls, the magnitude of recruitment suggests that post-recruitment processes influence the local abundance of adult colonies. Such processes have been reported to be important in regulating the populations of shallow-water

broadcast spawning corals (Vermeij and Sandin 2008). Based on the mean abundance of recruits on the top surfaces of the collectors on the north wall (0.57 recruits/100 cm^2) and south wall (1.42 recruits/100 cm^2), estimated abundance of adult colonies would range between 5,700 and 14,200 colonies per 10 m^2, 3.5 orders of magnitude greater than the measured mean abundance of colonies at these depths (2.7 to 4.1 colonies per 10 m^2 – Watanabe et al. 2009). Additionally, the majority of recruits were at the primary polyp stage, with a sharp decline in abundance in later stages. Given that the shape of the height-frequency distributions of *P. resedaeformis* recruits suggests continuous recruitment, in accordance with a previous study (Mercier and Hamel 2011), we consider it unlikely that recent, large pulses in recruitment are the sources of these patterns at both locations.

The influence of post-recruitment processes on the local abundance of adult colonies is unknown in deep-water gorgonian corals. In our study, structural complexity influenced recruitment of *P. resedaeformis*, as larvae most often settled on other components of the collectors, rather than on the top flat surfaces. We suggest that survival of coral recruits may have been the result of the presence of refuges from biological disturbance. It is possible that *P. resedaeformis* is unable to recruit (despite high larval supply) on available suitable substrate (i.e. pebbles, cobbles and boulders) due to the presence of other benthic organisms creating a disturbance and affecting survival in the early life history of this species. In Northeast Channel, the density of the brittle star *Ophiacantha abyssicola* has been reported at more than 1,000 individuals/m^2 (Metaxas and Griffin 2004). These suspension-feeding brittle stars were abundant at the north and

south wall sites in the vicinity of the collectors, and on the collectors when we retrieved them. They were relatively more abundant on the north wall than on the south wall, which could explain why more recruits were retrieved on the top flat surfaces of the collectors on the south wall (1.42 recruits/100 cm^2 compared to 0.57 recruits/100 cm^2 on the north wall). Further, recruits on basalt rocks were relatively larger than those on mesh pads, possibly because the space between the basalt rock and the plastic container provided a refuge from such disturbance.

The 3-dimensional structure of the collectors may have also altered fine-scale flow, possibly enhancing the survival of coral recruits by altering the encounter rate with food particles and reducing sedimentation. In dynamic deep-water habitats, food supply is through the export of surface primary production, presumably through vertical deposition and lateral advection in areas of strong currents. The presence of rich megafaunal communities in deep-water canyons (Huvenne et al. 2011) and on seamounts (Rowden et al. 2010) suggests that food delivery is enhanced in these habitats, but the magnitude of this flux is unknown. At spatial scales of 10s to 100s of km's, food supply is considered the dominant factor influencing the distribution of *P. resedaeformis* and *P. arborea* (Mortensen and Buhl-Mortensen 2004; Bryan and Metaxas 2006; Tong et al. 2012). At scales of meters to 10s of meters, in both moderate and steep reliefs, the abundance of these gorgonian corals is greater in the presence of structural complexity (cobbles, pebbles, and boulders) (Tong et al. 2012), which can enhance the resuspension of organic matter by creating turbulent flow near the seafloor (Mortensen and Buhl-Mortensen 2004). Enhanced recruitment of suspension-feeding invertebrates in cryptic

microhabitats, such as cracks and undersides of plates, rather than due to surface composition (basalt rock vs. plastics), has also been reported near hydrothermal vents (Mullineaux et al. 1998). Strong currents and turbidity near the seafloor concurrently reduce sedimentation, which can affect the suspension-feeding capacity of gorgonian corals. Encounter rate with food particles may hence not be sufficient to ensure the development of each primary polyp into a juvenile colony. The rates of export of primary production to the benthos off the continental margin of Atlantic Canada are not currently known. Such knowledge is urgently needed, as the dynamics of surface primary productivity are shifting in various water bodies worldwide, potentially affecting deep-dwelling suspension-feeders (Smith et al. 2009).

Unlike *P. resedaeformis*, the reproductive strategy of *P. arborea* has not been studied to date. *P. arborea* is typically larger than *P. resedaeformis*, forming a concave shape oriented perpendicular to the dominant direction of currents (Mortensen and Buhl-Mortensen 2005). This species is thought to feed primarily on fresh phytodetritus (Sherwood et al. 2008), which could explain their shape to maximize the encounter rate with food particles in areas of strong currents, and their local distribution (they are often found on vertical structures (Mortensen and Buhl-Mortensen 2004; Watanabe et al. 2009; Tong et al. 2012)). The abundance of *P. arborea* colonies does not follow a clear bathymetric pattern, but this species tends to be found at greater depths than *P. resedaeformis* (Mortensen and Buhl-Mortensen 2004; Wareham and Edinger 2007; Watanabe et al. 2009; Edinger et al. 2011; Tong et al. 2012). In our study, the largest recruit (> 20 polyps) was identified as *P. arborea*, and was retrieved at the floor of the

canyon. It was the only location where 1) a large boulder (> 3 m in diameter) was present, and 2) colonies of *P. arborea* were present within meters of the collectors, including one exceeding 1.5 m in height. It is possible therefore that the floor of the canyon was more susceptible to recruitment of *P. arborea*. Further, we consider it unlikely that the lack of *P. arborea* recruits may be due to space competition, given the high abundance of *P. resedaeformis* recruits and because much of the space available on the collectors had not been colonized. Given the important difference in recruitment between *P. arborea* and *P. resedaeformis*, and the presumed limited range of settlement for *P. arborea* (brooders release competent larvae, which can substantially reduce time spent in the water column (Richmond 1997)), we suggest that this species may be a brooder.

Overall, we conclude that both *P. resedaeformis* and *P. arborea* are limited in their ability to maintain their populations in the Northeast Channel Coral Conservation Area, although the reason differs between the 2 species. Deep-water gorgonian corals are long-lived invertebrates (10s to 100s of years), and processes affecting early life stages must be integrated over a longer period of time than for shallow-water species. After 4 years, we found very few recruits of *P. arborea*, which suggests low larval supply in the area. In contrast, despite high recruitment for *P. resedaeformis*, our results suggest extremely high mortality for this species in its early life stages: approximately 20% of the coral recruits formed a colony, and < 1% of these were at a stage of ≥ 4 polyps. We emphasize that our study provides indirect evidence supporting hypotheses on the reproductive strategy of each species (*P. resedaeformis* as a broadcast spawner and *P.*

arborea as a brooder), and that more information on the reproductive biology of each species is needed. We have also shown that recruitment is enhanced by the structural complexity of the recipient habitat, and proposed biological disturbance and access to limited food resources in the water column as ecological mechanisms possibly explaining this enhanced recruitment and high juvenile mortality early on in the benthic stage.

CHAPTER 3

USING OBJECT-BASED IMAGE ANALYSIS TO DETERMINE SEAFLOOR FINE-SCALE FEATURES AND COMPLEXITY[2]

3.1 Abstract

Autonomous and remotely-operated underwater vehicles equipped with high-definition video and photographic cameras are used to perform benthic surveys. These devices record fine-scale (<1 m) seafloor features (seafloor complexity) and their local (10-100s m) variability (seafloor heterogeneity). Here, we introduce a methodology to efficiently process this optical imagery using object-based image analysis, which reduces the pixels in high-resolution digital images into a collection of 'image-objects' of homogeneous color and/or luminosity. This approach uses intuitive user-defined parameters and reproducible computer code, which aims to facilitate comparisons between habitats and geographic regions. We test this methodology with 511 images taken on the seafloor of a glaciated continental shelf (Gulf of Maine, northwest Atlantic), and describe 3 applications: (1) estimating percent cover of conspicuous epibenthic fauna by building a Random Forest binary classifier assigning an identity to image-objects; (2) correlating image complexity (number of image-objects) with mean particle grain size; and (3) estimating seafloor heterogeneity from local variability in image complexity

[2] Lacharité, M., A. Metaxas, and P. Lawton. 2015. Using object-based image analysis to determine seafloor fine-scale features and complexity. Limnology & Oceanography: Methods **13**: 553-567.

My coauthor A. Metaxas supervised survey design, development of the method, and analyses, and edited the manuscript. My coauthor P. Lawton supervised survey design, provided data, and edited the manuscript.

within and between 2 physiographic regions. Percent cover of epibenthic fauna estimated by the Random Forest binary classifier was in close agreement with the human visual assessment. Mean particle grain size (ϕ scale) was inversely correlated with image complexity (maximum Spearman's ρ = -0.89, $p < 0.01$) with images dominated by pebbles, cobbles, boulders (low on ϕ scale) yielding high image complexity. Predictive relationships of sediment composition were established using polynomial regression. Lastly, our approach could differentiate habitats within and between physiographic regions by using mean seafloor complexity and local variability along transects.

3.2 Introduction

Benthic habitat structure is composed of 2 factors: *complexity*, the absolute abundance of structural components (e.g. rocks, mounds); and *heterogeneity*, the variation in complexity due to changes in the relative abundance of these structural components (McCoy and Bell 1991; Sebens 1991). On sedimented substratum, complexity arises from the distribution of sediment grain size and small-scale topographic features (e.g. pits and burrows) resulting from local hydrodynamics and bioturbation. On hard substratum, in rocky intertidal and subtidal habitats, complexity is most often measured with a surface to area ratio [e.g. fractal dimensions (Kostylev et al. 2005), and the chain-and-tape approach (Risk 1972)], which is influenced by the presence of crevices, rock walls or biological structures. Seafloor complexity influences larval settlement (e.g. Walters and Wethey 1996), the abundance and diversity of invertebrate assemblages (e.g. Kostylev et al. 2005; Matias et al. 2010), predator-prey interactions (e.g. Grabowski 2004), and the concentration of organic matter (e.g. Abelson et al. 1993).

Amongst other factors, spatial variability in fine-scale (< 1 m) seafloor complexity (i.e. seafloor heterogeneity) can influence the distribution of species in both shallow coastal waters (e.g. Cusson and Bourget 1997) and deeper waters on continental shelves and margins (Buhl-Mortensen et al. 2012; Robert et al. 2014). The proximity of suitable habitat to the source population is thought to affect biological patterns, particularly during the dispersing larval phase of marine benthic invertebrates (Garcia-Sanz et al. 2012; Robert et al. 2014). Variability in seafloor complexity can be gradual and monotonic or sharp with distinct changes along small spatial scales (Jacquez et al. 2000). These patterns may influence both the distribution of benthic organisms, and also be indicative of anthropogenic impacts; abrupt changes in habitat characteristics have been linked to human-induced disturbance in terrestrial ecosystems (Strayer et al. 2003). On glaciated continental shelves, the retreat of ice created complex geomorphological features (e.g. drumlins, basins) and left stratified debris along a typical vertical sequence of sediment depositions (reviewed in Syvitski 1991). In Atlantic Canadian continental shelves, these deglacial processes during the late Pleistocene, coupled with circulation patterns and periods of erosion, created a heterogeneous, unsorted, and often unconsolidated, mixture of sediment grain sizes (from mud/silt to large boulders), interspersed with bedrock outcrops, yielding complex patterns of surficial geology. These processes resulted in strong spatial environmental gradients at fine- (<1 m) to meso- (1-10s km) scales (Fader et al. 1977).

In benthic habitat mapping, imagery from acoustic surveys from side-scan sonar, and both single- and multi-beam echosounders is often used to determine substratum

composition based on backscatter strength and texture (see Brown et al. 2011 for review). In situ observations of sediment properties and/or biological assemblages using either sediment core samples or optical surveys have most often been used to interpret ('groundtruth') results from these acoustic surveys (e.g. Kostylev et al. 2001). Some studies have directly incorporated measurements of sediment properties at multiple spatial scales (e.g. Todd and Kostylev 2011). Arguably, to be useful at the seascape scale ('seascape' is defined here as an area encompassing 2 or more habitat types), seafloor complexity must be measured over wide geographic areas. Remotely-operated vehicles and autonomous underwater vehicles equipped with high-definition video and photographic cameras now collect a vast quantity of optical imagery of the seafloor that can be used to determine its complexity at fine spatial scales (< 1 m) and determine the variability of these features at larger spatial scales (Wynn et al. 2014).

Optical remote sensing of the seafloor generates a large quantity of information, as hours of video transects can easily translate into 1,000s to 10,000s of still images. Since it is difficult to standardize the processing of optical imagery, new objective approaches, adapted from concepts of computer vision and image processing, are being developed to accelerate processing speed, remove subjectivity of interpretation and foster collaboration through the transfer of tools (Seiler et al. 2012; Lambert et al. 2013). Image processing methods can be broadly divided into 2 categories: feature detection and whole-scene pattern recognition. Feature detection aims to identify specific objects in a scene using a training dataset. In benthic studies, it has been used with stationary cameras in the deep sea to detect specific organisms and track their movement (Aguzzi et al. 2009;

Aguzzi et al. 2011). Whole-scene pattern recognition has been used to classify images into discrete categories of habitats (Teixido et al. 2011; Seiler et al. 2012; Lambert et al. 2013).

Here, we develop a method using digital images of the seafloor to build a continuous scale of seafloor complexity and use it to identify features at a scale of <1 m. The method is based on object-based image analysis, which generates image-objects or 'superpixels' with a homogeneous signature that can include one or more dimensions in the feature space. Based on principles of image segmentation (Pal and Pal 1993), it has been used more extensively since the early 2000s in remote sensing studies particularly on land (reviewed in Blaschke 2010), but also increasingly in marine systems with acoustic backscatter surveys (Lucieer 2008; Lucieer and Lamarche 2011; Lucieer et al. 2013; Diesing et al. 2014). To our knowledge, it has not been used at finer spatial scales in the context of benthic studies. Previous benthic studies of whole-pattern recognition (Seiler et al. 2012; Lambert et al. 2013) used pixel-based approaches to classify images; we use a region-based approach. Specifically, we first adapt image segmentation algorithms to segment seafloor digital images into an array of image-objects, the variability of which is used to estimate image complexity as a proxy of seafloor complexity. In our study, an 'image-object' is meant to represent an area of the seafloor with homogeneous texture and/or color, not necessarily a real object, since this distinction is currently hard to establish (see 'Comments & Recommendations'). We then use this approach in deep waters (>100 m) of an Atlantic Canadian glaciated continental shelf to: 1) determine fine-scale substrate features using supervised machine-learning

classification of image-objects; 2) test whether we can infer mean particle grain size by using image complexity; and 3) evaluate variability in fine-scale seafloor complexity at 2 spatial scales: local (10-100s m) and mesoscale (1-10s km).

3.3 Materials & Procedures

3.3.1 Study area

The Gulf of Maine is a relic of the retreat of the Laurentide ice sheet, which extended to the continental shelf break at the last glacial maximum ~20,000 years ago (Schnitker et al. 2001; Shaw et al. 2006). Water depths reach a maximum of ~350 m in 3 deep basins (Jordan, Georges and Wilkinson Basins) separated from one another by large ridges. The Gulf proper is bordered along the continental margin by Georges Bank and Browns Bank. The surficial geology of the deep waters (>60 m) of the eastern Gulf of Maine is typical of glaciated continental shelves, mostly comprised of moraine debris, ice-contact sediment or 'glacial till' (Fader et al. 1977). This wide range of particle grain sizes co-occurring at fine spatial scales (<1 m) makes it difficult to determine variability in fine-scale geological features using traditional sediment samples. The complex bathymetry and surficial geology create heterogeneity in benthic habitats in the region, thought to influence patterns of biodiversity (Incze et al. 2010).

3.3.2 Benthic photographic transects

Digital images of the seafloor were collected along transects in 5 physiographic regions in the eastern Gulf of Maine and adjacent Scotian shelf (Table 3.1, Fig. 3.1) in July and August 2009 using Campod, an instrumented tripod equipped with video and still cameras (Gordon Jr. et al. 2007) aboard the Canadian Coast Guard Ship Hudson.

Campod has an open profile and a wide stance to minimize disturbance to the seafloor, and is operated in a near-seafloor drift mode, with the capability to land on the seafloor to collect standardized imagery (using a high-resolution color photographic camera (Nikon D300) with a resolution of > 12 megapixels facing downward). An image was taken approximately every minute along the transect track, and surface area of the field of view was calculated based on lasers 10 cm apart. Due to lack of illumination in the outer portion of images, original images were cropped to a standardized field of view of 0.375 m^2 (height: 0.5 m; length: 0.75 m). Campod is equipped with an ultra-short-baseline (USBL) navigation system (ORE Trackpoint II), allowing its precise positioning on the seafloor. Distance between images was rounded to the nearest meter. Overall, 26 transects were performed in the 5 physiographic regions, ranging in length from ~700 m to 1100 m, producing a total dataset of 2582 images (Table 3.1, Fig. 3.1). To develop the proposed method, we subsampled the original dataset (1 every 5 images), resulting in a subsample dataset of 511 images.

Table 3.1: Location and depth range of benthic transects in the Gulf of Maine and adjacent Scotian Shelf (northwest Atlantic). Also shown are the total number of images collected along transects and the subsample dataset that is used to develop the proposed approach.

Region	GPS coordinates	# Transects	Depth range (m)	Total # of images	Number of subsample images
Jordan Basin	43°39'46''N 66°56'57''W	9	77 - 210	846	162
Sewell Ridge	42°43'39''N 67°07'11''W	4	209 - 265	502	99
Georges Basin	42°33'54''N 66°53'01''W	2	254 – 318	264	51
Roseway Basin	43°23'58''N 64°47'54''W	5	64 – 163	267	51
Browns Channel	42°53'27''N 66°05'17''W	6	110 - 263	703	148

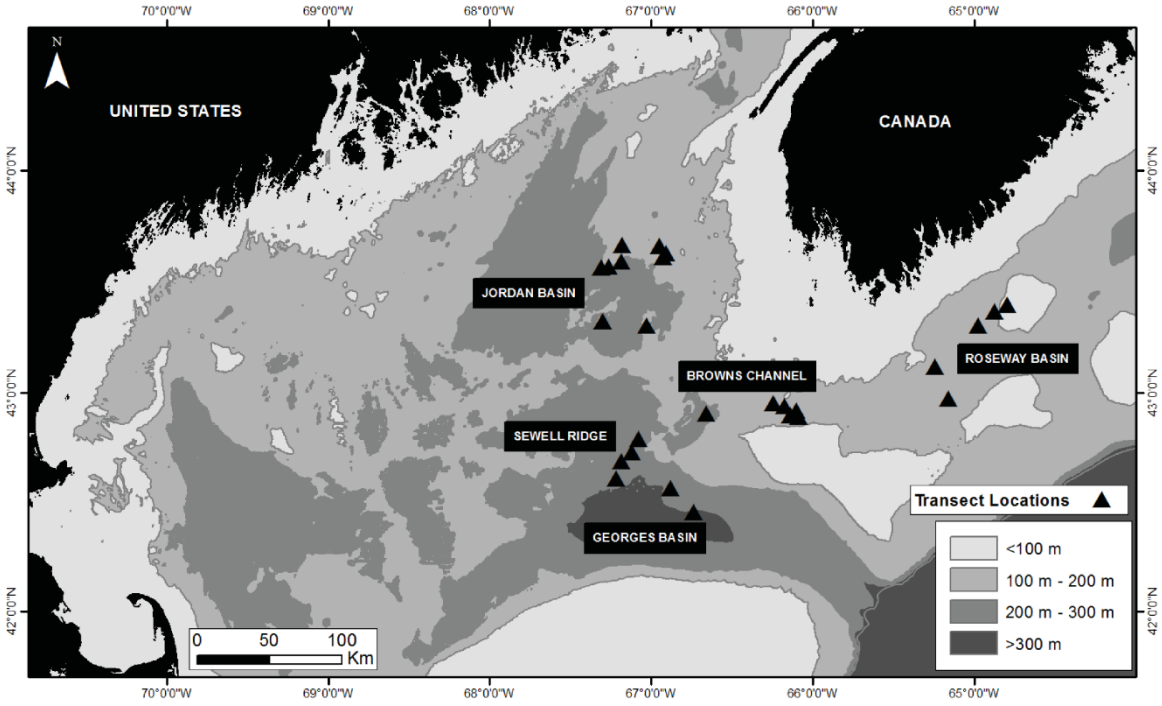

Figure 3.1: Gulf of Maine and adjacent Scotian Shelf (Northwest Atlantic) with locations of benthic transects (n = 26) in Jordan Basin, Sewell Ridge, Georges Basin, Browns Channel and Roseway Basin.

3.3.3 Object-based image analysis of seafloor images

Object-based image analysis aims to reduce the number of pixels in an image into a collection of 'superpixels' or 'image-objects' representing homogeneous regions of luminosity, texture and/or color (e.g. Kettig and Landgrebe 1976; Blaschke 2010). To process digital images of the seafloor, we adapted from the literature an algorithm using object-based image analysis (Haris et al. 1998, Castilla 2003 (unpublished thesis) and references therein) described below and implemented it in MATLAB (©MathWorks). The code is available online through GitHub (GitHub.com; repository: mlacharite/SeafloorOBIA). It requires the MATLAB image processing toolbox. Object-based image analysis is composed of 2 main steps: image segmentation and assignment of an 'identity' to the resulting image-objects after segmentation. Broadly, we achieved image segmentation by first over-segmenting the image and recursively merging image-objects ('region merging') until all image-objects were larger than a minimum size predetermined by the user (Figs. 3.2, 3.3).

Seabed images were taken using the additive RGB (red, green, blue) color model. Original RGB images were re-sized to a standard pixel resolution and transformed into the CIELab color space (L: luminosity; a, b: color components). CIELab was used because it is a Euclidean color space, is designed to be comparable to human vision, and has been proven to be powerful in image segmentation (Ganesan et al. 2010). A modified Euclidean distance (Sharma et al. 2005) was used because the typical Euclidean distance is overestimated close to the central axis of the CIELab color space composed of shades

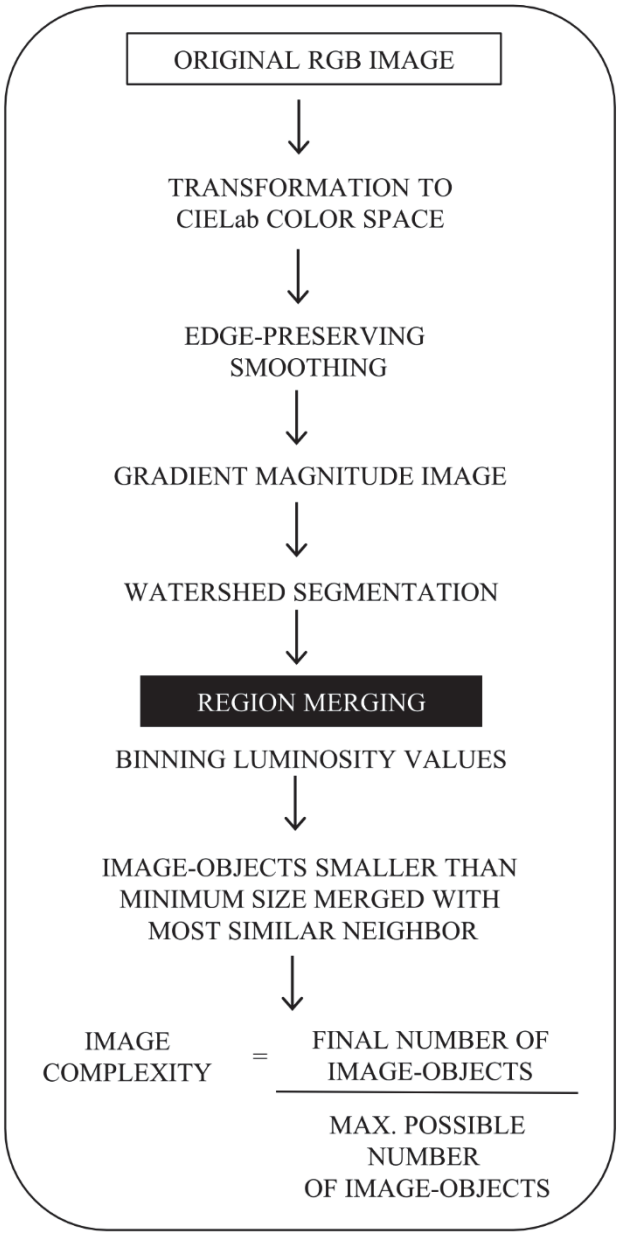

Figure 3.2: Object-based image analysis algorithm used to infer image complexity in digital images of the seafloor.

of brown and grey, which are the shades of most images of the seafloor in the surveyed region. Since adjacent pixels in high-resolution digital images tend to be 'noisy', smoothing is required before the image is segmented. To preserve boundaries between potential image-objects and, in some cases, to enhance contrasts between them, we used an edge-preserving smoothing algorithm [Castilla 2003 (unpublished thesis) adapted from Perona and Malik 1990; Fig. 3.3b]. For each pixel of the smoothed image, we calculated the modified Euclidean distance in the CIELab color space between neighbors on opposite sides (top-bottom; left-right). This yielded a gradient magnitude image of the same size as the original image where the value of each pixel is proportional to the contrasts in color and luminosity among its neighbors (Fig. 3.3c). Watershed segmentation (Vincent and Soille 1991) was applied to the gradient magnitude image (Fig. 3.3d). This segmentation algorithm, similarly to a digital elevation model, creates image-objects by merging neighboring pixels in 'basins' (regions of low contrast in luminosity and color) that are surrounded by 'peaks' (regions of high contrast in luminosity and color). Because watershed segmentation tends to 'over-segment' the image (i.e. create too many, spurious image-objects), region merging of similar image-objects is required.

During region merging, image-objects were first binned based on their mean luminosity, since it is responsible for most of the contrast observed in digital images. Luminosity in the CIELab color space ranges from 0 to 100. This range can be divided into an arbitrary number of bins representing a certain interval of interest, and each image-object assigned to a bin. In the original image, image-objects in the same bin are

then merged, resulting in larger image-objects if image-objects from the same bin are neighbors. High-resolution images of the seafloor can render very small, potentially meaningless, objects, such as individual grains of sand. Therefore, the last step of the image segmentation was to merge neighboring image-objects based on a minimum size determined manually as number of pixels representing a defined area on the seafloor (Fig. 3.3e). Image-objects smaller than this minimum size were merged recursively with their most similar neighbor. Similarity was established with a modified Euclidean distance in CIELab (Sharma et al. 2005) where short distance indicated higher similarity. The algorithm stopped when all image-objects were larger than the minimum size.

We define 'image complexity' for digital images as a dimensionless measure of complexity: the number of image-objects detected by the algorithm divided by the maximum potential number of image-objects given the minimum size of each image-object. For example, an image covering a surface of 3750 cm^2 could potentially detect 3750 image-objects if the minimum size is set at 1 cm^2. This allows comparisons of images with a similar size of field of view, but varying pixel resolution.

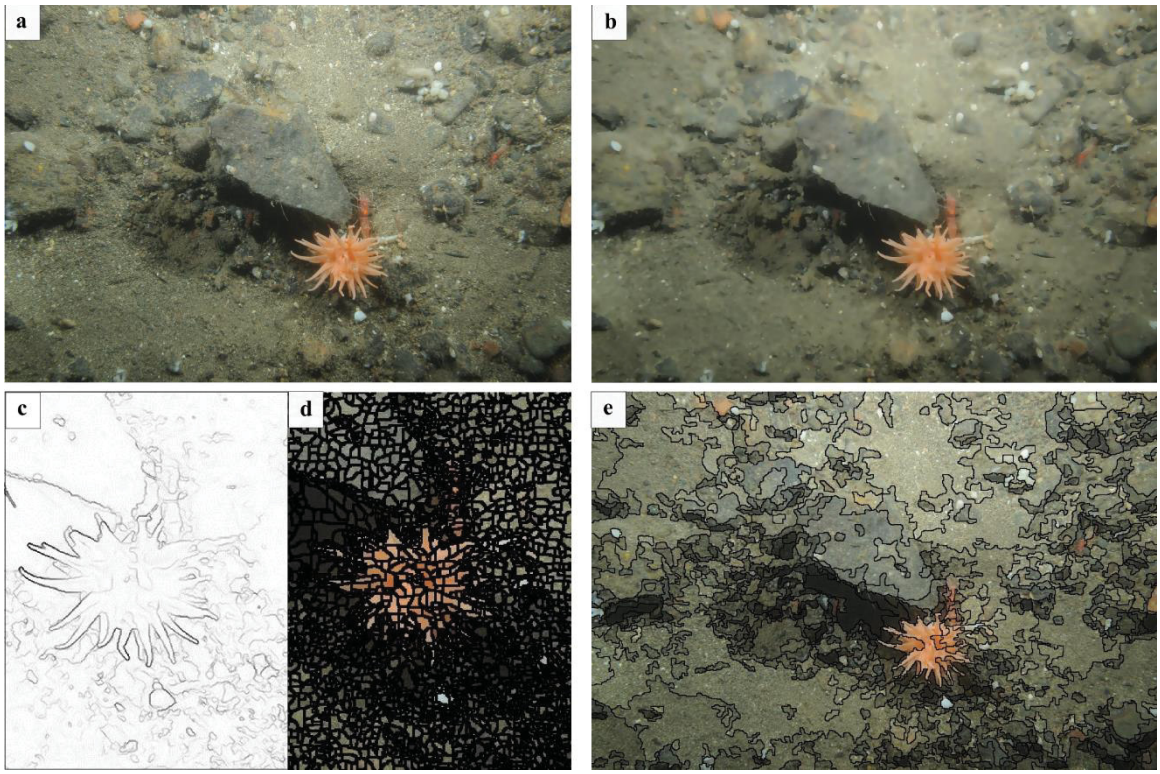

Figure 3.3: Steps of image segmentation algorithm implemented in the proposed method (luminosity histogram bin size: 5; minimum size of image-objects: 1 cm^2). (a) Original RGB image covering 0.375 m^2 on the seafloor (0.75 m x 0.50 m). (b) Image rendition after edge-preserving smoothing (20 iterations; Castilla 2003 (unpublished thesis) adapted from Perona & Malick 1990). (c) Portion of the gradient magnitude image built from the smoothed image. Darker lines indicate stronger gradients in the CIELab color space. (d) Portion of the image after watershed segmentation (20411 image-objects detected). (e) Final image segmentation (589 image-objects).

3.3.4 Application example one: Assigning an identity to image-objects using a Random Forest classifier

Each image-object can be assigned an 'identity' based on a set of user-defined characteristics used as predictor variables. Here, we tested whether object-based image analysis of digital images of the seafloor can be used to estimate percent cover of epibenthic fauna in the 5 physiographic regions surveyed.

A Random Forest classifier is a machine-learning algorithm that uses an ensemble of binary decision trees to classify an observation based on 'tree votes' in a given set of categories (Breiman 2001). Random Forest is easy to implement, since only 2 parameters need to be defined: the number of decision trees in the forest and the number of predictor variables that are randomly selected at each split. It can also handle categorical and unbalanced data, making it more flexible for analysing large, multivariate datasets. The accuracy of Random Forest classifiers has been demonstrated in studies using acoustic surveys to classify benthic habitats (Diesing et al. 2014; Stephens and Diesing 2014). Here, we built the classifier using a training dataset of 500 randomly-selected image-objects of 'epibenthic fauna' (i.e. conspicuous sponges, anemones, corals, bivalves, crinoids, and echinoderms greater than > 2 cm in diameter for consistency in visual detection) and 500 image-objects that did not represent epibenthic fauna. To illustrate the use of the classifier, the image-objects were generated with only 1 combination of user-defined parameters in the segmentation algorithm: histogram bin size of 5 units of luminosity and a minimum size of image-objects of 1 cm^2. Predictor variables included mean components of the CIELab color space (luminosity and 2 color components), and mean texture that was determined using rotation-invariant linear binary patterns (Ojala et al. 2002) at 3 scales (3x3, 5x5, 7x7 pixels). Texture is a measure of variability in grey-scale pixel values. Other methods have been used to measure texture in seafloor acoustic imagery (e.g. grey-level co-occurrence matrices – Huvenne et al. 2002), but linear binary patterns have proven powerful for fine-scale digital images of the seafloor (Seiler et al. 2012). Given the binary nature of the ensemble classifier, image-objects were assigned to a category based on voting thresholds from the decision trees (50%, 60%, 65% and 70%).

Each tree in the forest assigns the image-object to a category based on the values of its predictor variables. Voting thresholds indicate the minimum proportion of trees needed to vote for the image-object as 'epibenthic fauna' to be classified as such. Increasing the threshold renders the analysis more 'conservative'.

The accuracy of the Random Forest classifier is measured with an 'out-of-bag' (oob) error estimate. Random Forest randomly separates the training dataset into 2 subsets: model building (~2/3 of observations) and model validation (~1/3 of observations). Predictions are made on the model-validation subset, and the percentage of misclassified values (i.e. oob error estimate) is recorded. A low oob error estimate therefore indicates a strong ensemble classifier. We tested 5 models with different combinations of predictor variables: 1) means of all 3 components of CIELab (L, a, b) and texture at 3 scales; 2) means of all 3 components of CIELab; 3) color components (a, b) and texture at 3 scales; 4) texture at 3 scales; 5) color (a, b). To determine the importance of predictor variables in classification accuracy, the Gini index was used. The Gini index measures the decrease in accuracy when the given predictor variable is randomly switched in the training dataset (Breiman 2001). High values of the Gini index therefore indicate that the predictor variable is important in determining classification accuracy.

Percent cover of epibenthic fauna was visually assessed by a human observer for all images (n = 511) using a grid-based method. Each image was divided into 400 grid cells (2.5 cm x 3.75 cm), and a grid cell was counted when epibenthic fauna covered >

50% of its surface area. Differences in cover (%) were calculated by subtracting the percent cover visually assessed from the percent cover generated by the Random Forest classifier. Therefore, positive values indicate that the Random Forest classifier overestimates percent cover relative to human visual assessment, while the opposite is true for negative values.

3.3.5 Application example two: Image complexity & particle grain size

Here, we tested whether there is a relationship between substrate types (distribution of particle grain size) and image complexity using a Spearman's correlation coefficient (ρ). The distribution of particle grain size was visually assessed by a human observer for all subsampled images (n = 511) by randomly selecting 200 points on each image and assigning a grain size category to each point using a modified Wentworth scale (Wentworth 1922; Sameoto et al. 2008): bedrock, boulder (>256 mm), cobble (64-256 mm), pebble (4-64 mm), sand (0.0625-4 mm), fine-grain sediment (<0.0625 mm), organism, and 'undetermined' (e.g. when the point fell on a small crevice). Due to inherent limitations in visual analysis of particle grain size, the category 'sand' included particles ranging from very fine sand to gravel. Mean grain size on a ϕ scale was calculated using a weighted average of the midpoints of the substrate categories (boulder = -8, cobble = -7, pebble = -4, sand = 1, fine-grain sediment = 6). To test the approach at the scale of the whole image, mean grain size was not calculated for images with >10% cover bedrock and organisms to avoid biases since these are not 'particles' (n = 134). To determine the sensitivity of the method to user-defined parameters (i.e. bin size of luminosity histogram and minimum size of image-objects during region merging), we

evaluated the correlation between image complexity and mean particle grain size (ϕ scale) using 12 combinations of parameters (histogram bin size: 2, 5, 10 units of luminosity; minimum size: 1 cm^2, 4 cm^2, 5 cm^2, 10 cm^2).

Establishing a strong correlation between image complexity and mean particle grain size is the first step in calibrating a predictive relationship for these 2 variables. Where correlation is strongest, we use polynomial regression with least-squares fit to predict mean particle grain size from image complexity. Normality of residuals was tested with Shapiro-Wilk tests.

3.3.6 Application example three: Local variability in substrate fine-scale features & complexity along transects

We aimed to illustrate the utility of object-based image analysis of digital images of the seafloor in inferring and comparing local variability (at a scale of 10-100s of meters) in fine-scale features and complexity among regions (i.e. seafloor *heterogeneity*). To achieve this, we determined image complexity for all images in 2 transects in Jordan Basin (JB1: length = 740 m, n = 75; JB2: length = 848 m, n = 74) and 2 transects in Georges Basin (GB1: length = 1043 m, n = 109; GB2: length = 1022 m, n = 66). These 2 basins differ in surficial geology and epibenthic faunal cover.

The Euclidean distance between each image and the location of the transect start (aerial view, in meters) was determined using UTM coordinates of the GPS positions of the drop camera, as derived from the USBL tracking system. The distance between images varied from < 1 m to > 60 m, with a mean of 11.7 m. Because standardized

intervals were needed for analyses, image complexity was linearly interpolated every 10 m along the transect. Linear interpolation was chosen because of its simplicity. Other interpolation methods such as cubic interpolation could be used. We did not test the effect of using linear interpolation on our results. To determine the presence of significant discontinuities in image complexity, we used a moving-window approach with a window size of 200 m to infer local-scale patterns (Fig. 3.4). Midpoint locations were selected every 10 m starting at 100 m from the beginning of the transect and ending 100 m from the end of the transect. Each midpoint location separated values of image complexity into 2 groups along the transect, each covering 100 m (n = 10 for each group). An intraclass correlation coefficient (ICC) was calculated between the 2 groups separated by the midpoint of the moving window, and this value of ICC was assigned to the midpoint location. High values of ICC indicate that values of image complexity are more correlated within groups than between groups, indicating a potential discontinuity. Two-sample *t*-tests were performed at each midpoint between the 2 groups to determine the statistical significance of this discontinuity.

All analyses were performed in the R computing environment (with packages 'randomForest' and 'ICC').

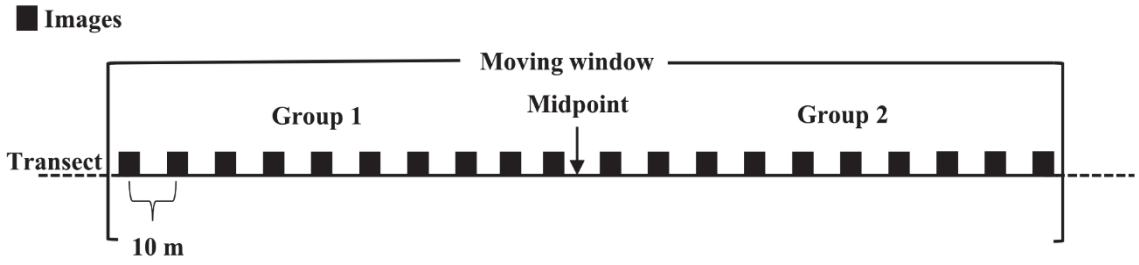

Figure 3.4: Schematic diagram of the moving-window approach used to determine variability in fine-scale benthic features. The moving window is 200 m in length and covers 20 images on the seafloor at intervals of 10 m. The midpoint separates the moving window in 2 groups of 10 images. Midpoint values range from 100 m from the start and end of the transect and moves by increments of 1 image.

3.4 Assessment

3.4.1 Application one: Assigning an identity to image-objects using a Random Forest classifier

Five different combinations of predictor variables were used to build the Random Forest classifier. Using all predictor variables [model 1: means of CIELab components (L, a, b) and texture at 3 scales] maximized the predicting power of the classifier by minimizing the out-of-bag error estimate (5.0%; number of trees: 100). The remaining 4 models yielded higher out-of-bag error estimates (means of all components (L, a, b): 11.9%; color (a, b) + texture: 5.6%, texture: 7.1%, color (a, b): 29%; number of trees: 100). Increasing the number of trees to 500 did not decrease the error estimates. When using all 6 predictor variables, texture at scales of 3x3 pixels (‘LBP1’) and 5x5 pixels (‘LBP2’), and luminosity (L component of CIELab) were the most important predictors in distinguishing image-objects of epibenthic fauna and non-epibenthic fauna (Fig. 3.5).

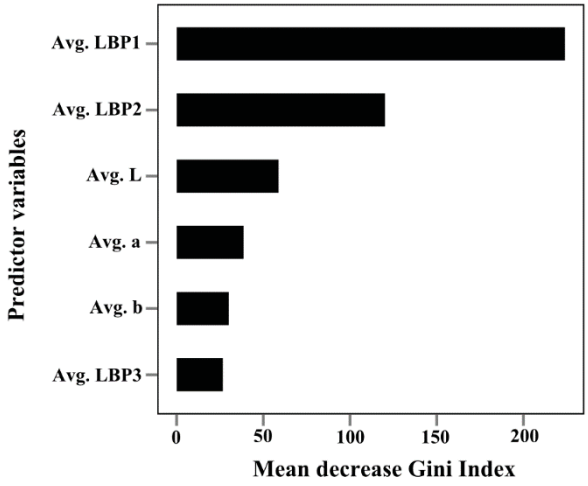

Figure 3.5: Mean decrease of Gini Index for each predictor variable when using the full model (i.e. including all predictor variables: average luminosity (L), average color components (a, b), and texture measured with average linear binary patterns at 3 scales for each pixel (3x3 pixels = 'LBP1', 5x5 pixels = 'LPB2', 7x7 pixels = 'LPB3') in the Random Forest ensemble classifier. Higher values indicate higher importance of the predictor variable in classification accuracy.

The best model (i.e. using all 6 predictor variables) was used to predict the identity of image-objects in all images (n = 511) with varying voting thresholds (50%, 60%, 65%, 70%). Overall, the percent cover estimates generated by the classifier were similar, but tended to be higher on average than those generated by human visual assessment (Fig. 3.6, Table 3.2). Increasing the voting threshold reduced this difference (50% voting threshold: mean difference = 6.3 %; 70% voting threshold: mean difference = 2.8%). Outliers were present with all voting thresholds, but positive outliers decreased in magnitude with increasing voting threshold (Fig. 3.6). Negative outliers did not decrease with increasing threshold, suggesting that underestimates of epibenthic fauna from the classifier relative to human visual assessment are not affected by voting thresholds. This is expected given that those underestimates were most often the result of

sediment covering fauna (see Discussion). Overall, the classifier tends to agree with the estimate provided by visual assessment. For the 70% voting threshold, 77% (n = 395 images) and 88% (n = 451 images) of percent cover estimates from the classifier fell within 5% and 10% of the estimate from visual assessment, respectively (Table 2). An example of the classification of image-objects with the Random Forest classifier (using all 6 predictor variables) is presented in Fig. 3.7.

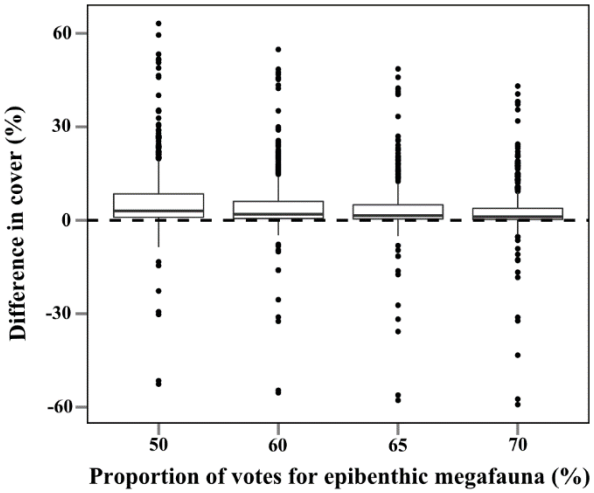

Figure 3.6: Difference in cover (%) between human visual assessment and the Random Forest classifier on the image-objects (using all 6 predictor variables). Positive values indicate the Random Forest classifier overestimates cover. Difference in cover is shown with 4 vote thresholds of the classifier: 50%, 60%, 65% and 70% of votes from trees (number of trees: 100) for the selected image-object to be categorized as 'epibenthic fauna'. All digital images were processed (n = 511) for each vote threshold.

Table 3.2: Differences between percent cover of epibenthic fauna determined using a Random Forest classifier (using all 6 predictor variables) on image-objects and a human visual assessment at 4 voting thresholds. Positive values indicate that the classifier overestimates percent cover. Shown are mean differences and standard deviations at each threshold (n = 511 images), and proportions of estimates generated by the classifier that fell within 5% and 10% of the percent cover estimated using human visual assessment.

Voting threshold (%)	Mean difference (%)	SD difference (%)	Proportion within 5% (%)	Proportion within 10% (%)
50	6.3	10.7	61	76
60	4.6	9.6	68	82
65	3.6	8.7	72	86
70	2.8	8.1	77	88

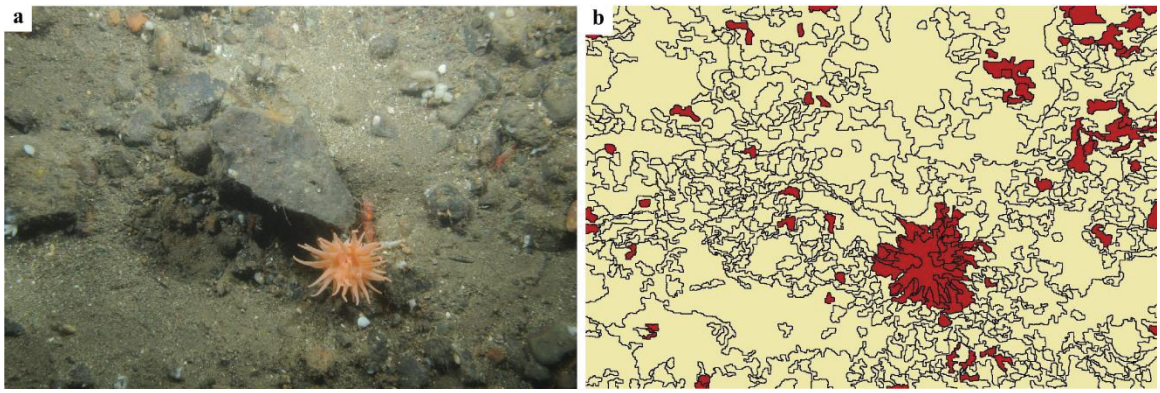

Figure 3.7: Classification of image-objects representing epibenthic fauna and not representing epibenthic fauna using a Random Forest ensemble classifier (using all 6 predictor variables). (a) Original RGB image covering 0.375 m^2 on the seafloor (0.75 m x 0.50 m). (b) Image segmentation (589 image-objects) and classification of epibenthic fauna (red image-objects) with a 'tree vote' threshold of 50% (majority vote) for epibenthic fauna.

3.4.2 Application two: Image complexity & particle grain size

Mean grain size assessed visually (ϕ scale; n = 377) was negatively correlated with image complexity computed with object-based image analysis (Table 3.3). A dominance of sand and fine-grain sediment (high on the ϕ scale) was associated with low image complexity, while the opposite was true for cobble, pebbles and boulders (low on the ϕ scale). Correlation coefficients ranged from -0.11 (Table 3.3; histogram bin size: 2 units of luminosity; minimum size of image-objects: 10 cm^2) to -0.89 (Table 3.3; histogram bin size: 5 units of luminosity; minimum size of image-objects: 1 cm^2). Correlation is slightly weaker with higher histogram bin size and minimum size of image-objects; the weakest correlation coefficients are obtained with a minimum size of image-objects of 10 cm^2 (Table 3.3). Overall, the algorithm is not sensitive to histogram bin size and the strongest correlation with mean particle grain size is found at small minimum sizes of image-objects (1 and 4 cm^2).

Table 3.3: Spearman's correlation coefficients (ρ) between image complexity computed with object-based image analysis and mean grain size (ϕ scale) measured with a grid-based human visual assessment. Correlation coefficients are indicated for 2 user-defined parameters applied during region merging: histogram bin size (3 values) and minimum size of image-objects (4 values). All correlation coefficients are statistically significant (n = 377 for each combination, $p \leq 0.05$).

		Bin size (units of L)		
		2	**5**	**10**
Min size of image-objects (cm^2)	**1**	-0.87	-0.89	-0.88
	4	-0.82	-0.86	-0.87
	5	-0.77	-0.84	-0.83
	10	-0.11	-0.64	-0.60

Given the strong correlation between image complexity and mean particle grain size, a predictive relationship between these 2 variables can be calibrated using polynomial regression with least-squares fit. Polynomial regression models of order 1 (simple linear regression) and order (quadratic function) were fitted to combinations of parameters with the strongest correlation (Table 3.4; all 3 bin sizes, minimum size of image-objects of 1 and 4 cm^2). Model residuals were normal only at a minimum size of image-objects of 1 cm^2 with quadratic functions (Table 3.4). The best predictive relationship was established as a quadratic function of image complexity with a minimum size of image-objects of 1 cm^2 and a bin size of 5 units of luminosity (Table 3.4; adjusted $R^2 = 0.81$).

Table 3.4: Relationships between image complexity (IC) and mean particle grain size (MGS; ϕ scale) using a minimum size of image-objects of 1 and 4 cm^2 and 3 bin sizes (2, 5 and 10 units of luminosity). Relationships were established with polynomial regression of order 1 (simple linear regression) and order 2 (quadratic function). Coefficients of determination (R^2; simple linear regression) and adjusted coefficients of determination (Adj. R^2; quadratic function) are provided. '*' denotes normality of residuals according to Shapiro-Wilk tests.

Min size of image-objects (1 cm^2)	Bin size (units of L)	Simple linear regression	R^2	Quadratic function	Adj. R^2
1	2	MGS = -29.2*IC + 7.9	0.77	MGS = -33.7*IC^2 – 12.1*IC + 6.0	0.77*
	5	MGS = -30.0*IC + 4.5	0.78	MGS = 75.7*IC^2 – 55.6*IC + 7.9	0.81*
	10	MGS = -54.3*IC + 3.9	0.72	MGS = 302.9*IC^2 – 107.7*IC + 7.9	0.78*
4	2	MGS = -33.6*IC + 10.5	0.66	MGS = -100.7*IC^2 + 32.3*IC + 2.8	0.70
	5	MGS = -27.8*IC + 4.6	0.75	MGS = 51.7*IC^2 – 42.1*IC + 5.9	0.77
	10	MGS = -42.3*IC + 3.6	0.69	MGS = 220.6*IC^2 – 91.1*IC + 5.2	0.76

3.4.3 Application three: Local variability in substrate fine-scale features & complexity along transects

Overall, image complexity was higher in Jordan Basin than in Georges Basin (Fig. 3.8). The highest mean complexity along transects was found in Jordan Basin-1 (Fig. 3.8a), while both transects in Georges Basin had similar complexities (Fig. 3.8b, d). In terms of local variability in fine-scale features (i.e. seafloor heterogeneity), Jordan Basin-2 was the most variable transect, with the highest proportion of significant discontinuities (Fig. 3.9c) and the highest mean intraclass correlation coefficient for all 4 transects (Fig. 3.9c). Both transects from Georges Basin exhibited similar patterns of local variability (Fig. 3.9b, d), which was overall lower than in Jordan Basin.

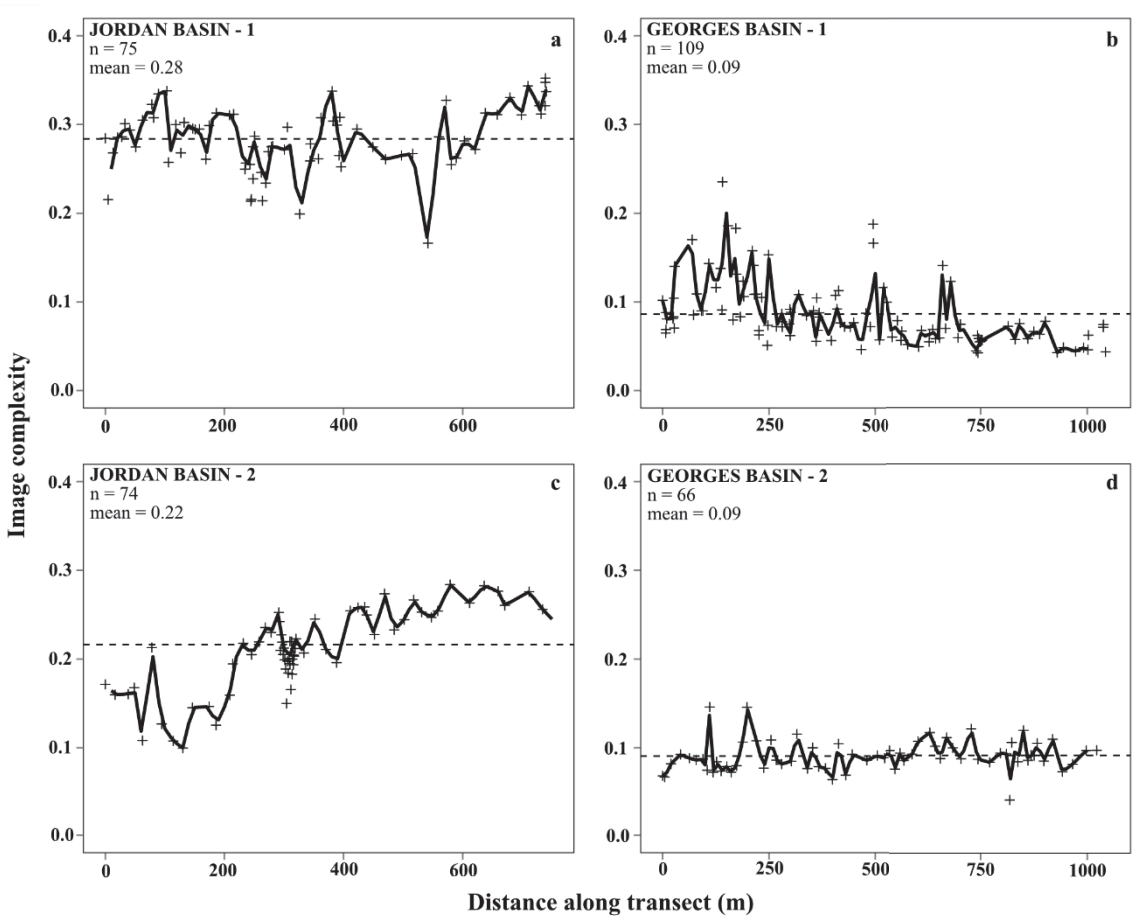

Figure 3.8: Image complexity along benthic transects in Jordan Basin (a,c) and Georges Basin (b,d) [length 750-1,000 m, 2 per basin; Gulf of Maine, NW Atlantic]. Raw data of image complexity are indicated with '+'. Full line **(-)** indicates linear interpolation of image complexity every 10 m on the seafloor (aerial view). Dashed line (--) is the mean image complexity calculated along the transect with the raw data. Also shown is the number of digital photographs used for each transect (n).

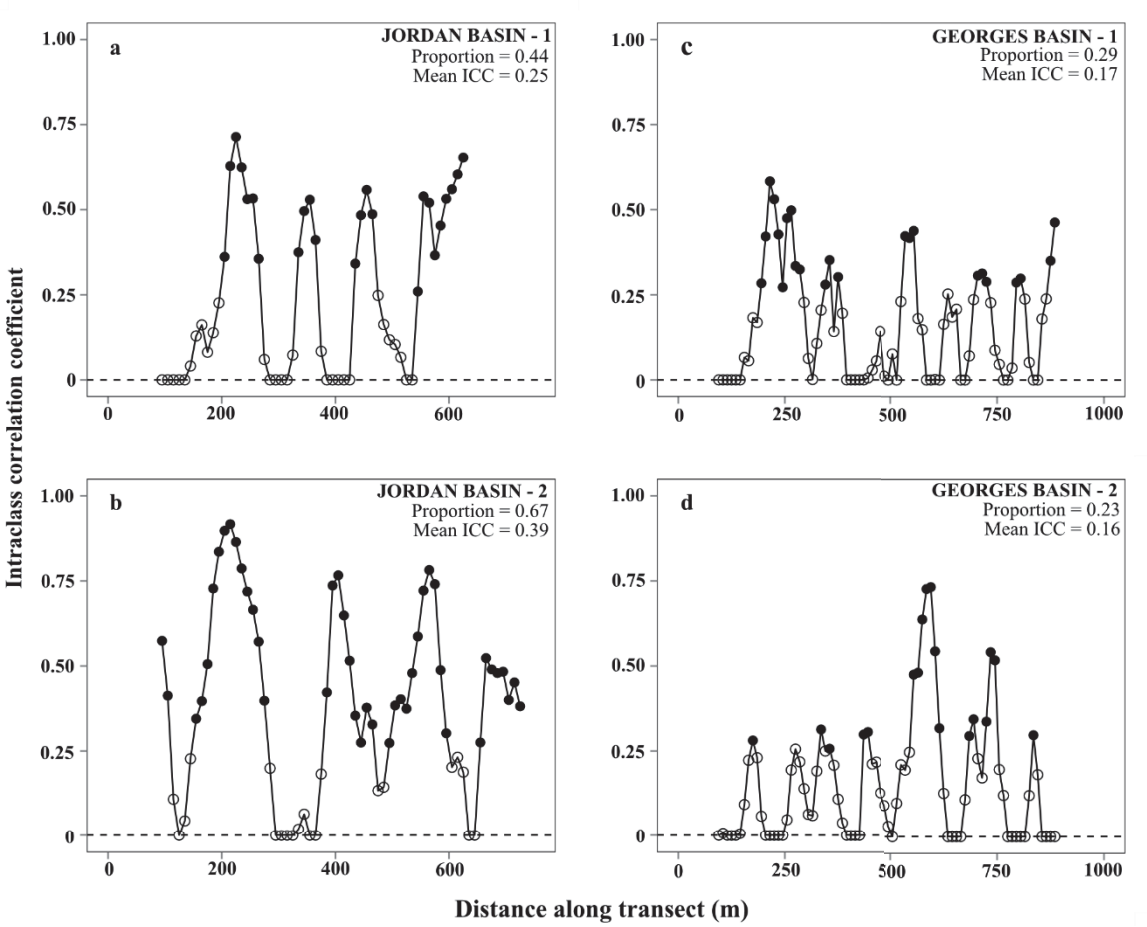

Figure 3.9: Intraclass correlation coefficient (ICC; window size: 200 m) calculated along 4 benthic transects in Jordan Basin (a,b) and Georges Basin (b,d) [2 per region; 750 m – 1,000 m in length]. Differences in groups separated by the midpoint of the moving window are tested with 2-sample *t*-tests ($p < 0.05$). Black symbols represent locations where significant discontinuities are detected, while symbols represent non-significant discontinuities. Also shown is the mean intraclass correlation coefficient along each transect.

3.5 Discussion

We presented here an approach that uses object-based image analysis of digital images of the seafloor to derive proxies for habitat complexity and heterogeneity, and determine features at fine spatial scales (<1 m), and their variability at larger spatial scales (10-100s m and 1-10s km). Because high-resolution digital images represent

individual features with many pixels, region-based segmentation, rather than pixel-based approaches, proved powerful for pattern recognition. This power was illustrated by the detection of percent cover of epibenthic fauna and the strong correlation between image complexity and sediment characteristics. Additionally, variability in seafloor characteristics was reflected in our proxy of 'image complexity', which was derived from the number of image-objects defined by the approach. This proxy can be used as an additional factor distinguishing variability within habitats and variability between habitats within a seascape. Using image complexity as a proxy is particularly useful in regions where sediments are unsorted (sediment distribution is 'skewed'), or where sporadic features could be ecologically meaningful, but currently hard to quantify. For example, the frequency of boulders in a homogeneous sedimentary environment can be detected and quantified using image complexity (high complexity relative to surrounding environment).

Our approach uses computer code (MATLAB) with intuitive parameters (e.g. minimum size of image-objects) and traceable steps that can be repeated and modified according to users' needs. Further developments in the approach could make use of open-source computer languages (e.g. Octave, R, Python) to minimize the financial costs of processing optical imagery, hence broadening the community of potential users. Therefore, the approach addresses a clear need of the scientific community for reproducible computational analyses (Barnes 2010; Peng 2011; Morin et al. 2012) and open science (Woelfle et al. 2011). In image-based benthic habitat studies, these analyses are needed to allow easier comparisons among habitats and geographic regions, while

removing the subjectivity of human visual interpretation. Using computer vision allows users to record all steps taken in either altering the image or processing it to obtain scientific information. Further, when using such an approach, the raw characteristics of the optical imagery (color, texture, surface area covered on the seafloor and pixel dimensions, for example) are more easily stored for future, yet undetermined analyses. This is particularly important in deep-water benthic habitats on continental shelves and beyond, where data are logistically difficult to obtain and hence scarce (Webb et al. 2010; Wright and Goodchild 1997). Our approach also reduces the time needed to process optical imagery, allowing users to focus efforts on data analysis and data storage. It takes 3-7 minutes to process an image on a local desktop computer (3GHz quad-core processor; 8GB RAM), when using 20 bins of luminosity and a minimum size of the image-objects of 1 cm^2, compared to an average of 10-15 minutes in our study for experienced human visual assessment. Further, using computer vision to process images is efficient, since computers do not have the time constraints associated with human resources, and the processing capacity can be largely quickened with parallel computing on computer clusters.

Determining the accuracy of the resulting segmentation and the 'true' identity of the image-objects are important issues to consider when using object-based image analysis with optical imagery at fine spatial scales (< 1 m in our study). Here, we used human visual assessment to determine the accuracy of the computer-generated segmentation by assigning a binary identity to image-objects and by comparing image complexity with measured mean grain size. Since fine-scale digital images of the seafloor

are highly complex, determining the 'true' boundaries of image-objects is not straightforward (see 'Comments & Recommendations'). However, unlike human visual assessment with associated untraceable margins of error, the benefit of our approach lies in the opportunity to record and compare the segmentation generated by several combinations of parameters (e.g. minimum size of image-objects), and hence determine its relative accuracy.

A challenging step of object-based image analysis is the assignment of an identity to the fragmented segments in an image. In our study, we used a Random Forest classifier with 6 predictor variables of the original image (mean components of the CIELab color space and texture measured with luminosity at 3 scales) to distinguish between image-objects representing epibenthic fauna. The computer-generated estimates of percent cover of epibenthic fauna generally agreed with human visual interpretation. Mean differences between estimates ranged from 2.8% to 6.3%. While the overall performance was acceptable, there were clear outliers. The difference between estimates was greater than ±25% in 12 images (2% of our dataset) in Jordan Basin and Browns Channel where the percent cover of epibenthic fauna was highest among all 5 physiographic regions. Such discrepancies were mainly due to the presence of shell debris on the seafloor (5 out of 7 images, mostly in Browns Channel) leading to overestimates from the classifier, while the accumulation of fine-grain sediment on epibenthic fauna led to underestimates (all 5 images).

The accuracy of the classification of image-objects ultimately depends both on how restrictive the training dataset is and on the machine-learning algorithm used. When looking for specific objects, feature detection, rather than pattern recognition, is more appropriate. For example, feature detection has been used to detect benthic crustaceans and bacterial mats (Aguzzi et al. 2011). Given our initial objective of exploration-based pattern recognition of seafloor fine-scale features, we did not use these approaches. This might be an important caveat in habitats with dense epibenthic fauna, such as in Browns Channel and in Jordan Basin, where the diversity of epibenthic fauna shapes and colors may be beyond the training dataset. Alternatively, machine-learning algorithms other than Random Forest could be used to classify image-objects, such as support vector machine, artificial neural networks or a Bayesian approach.

In our study, image complexity correlated strongly with sediment characteristics, measured as mean grain size, and our approach was also overall not sensitive to user-defined parameters (histogram bin size and minimum size of image-objects). Further, we were able to establish significant predictive relationships between image complexity and mean particle grain size. We recommend however that this calibration be repeated when using the method in other areas. This is meant to increase the accuracy of the estimates of mean particle grain size in the area of interest, and also allow the comparison of this relationship between habitats and regions. Linear modeling of autocorrelation curves calculated from 2D correlation coefficients in digital images has also been used to estimate the distribution of sediment grain size on the seafloor (Rubin 2004; Barnard et al. 2007; Buscombe 2008). This method requires a training dataset of images of

homogeneous sediment sizes and is generally used in controlled environmental conditions, such as on beaches or in the laboratory. The potential use of this method for in situ deep-water studies on glaciated continental shelves has not been investigated, but could be limited, given the prevalence of mixtures of sediment grain size at fine spatial scales (<1 m). The decreasing density of epibenthic fauna with increasing depth (Rex et al. 2006) alters measures of complexity; thus, using imaging techniques to estimate the distribution of sediment grain size over large geographic areas is a promising area of research.

Local variability of the composition of the substratum (10-100s m), as a measure of habitat heterogeneity, is an important indicator of the distribution of benthic biological assemblages on continental shelves and margins (Buhl-Mortensen et al. 2012; Robert et al. 2014). Substratum composition is most often determined based on percent cover of a particular grain (e.g. percent gravel or sand), but it does not explicitly incorporate the fine-scale spatial arrangement and composition of the whole sediment distribution. Our image-based approach produces a continuous scale of seafloor complexity, which can distinguish gradients in substratum composition. For example, despite having a lower mean complexity, Jordan Basin-2 was more variable at a scale of 10-100s m than Jordan Basin-1, and we were able to quantify this difference. The flexibility of the continuous scale allows the incorporation of seafloor complexity into both discrete and continuous (or multivariate) habitat models. Discrete habitat models use a habitat classification scheme (e.g. Huang et al. 2011; Kaskela et al. 2012) to partition the seascape into distinct habitat types (see Brown et al. 2011 for review). For example, in our study, Jordan Basin

had an overall greater seafloor complexity (and variability in seafloor complexity) than Georges Basin. This information can be used to make comparisons between physiographic regions and guide habitat classification. Alternatively, multivariate statistical models (e.g. multiple regression, regression trees, factor analysis) aim to determine the relationship between a suite of environmental variables and the distribution of biological assemblages (e.g. Pitcher et al. 2012; Robert et al. 2014) or specific species (e.g. Tong et al. 2012). In such cases, seafloor complexity can be incorporated as a covariate.

3.6 Comments & Recommendations

The use of computer vision for pattern recognition in image-based benthic studies can be limited by inconsistencies in luminosity, given the central role of luminosity in distinguishing image-objects by establishing their characteristics with measures of texture. In our study, all digital images were taken at a similar angle of the seafloor, and luminosity was therefore constant. However, when using remotely-operated vehicles or automated underwater vehicles, where luminosity can vary more significantly, the effect of this variation on measurements of seafloor complexity should be accounted for. The color space CIELab is useful for that purpose as it segregates the luminosity signal ('L'), allowing its direct manipulation. Histogram equalization of luminosity is a possible avenue of research to calibrate luminosity within and between images along transects.

Because of the complexity of fine-scale digital images of the seafloor, the detection of features of interest will fall within a certain margin of error when compared

to human visual interpretation. Accuracy of interpretation is also hindered by the lack of consensus of what a true 'image-object' should represent on the seafloor. Distinguishing fauna or flora is feasible as clear boundaries can usually be established, but characterizing the particle grain size of the seafloor remains difficult. In our study, we have only attempted to distinguish fauna from the underlying substratum. Our approach proposes that mean particle grain size could be estimated with the remainder of image complexity once the overlying biological signal has been removed. A finer spatial partition of the particle grain size distribution of the substratum, for example distinguishing areas of mixed sediments from areas of sand, would require further studies. High-resolution images of the seafloor could potentially resolve individual grains of sand. Therefore, the end-product of the identity of the segmentation is largely determined by the area on the seafloor targeted by the user and by the extent of the training the algorithm has been subjected to.

Lastly, using computer code to process optical imagery of the seafloor is an efficient way to facilitate data manipulation and eventual long-term storage. Imagery is a challenging sampling tool in marine systems, and adequate methods to process and store these data are still emerging. Our approach is flexible enough to be reproducible and adaptable, ensuring the possibility of continuous improvements as new developments in benthic image processing are made.

CHAPTER 4

FINE-SCALE SUBSTRATE FEATURES INFLUENCE EPIBENTHIC MEGAFAUNAL DIVERSITY ON THE DEEP EASTERN CANADIAN MARGIN[3]

4.1 Abstract

The influence of sediment heterogeneity on deep-water benthic megafauna may depend on the range of particle grain size, since the availability of substrate, in particular hard substrate, is an important habitat requirement. On glaciated continental margins, sediment heterogeneity varies at fine to local spatial scales (< 1 m - 100 m), but remains difficult to quantify. In this study, we performed benthic video transects with the remotely-operated vehicle ROPOS at 5 locations along a depth gradient (~1100 to 3000 m; total transecting length: 9908 m) in the Northeast Fan on the continental margin off the Gulf of Maine (northwest Atlantic). Substrate complexity was quantified using object-based image analysis, a novel approach that uses image complexity to infer fine-scale substrate features. The density of epibenthic megafauna was recorded, and diversity was calculated with rarefaction and indices (Shannon-Wiener Index, Pielou's evenness, morphospecies richness). Megafaunal abundance decreased markedly between the shallowest (~1100 m) location and the remaining locations, mostly due to a diverse and abundant community of deep-water corals (alcyonaceans). Both diversity and substrate complexity were highest at the shallowest and deepest (~3000 m) locations, and lowest at

[3] Lacharité, M., and A. Metaxas. Submitted to Deep-Sea Research Part I: Oceanographic Research Papers in March 2016.
My coauthor Dr. Anna Metaxas supervised the development of the study and analyses, and edited the manuscript.

intermediate depths (~2000 m). We concluded that sediment heterogeneity influences diversity, but not abundance of megafauna in the area. In particular, the sporadic presence of boulders provided heterogeneity at a local scale in an otherwise homogeneous substrate of fine-grain sediment. Given their potential ecological importance in the deep sea, seafloor fine-scale features should be included into habitat studies, but quantifying their distribution at larger spatial scales remains challenging.

4.2 Introduction

Habitat heterogeneity on deep continental margins, which extend from the shelf break to the base of the continental slope and rise (i.e. depths of ~200 to ~3-4000 m), is an important driver of patterns in benthic invertebrate communities at multiple spatial scales (reviewed in Levin and Dayton 2009; Levin and Sibuet 2012). Vertical gradients in light, pressure, temperature, oxygen, and food availability lead to depth zonation in fauna, with the most-reported faunal change occurring at ~1000 m depth (Carney 2005). Within these large-scale gradients, the role of finer-scale environmental factors, such as sediment characteristics, in determining biological patterns is less clear. Studies on the relationship between sediment heterogeneity (particle size spectra) and deep-sea benthos have mostly focused on macrofaunal and meiofaunal communities in soft-sediment habitats. A positive relationship between sediment heterogeneity and diversity has been suggested in these faunal groups (Gray 1974, Levin et al. 2001), and evidence supporting this hypothesis has been reported in the North Atlantic (Etter and Grassle 1992), in submarine canyons off the Hawaiian Archipelago (De Leo et al. 2014), and off the coast of New Zealand (Leduc et al. 2012). However, the strength of the pattern (Netto et al. 2005)

and/or the potential correlation between the distribution of sediment and other environmental factors, such as organic matter content (Snelgrove and Butman 1994) remain unresolved.

The effect of sediment heterogeneity on deep-water benthic megafauna (> 2-3 cm) may depend on the range of particle grain sizes. In the deep waters of the Fram Strait (~1300 to 5400 depth), sediment heterogeneity was not found to influence benthic megafaunal communities (Soltwedel et al. 2009). However, the sediment sampled in that study had a narrow range of median particle grain size (φ: 6.3 – 8, 'silt'). In contrast, differences in megafaunal communities were observed with a wider particle size spectrum on the Porcupine Abyssal Plain (silt, mud and sand; Durden et al. 2015), in the Faroe-Shetland Channel (silt to pebbles; Jones et al. 2007) and on a deep-water rocky reef (1796-2373 m) in the Fram Strait (sand to boulders; Meyer et al. 2014). At shallower depths (< 1000 m), differences in megafaunal communities were also observed among areas with different substrate types ('hard' vs. 'soft') in the Canadian Arctic (Roy et al. 2014), on the continental shelf west of the island of Svalbard (Bergmann et al. 2011), and in submarine canyons off southeastern Australia (Schlacher et al. 2007). Further, the sporadic presence of coarse sediment and/or hard substrate at various scales has been reported as influencing megafaunal communities, in particular on deep-water rocky reefs (Meyer et al. 2014), exposed bedrock on vertical walls and overhanging cliffs in submarine canyons (Huvenne et al. 2011; Johnson et al. 2013; Roberts et al. 2015), and at a finer spatial scale, stones, boulders and anthropogenic debris (Schulz et al. 2010).

Glaciation has impacted the surficial geology of the habitats of marine benthic ecosystems. 'Glacial till' ('glacial-marine sediment') consists of poorly-sorted, unconsolidated sediment deposited by glaciers during the last ice age, and is composed of coarse-grained sediment - such as gravel and boulders – interspersed in a matrix of finer-grain sediment. This surficial geology is typically present in high-latitude continental margins, particularly in the Arctic, sub-Arctic, and Antarctic, but can also be found at lower latitudes due to the extent of the ice margin. At the glacial terminus, meltwater flow deposited sediment loads ('outwash') that formed submarine 'fans'. These fans are thus often found at the mouth of important subglacial tunnels. Glacial till causes variability in particle grain size on the seafloor at fine to local scales (< 1 m to 10-100s m), likely resulting in increased habitat heterogeneity for benthic organisms. However, some difficulty remains in characterizing these habitat features adequately to determine their influence on benthic fauna.

Characteristics of substrate types include both the distribution and spatial arrangement of sediment particles of different grain sizes (including exposed bedrock) that ultimately form the structural components available to benthic organisms. Substrate *complexity* quantifies this arrangement (e.g. abundance), while *heterogeneity* reflects variation in complexity (McCoy and Bell 1991; Sebens 1991). In this study, we focus on substrate complexity and heterogeneity in space. Methods to quantify sediment properties of the substrate in the deep ocean typically rely on coring, which is adequate in soft-bottom habitats, but not in habitats where coarse sediment (and exposed bedrock) is present. Imaging techniques are more adequate for detecting a wider range of sediment

and sporadic features on the seafloor. Grid-based approaches, using a simplified scale of particle grain size, have been used to determine mean/median particle grain size (Jones et al. 2007; Sameoto et al. 2008; Meyer et al. 2014; Meyer et al. 2015). Here, we use an automated approach based on object-based image analysis to determine the complexity of the substrate along a continuous scale, which has the advantages of detecting gradients and boundaries in substrate characteristics, as well as sporadic features (Lacharité et al. 2015).

In this study, we: 1) characterized substrate complexity and heterogeneity using optical imagery along a depth gradient (~1,000 m -3,000 m) in the 'Northeast Fan', an area adjacent to the Gulf of Maine downslope of submarine canyons on the eastern Canadian margin; and 2) assessed the relationship between substrate features at fine to local scales (1-10s of m) with the abundance and diversity of epibenthic megafaunal communities.

4.3 Materials and Methods

4.3.1 Study area

The Gulf of Maine (northwest Atlantic) is a relic of the last glaciation event in northeastern North America (Schnitker et al. 2001; Shaw et al. 2006). Deep basins in the Gulf proper are bordered at the edge of the continental shelf by the shallow Georges and Browns Banks, separated by the deep Northeast Channel (Fig. 4.1a). At the shelf edge of the channel, submarine canyons cut across the continental slope to a depth of ~900-1000 m, where the seafloor levels off on the continental rise (Fig. 4.1b, the 'Northeast Fan'). The surficial geology in the submarine canyons is typical of glaciated continental

margins: a mixture of ice-contact sediment (pebbles, cobbles, boulders) amidst a matrix of sand and/or mud (Edinger et al. 2011). In the Northeast Fan, at the floor of the Middle Canyon, the presence of large boulders has been reported (Lacharité and Metaxas 2013), but a comprehensive description of the surficial geology of the area is still lacking.

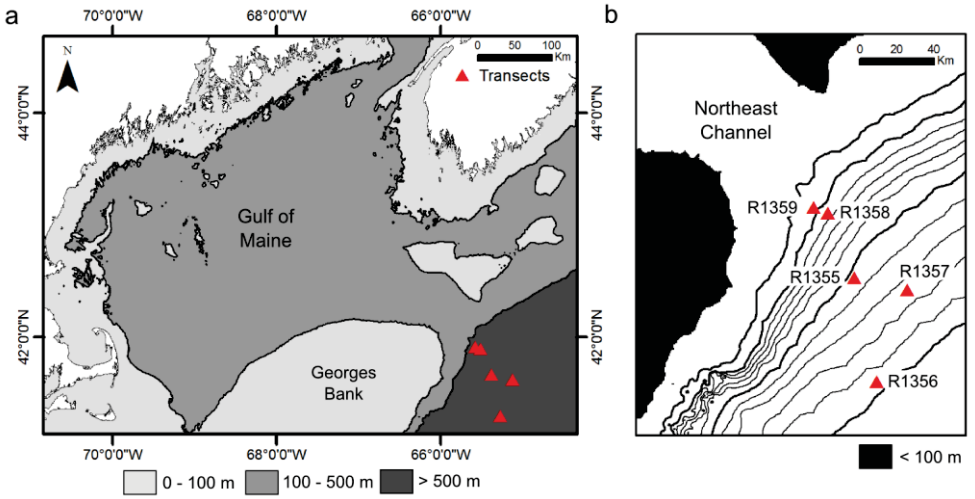

Figure 4.1: Locations of the benthic video surveys. Depth is indicated below the panels. (a) Gulf of Maine (northwest Atlantic). (b) Northeast Fan (continental slope off Northeast Channel). Bold contour lines represent depths of 500 m, 1000 m, 2000 m and 3000 m. Between 1000 m and 3000 m, 200-m isobaths are shown.

4.3.2 Video transects in the Northeast Fan

Video transects were performed with the ROV ROPOS in 5 locations in the Northeast Fan of the Gulf of Maine (continental slope and rise) across a depth gradient (964 m – 2956 m) in August 2010 aboard the *CCGS Hudson* (Fig. 4.1, Table 4.1). ROPOS was equipped with 2 high-definition cameras: one facing downward perpendicular to the seafloor (Insite Pacific Mini Zeus 1080i HD), and one facing forward of the vehicle at an oblique angle (Insite Pacific Zeus-Plus 1080i HD). Each

camera was equipped with lasers 16.5-cm and 10-cm apart, for the downward-looking and forward-looking cameras, respectively. Sections of transects considered too far or near the bottom (based on field of view in downward-looking camera, see below '2.3 Video data processing') were not included for analysis. Transect length available for analysis varied between locations from 942 m (R1355; mean depth: 2092 m) to 2089 m (R1357; mean depth: 2515 m), with an overall combined length of 8439 m used for analysis. Transects were performed at an average height of 0.9-1.6 m above the seafloor. Most transects were performed along isobaths, except the shallowest dive at a mean depth of 1095 m (dive R1359), which was performed upslope. For all transects, a constant heading was maintained, but paths in transects often deviated from a straight line due to local currents. Therefore, position is reported as 'Distance along transect', which was treated as a path. Some transects were separated into 2 contiguous segments (dives R1358, R1356) performed with a different heading. These segments were pooled for analyses. The ROV ROPOS is equipped with a USBL responder allowing precise positioning on the seafloor, and a CTD profiler (SBE 19plusV2). Mean temperature and oxygen concentration along transects is shown in Table 4.1.

Table 4.1: Video transects performed with the ROV ROPOS in the Northeast Fan (continental margin of the Gulf of Maine, northwest Atlantic), in August 2010. The length of transects used to normalize abundance data from the forward-facing camera is indicated in 'Portion used [m]'.

Dive	Segment	Latitude	Longitude	Total length [m]	Portion used [m]	Mean height above seafloor [m; min-max]	Depth range [m]	Mean depth [m]	Mean temperature [°C]	Mean oxygen concentration [ml/L]
1359	01	41°55'01"N	65°35'10"W	2867	1967	1.6 [0.8 - 3.6]	964 – 1187	1095	4.38	5.56
1358	01	41°53'54"N	65°31'07"W	1150	965	1.4 [1.0 - 2.5]	1451 – 1521	1458	4.05	5.68
	02	41°53'23"N	65°31'05"W	991	873	1.5 [1.2 – 2.0]	1352 – 1471			
1355	02	41°39'33"N	65°23'15"W	942	942	1.3 [1.00 – 1.9]	2060 – 2119	2092	3.44	5.79
1357	01	41°35'56"N	65°07'16"W	2113	2089	1.1 [0.8-1.4]	2508 – 2526	2515	3.00	5.80
1356	01	41°17'05"N	65°16'30"W	1073	953	0.9 [0.6-1.7]	2878 – 2956	2887	2.63	5.91
	02	41°16'44"N	65°16'29"W	772	650	1.1 [0.6-1.8]	2819 – 2880			

4.3.3 Video data processing

Since the field of view differed between cameras, both cameras are processed to reflect changes in epibenthic megafaunal community composition. Only the downward-looking camera is used to assess substrate complexity.

4.3.3.1 *Downward-looking camera*

Along each transect, frame grabs (static images) were extracted from the downward-looking camera every 10 seconds to avoid overlap in the field of view. To infer local-scale patterns (10s – 100s of meters), a subset of these extracted images was used for analysis. The frequency of sampled images depended on the variability in substrate features: changes in substrate complexity, the presence of sporadic features (e.g. large boulders), and the presence of conspicuous fauna. To be consistent across depths, subsequent images were sampled at a maximum distance of 10 m apart even when no variability was observed on the seafloor. Images with poor luminosity, with an obstructed field of view (e.g., presence of fish), and/or showing blurriness were omitted. The mean distance along the transect between sampled images varied between 6 m (R1356; mean depth: 2887 m) and 14 m (R1358; mean depth: 1458 m) (Table 4.2). A total of 877 sampled images were included in the analysis. Images were cropped to 1 m^2 (1.25 m x 0.8 m), which represented on average 61% of the field of view of the original images (range: 35-100%). All epibenthic organisms larger than 2-3 cm were recorded and identified to the lowest possible taxonomic level. Identification was based on reported occurrences in the study area (OBIS; www.iobis.org) and published literature. Since specimens were not collected, some taxa could not be identified to species level, hence taxa are referred here as ‘morphospecies’.

Table 4.2: Summary of images obtained from the downward-looking camera on the ROV ROPOS used to assess the variability of substrate complexity along transects.

Dive	Segment	Total # of images	Mean distance between images [m; ± sd]	# Images w/o fauna
1359	01	170	13 [±5]	107
1358	01	77	14 [± 4]	71
	02	83	11 [± 3]	59
1355	02	92	10 [± 2]	0
1357	01	233	9 [± 2]	180
1356	01	114	9 [± 4]	70
	02	108	6 [± 3]	57

For each image, image complexity was determined using object-based image analysis (Lacharité et al. 2015). This approach decomposes a pixel-based image into regions of homogeneous color and texture referred to as 'image-objects'. Image complexity is a dimensionless proxy of substrate complexity, since the number of image-objects is strongly correlated with the distribution of sediment particle grain size on the seafloor (Lacharité et al. 2015). Higher complexity indicates coarser sediment (Fig. 4.2). The approach requires the input of 2 parameters: the minimum size of each image-object (to restrict the algorithm from decomposing the image into very small, potentially spurious, image-objects) and the number of equal bins dividing the luminosity axis in the CIELab color space. In this study, we used a minimum size of image-objects equal to 5 cm^2 (i.e. the approximate size of 'coarse gravel') and 20 bins. Image complexity is reported as a dimensionless number: the number of image-objects detected in the image divided by the theoretical maximum number of image-objects, given the minimum size of image-objects and the surface area covered by the images. In this study, the theoretical maximum is 2000 image-objects.

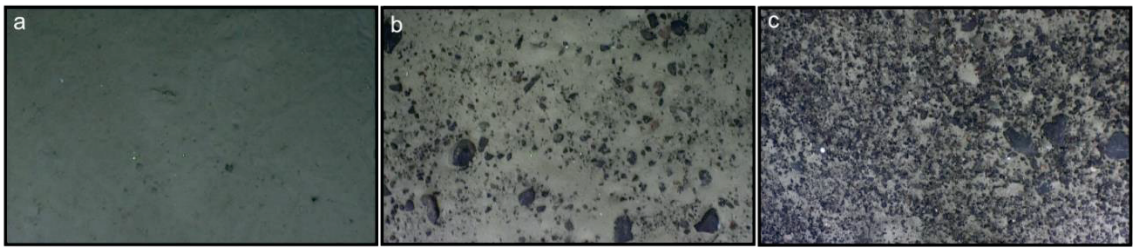

Figure 4.2: Examples of substrate types defined with dimensionless image complexity (Lacharité et al. 2015). (a) Dive R1357, depth: 2509 m, image complexity: 0.02; (b) Dive R1356, 2914m, image complexity: 0.11; (c) Dive R1356, 2821 m, image complexity: 0.39. [Surface area: 1 m^2 – 1.25 m x 0.80 m]

4.3.3.2 *Forward-looking camera*

The position of individuals and colonies of megafauna visible in the most illuminated portion of the forward-looking video and larger than ~10 cm was recorded continuously along transects. Smaller organisms and/or organisms lying flat against the seafloor (e.g. ophiuroids, small echinoids) were not recorded. The field of view in the forward-looking camera was on average ~4-5 m wide, but varying due to changes in altitude (especially in areas where boulders were more prevalent or to adjust for the slope of the seafloor), and the pitch and roll of the ROV. Only in the deepest dive R1356 was the field of view marginally smaller (3.5-4 m wide) due to low altitude. We did not detect any significant bias in and between dives that could affect our results. Because of the variability in visibility, and the coupling of a downward-looking camera that is more robust in estimating surface area on the seafloor, we did not attempt to measure surface area of the image for the forward-looking camera.

4.3.4 Analysis of biological communities

4.3.4.1 *Abundance of megafauna*

In downward-looking images, abundance of megafauna is recorded as number of individuals or colonies per m^2 (presence/absence for poriferans is recorded as 1/0). In the forward-looking video, the abundance of megafauna is standardized to number of individuals and colonies per 100 m surveyed along transects.

4.3.4.2 *Community composition*

Morphospecies were assigned into broader taxonomic groups to determine patterns in community composition. Most of the groups represented either orders in the phylum Cnidaria (Actiniaria, Alcyonacea, Antipatharia, Ceriantharia, Pennatulacea, Scleractinia) or classes in the phylum Echinodermata (Echinoidea, Crinoidea, Holothuroidea, Ophiuroidea, Asteroidea). Some morphospecies were assigned to phylum because of their low abundance and/or diversity (Mollusca, Arthropoda), or our inability to identify morphospecies to a lower taxonomic level (Porifera).

For the description of community composition, all individuals were pooled for each dive from both cameras, yielding a single community per location. To avoid multiple counts of the same individuals or colonies, for morphospecies detected in both cameras, only abundance from the forward-looking camera was used for analysis. Differences in community composition between locations were assessed by determining the relative abundance of each taxonomic group in each community. In each taxonomic group, vertical zonation was determined using relative abundance between locations when pooling all individuals or colonies recorded in the survey.

4.3.4.3 *Diversity*

Diversity in transects was assessed with morphospecies richness, Shannon-Wiener (*H*'; natural log) and Pielou's evenness (*J'*). At each location, a single sample of the community was used for each camera by pooling either all images from the downward-looking camera or all individuals from the forward-looking video. Rarefaction analysis (Gotelli and Colwell 2010) was used to compare morphospecies richness between locations. For the forward-looking video, individual-based morphospecies richness was estimated for 45 (minimum surveyed) and 90 individuals. For the downward-looking images, sample-based morphospecies richness (each image was considered a sample in this analysis) was estimated for 80 and 160 images. Variability in the accumulation of morphospecies along transects was described using accumulation curves ('collector' method) for both the forward-looking video and downward-looking images.

4.4 Results

Indicated depths refer to mean depths at each location (5) along the depth gradient (i.e., 1095 m, 1458 m, 2092 m, 2515 m, and 2887 m).

4.4.1 Substrate complexity across depths in the Northeast Fan

Median image complexity and variability in complexity differed between locations, indicating a change in substrate types across the depth gradient and within transects (Fig. 4.3). Higher complexity, increased variability in complexity along transects, and outliers (image complexity values upward of 0.25 in images with and without fauna) were found at the shallowest (1095 m) and deepest (2887 m) locations in

images with and without fauna (Fig. 4.3). This suggests a greater proportion of coarse substrate such as pebbles and cobbles in these locations. In contrast, lowest median complexity was found at 2092 m, despite the fact that all images included fauna (Fig. 4.3), suggesting a dominance of soft substrate, such as sand and mud.

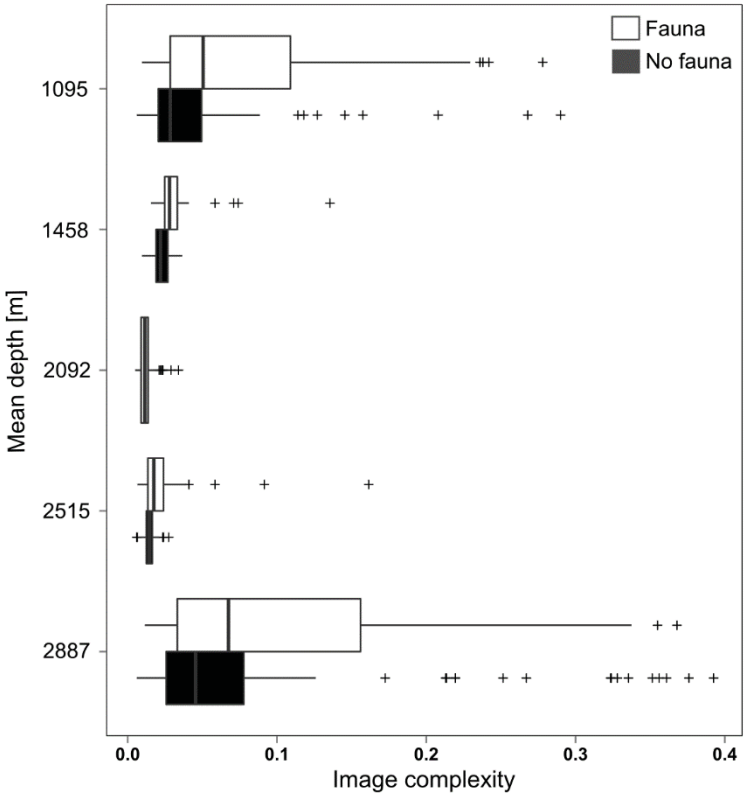

Figure 4.3: Boxplots of image complexity across the depth gradient computed with object-based image analysis in images with fauna (white) and where no fauna is detected (black). All images in each dive are pooled. Mean depth along transects at each location is shown.

Variability in substrate complexity along transects over scales of 10-100 m was detected with our image-based approach in some transects, namely at the shallowest (1095 m) and deepest (2887 m) locations. This variability indicated the presence of either boundaries or gradients. At the shallowest location, where we performed an upslope transect rather than one along an isobath, a boundary existed at the mouth of the submarine canyon and across the continental margin, indicated by a transition from lower complexity on the slope, where soft substrate is more prevalent, to higher complexity in the canyon due to the increased presence of coarser substrate (Fig. 4.4a,b). In contrast, variability in substrate complexity at greater depths (mean depth: 2887 m) was due to intermittent patches of coarse sediment (pebbles, cobbles and large boulders), and was seemingly unrelated to local variability in bathymetry (Fig. 4.4c,d).

The presence of sporadic features, such as large boulders, interspersed in a matrix of sand and mud generates variability in substrate complexity at very fine spatial scales. With our approach, these features are detected with clear outliers in image complexity along transects, as observed at 1458 m (Fig. 4.3, Fig. 4.5a,c) and 2515 m (Fig. 4.3, Fig. 4.5b,d). Most of these sporadic features harbored megafauna, such as brisingid seastars, deep-water corals and anemones (Fig. 4.5).

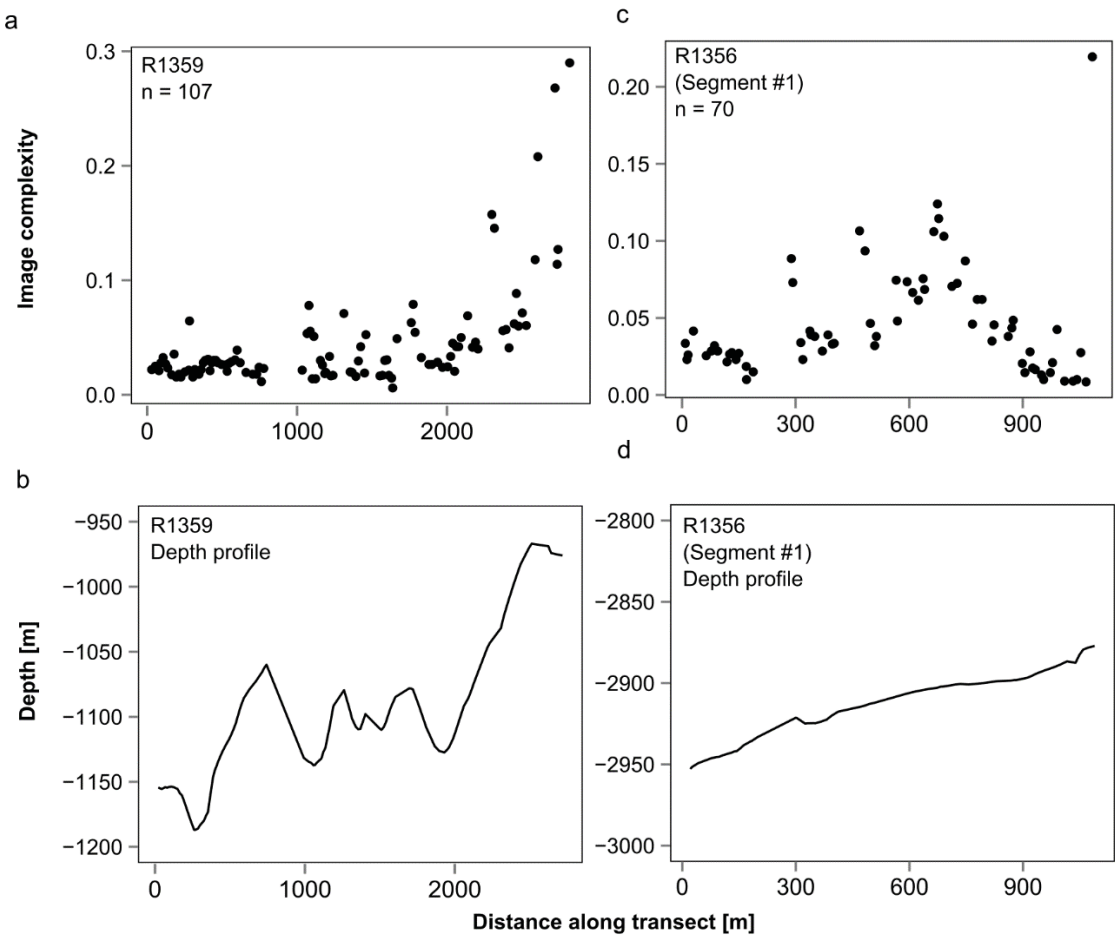

Figure 4.4: Gradients in image complexity reflecting substrate complexity. Image complexity (a) and depth profile (b) for dive R1359 (mean depth: 1095 m). Image complexity (c) and depth profile (d) for transect #1 of dive R1356 (mean depth: 2887 m). Complexity is shown for images with no fauna only. Distance along transect (m) represents real distance on the seafloor (i.e. including portions not used for analysis).

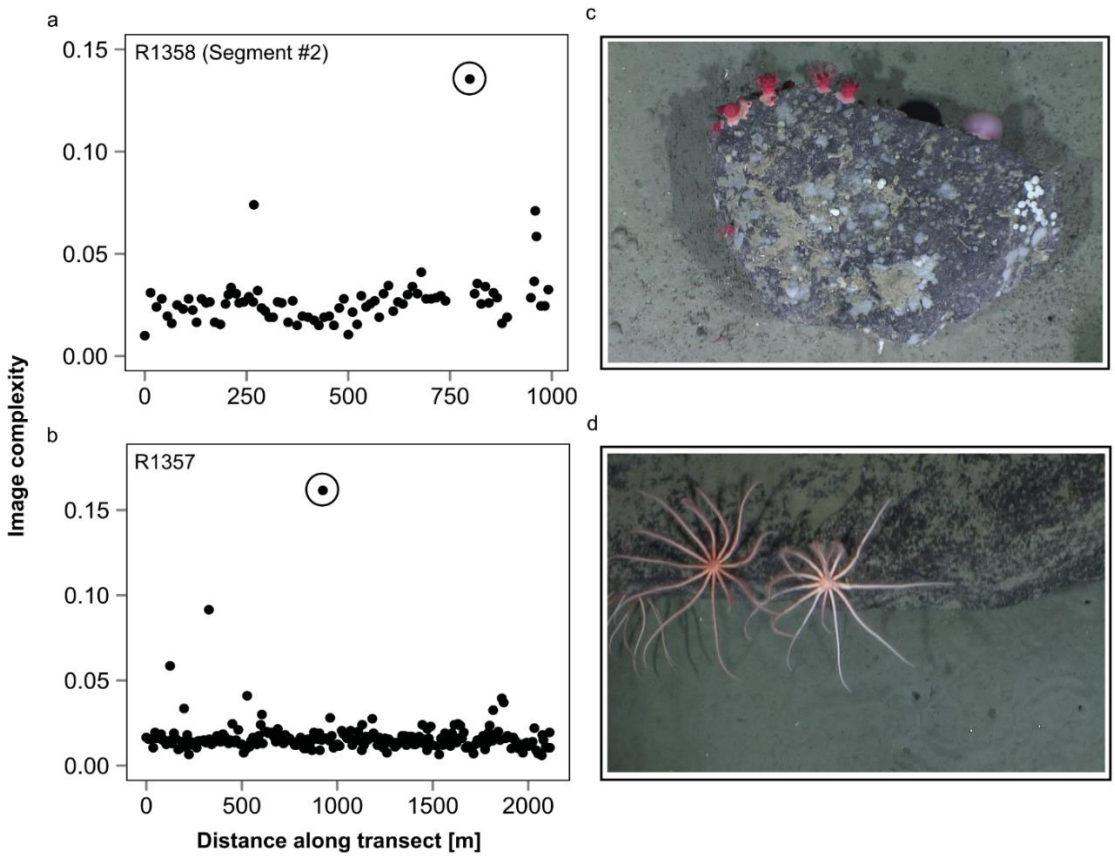

Figure 4.5: Outliers in substrate (image) complexity along transects in dives R1358 (a) and R1357 (b). Images [surface area: 1 m^2] associated with circled outliers in each dive are shown on the right-hand panels (c,d for dives R1358 and R1357 respectively). Complexity is shown for all images, regardless of the presence of fauna. Distance along transect (m) represents real distance on the seafloor (i.e. including portions not used for analysis).

4.4.2 Epibenthic megafaunal communities

4.4.2.1 *Abundance*

Total abundance of megafauna varied across the depth gradient, and between cameras (Fig. 4.6). The mid-depth location (2092 m) showed the highest abundance of organisms in the downward-looking images due to the high density of the brittle star *Ophiomusium lymani* recorded at this depth (Table 4.3), and all other dives showed similar mean density (Fig. 4.6a). Abundance was maximized in the location at 1458 m (Fig. 4.6a), as a result of the presence of a boulder covered with megafauna (Fig. 4.5c). The highest abundance in the forward-looking video was recorded at the shallowest location (1095 m; Fig. 4.6b), and was due to the high abundance of alyonacean corals, particularly *Anthomastus grandiflorus* (Table 4.3; abundance did not vary among the remaining locations (Fig. 4.6b). Within these locations, the highest abundance was recorded at 2515 m (Fig. 4.6b), and was mostly due to the brisingid sea star *Freyella elegans*, the alcyonacean *Chrysogorgia* sp., and a holothuroid morphospecies (Table 4.3). The first 2 species were observed on boulders (Fig. 4.7e), while the holothuroid (Fig. 4.7a) was mostly found on soft to mixed substrate.

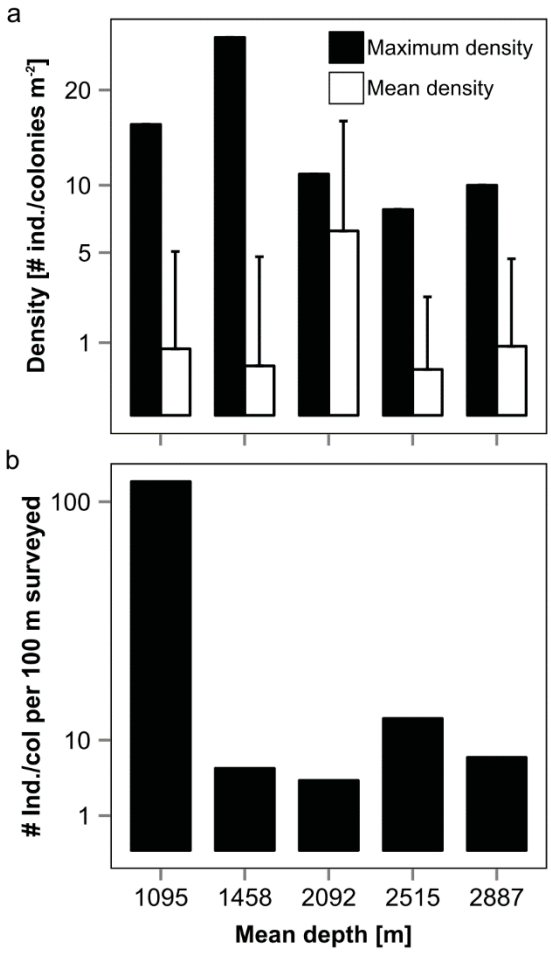

Figure 4.6: Morphospecies abundance between locations. (a) Mean (+ SD, n: see Table 2) and maximum density of epibenthic megafauna observed in downward-looking camera. (b) Total abundance of epibenthic megafauna in the forward-looking video standardized to length of each transect. Mean depth [m] of each transect is shown. Abundance is reported on a square-root scale.

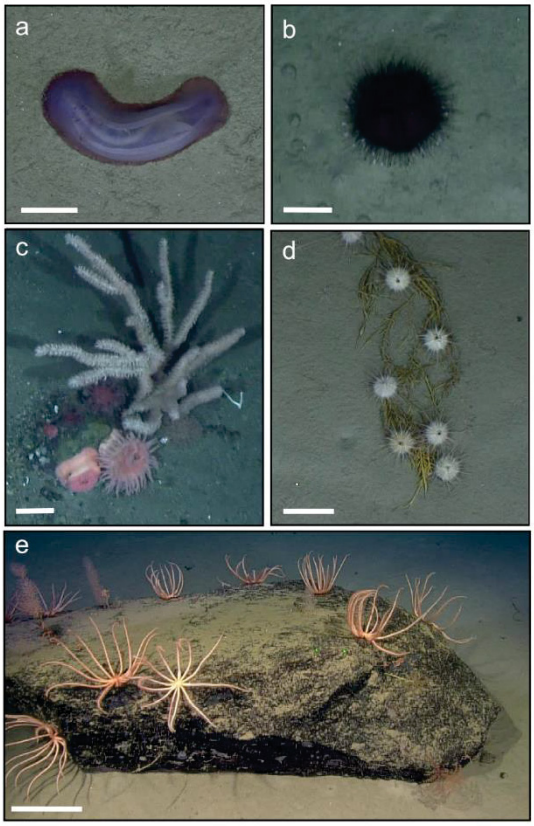

Figure 4.7: Epibenthic megafaunal morphospecies recorded in the Northeast Fan. (a) Sea cucumber 1 (purple). Scale: 5 cm. R1357, depth: 2525 m. (b) *Hygrosoma petersii***.** Scale: 10 cm. R1358, depth: 1498 m. (c) *Kerotoisis ornata*, *Anthomastus grandiflorus*, and Actiniaria sp. 2. Scale: 10 cm. R1359, depth; 1114 m. (d) *Gracilechinus affinis* on drift algae. Scale: 10 cm. R1357, depth: 2525 m. (e) Brisingid seastar (*Freyella elegans*), *Chrysogorgia* sp., and *Bathypathes* sp. on a large boulder. Scale: 25 cm. R1357, depth: 2510 m.

Table 4.3: Abundance of epibenthic megafaunal taxa across depths. For downward-looking images, abundance is recorded as mean number of individuals/colonies·m^{-2} (± SD). For the forward-looking video, abundance is recorded as the normalized number of individuals/colonies per 100 m surveyed (4 morphospecies are not included since the taxonomic group could not be identified.)

		Downward-looking images (# individuals/colonies m^{-2}, ± SD)					Forward-looking video (total # individuals/colonies per 100 m)				
Taxonomic group	**Morphospecies**	**R1359**	**R1358**	**R1355**	**R1357**	**R1356**	**R1359**	**R1358**	**R1355**	**R1357**	**R1356**
Actiniaria	*Actinoscyphia* sp.	0.04 (0.24)	0.03 (0.16)	0	0	0	1.2	0.8	0.1	0	0
	Actiniaria sp. 1	0.02 (0.19)	0.01 (0.11)	0	0	0	0.6	0.07	0	0	0
	Actiniaria sp. 2	0.02 (0.19)	0	0	0	0	0.7	0	0	0	0
	Actiniaria sp. 3	0	0	0	0	0	0.05	0	0	0	0
Alcyonacea	*Acanella arbuscula*	0.05 (0.21)	0.01 (0.08)	0	0	0	10.6	0.5	0	0	0
	Acanthogorgia armata	0.01 (0.08)	0	0	0	0	0.6	0	0	0	0
	Anthomastus grandiflorus	0.23 (0.80)	0.04 (0.47)	0	0	0	55.7	0.4	0	0	0
	Anthothela grandiflora	0	0	0	0	0	0.05	0	0	0	0
	Chrysogorgia sp.	0	0	0	0.03 (0.34)	0.01 (0.10)	0	0	0.1	3.2	1.1
	Clavularia sp.	0	0	0	0	0	0.3	0	0	0	0
	Nephtheidae sp.	0	0	0	0.04 (0.065)	0	0	0	0	2.3	0
	Keratoisis ornata	0.05 (0.22)	0	0	0	0	13.1	0	0	0	0
	Paragorgia arborea	0	0	0	0	0	0.05	0	0	0	0
	Radicipes spp.	0.03 (0.20)	0	0	0	0	10.7	0	0	0	0
Antipatharia	*Bathypathes* sp.	0	0	0	0	0	0	0	0	0.05	0.1
Ceriantharia	Cerianthid	0	0	0.01 (0.10)	0	0	0	0	0	0.05	0
Pennatulacea	*Halipteris finmarchica*	0.02 (0.13)	0	0	0	0	13.1	0	0	0	0
	Pennatula borealis	0	0	0	0	0	0.7	0	0	0	0
	Umbellula sp.	0	0	0	0	0	0	0	0	0	0.4
Scleractinia	*Javania* sp.	0.01 (0.08)	0	0	0	0	1.0	0	0	0	0
	Flabellum sp.	0	0	0	0.06 (0.24)	0	-	-	-	-	-
Cnidaria	Unknown coral 1	0.006 (0.08)	0	0	0	0	0	0	0	0	0
	Unknown coral 2	0.01 (0.11)	0	0	0	0	0.6	0	0	0	0
	Unknown soft coral	0	0	0	0	0	0	0	0.1	0	0
	Unknown cnidarian	0.02 (0.13)	0.12 (0.43)	0	0	0.05 (0.23)	-	-	-	-	-

Table 4.3 *(continued)*

		Downward-looking images (# individuals/colonies m^{-2}, ± SD)					Forward-looking video (total # individuals/colonies per 100 m)				
Taxonomic group	**Morphospecies**	**R1359**	**R1358**	**R1355**	**R1357**	**R1356**	**R1359**	**R1358**	**R1355**	**R1357**	**R1356**
Echinoidea	*Hygrosoma petersii*	0	0.01 (0.11)	0.01 (0.10)	0	0	0	0.5	0.2	0	0
	Gracilechinus affinis	0	0	0.30 (0.53)	0.08 (0.30)	0.59 (1.15)	-	-	-	-	-
	Phormosoma placenta	0	0.01 (0.11)	0	0	0	0	3.0	0	0	0
	Echinoidea sp.	0.02 (0.15)	0.01 (0.08)	0	0	0	2.3	0	0	0	0
Crinoidea	Stalked crinoidea	0	0	0.01 (0.10)	0	0	0	0	0.1	0.3	0
Holothuroidea	Psychropotidae sp.	0	0	0	0.004 (0.066)	0.04 (0.19)	0	0	3.4	3.2	2.3
	Holothuroidea sp.	0	0	0	0	0.01 (0.12)	0	0	0	0.2	1.2
Ophiuroidea	*Ophiomusium lymani*	0.03 (0.17)	0.06 (0.30)	6.07 (2.26)	0.02 (0.13)	0.06 (0.25)	-	-	-	-	-
	Ophiacantha sp.	0	0	0.01 (0.10)	0.13 (0.65)	0	-	-	-	-	-
Asteroidea	*Ceramaster granularis*	0.01 (0.11)	0	0	0	0	0.4	0	0	0	0
	Neomorphoaster forcipatus	0.01 (0.11)	0	0	0	0	1.3	0	0	0	0
	Porania pulvillus insignis	0	0	0	0	0	0.05	0	0	0	0
	Asteroidea sp. 1[1]	0.02 (0.13)	0	0	0	0.005 (0.08)	2.1	0	0	0	0.2
	Asteroidea sp. 2	0.006 (0.08)	0	0	0	0	0.1	0	0	0	0
	Asteroidea sp. 3[2]	0	0	0.01 (0.10)	0	0.01 (0.10)	0	0	0	0	0.2
	Asteroidea sp. 4	0	0	0	0	0	0	0	0	0	0.06
	Freyella elegans	0	0	0	0.06 (0.30)	0.04 (0.23)	0	0	0	4.9	1.1
Mollusca	*Graneledone verrucosa*	0	0	0	0	0	0.05	0	0	0	0
Arthropoda	*Neolithodes grimaldii*	0.01 (0.08)	0	0	0	0	0.1	0	0	0	0
	Decapod (crab)	0.01 (0.08)	0	0	0	0	0	0	0	0	0
	Pycnogonida	0	0	0	0.004 (0.07)	0	0	0	0	0	0

1. Possibly Poraniidae sp.
2. Possibly Pedicellasteridae sp.

Table 4.3 *(continued)*

		Downward-looking images (# individuals/colonies m^{-2}, ± SD)					Forward-looking video (total # individuals/colonies per 100 m)				
Taxonomic group	**Morphospecies**	**R1359**	**R1358**	**R1355**	**R1357**	**R1356**	**R1359**	**R1358**	**R1355**	**R1357**	**R1356**
Porifera[3]	Erect sponge 1 (white)	0	0	0	0	3	0	0	0	0	6
	Erect sponge 2 (white)	3	1	0	0	0	-	-	-	-	-
	Erect sponge 3 (white)	0	0	0	0	0	0	4	0	1	0
	Encrusting sponge 1 (yellow)	6	0	0	0	0	-	-	-	-	-
	Encrusting sponge 2 (grey)	0	1	0	0	0	-	-	-	-	-
	Encrusting sponge 3 (white)	7	6	0	0	16	-	-	-	-	-

3. Porifera morphospecies are recorded as number of occurrences.

4.4.2.2 *Community composition*

The composition of megafaunal communities differed among depths (Fig. 4.8a). Alcyonaceans (soft corals), ophiuroids (brittle stars) and echinoids (sea urchins) were overall numerically dominant, but patterns in dominance varied with depth. Alcyonaceans formed most of the community at the shallowest location (1095 m; Fig. 4.7c), while echinoids dominated communities with 3 different species: *Hygrosoma petersii* and *Phormosoma placenta* at 1458 m (Table 4.3; Fig. 4.7b), and *Gracilechinus affinis* at the deepest location (2887 m; Table 4.3; Fig. 4.7d). Ophiuroids dominated the community at 2095 m, due to the presence of *Ophiomusium lymani* (Table 4.3). No clear dominance was detected at 2515 m.

Patterns in vertical zonation differed among taxomonic groups (Fig. 4.8b). Morphospecies of deep-water corals (pennatulaceans, alcyonaceans and scleractinians) were often restricted to 2-3 depths, being clearly more prevalent at the shallowest location (1095 m). In contrast, holothuroids were only found at depths >2000 m. Echinoids and poriferans were the most broadly distributed taxonomic groups, with echinoids being present at all depths. Most of the ophiuroids recorded in this study were found on soft substrate at 2095 m. Most asteroids (sea stars) were found at the shallowest (1095 m) and deepest (2887 m) locations. The brisingid sea star *Freyella elegans* (Fig. 4.5d, 4.7e) was numerically abundant at 2515 m and 2887 m. (Table 4.3).

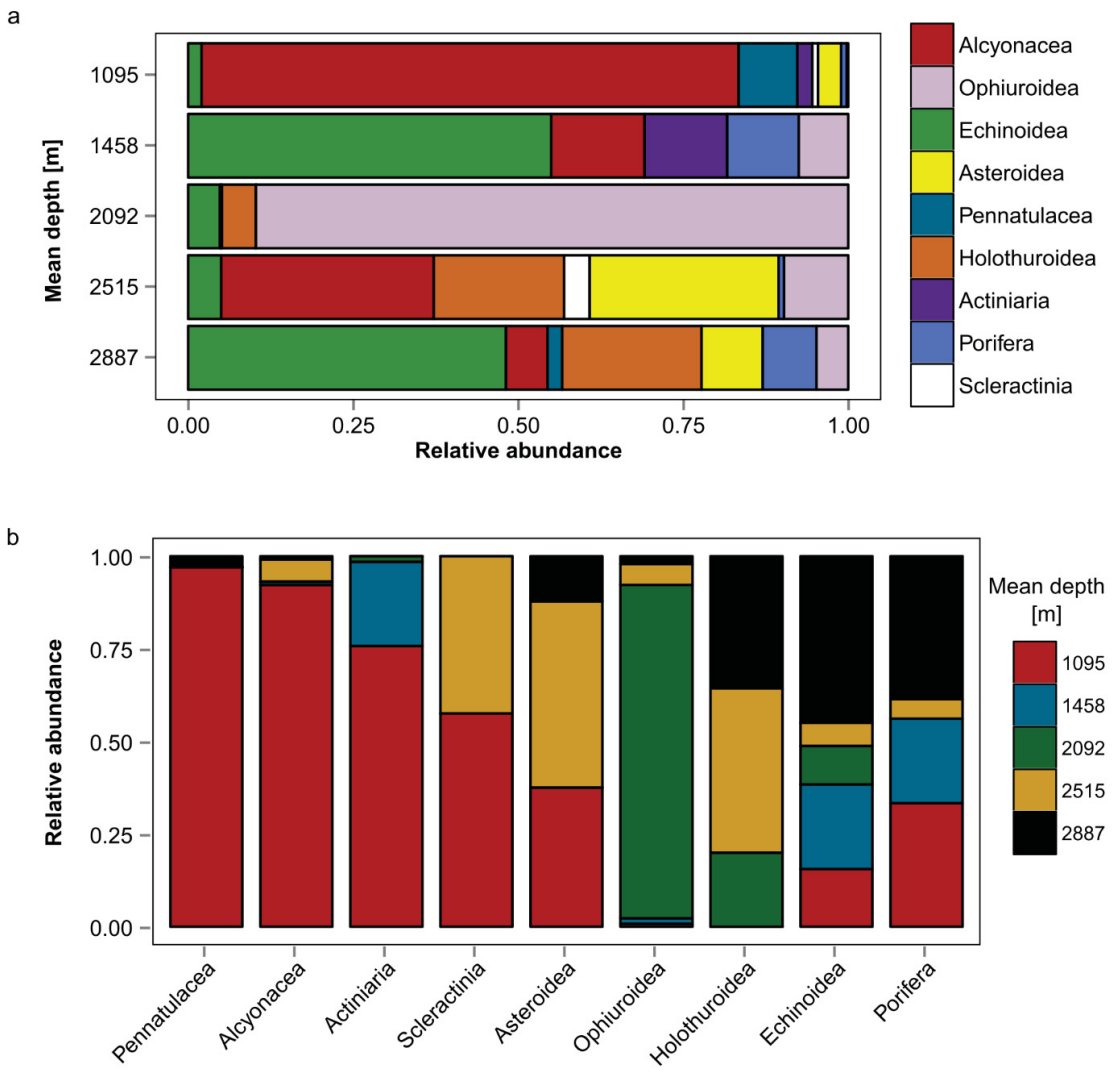

Figure 4.8: Composition of epibenthic megafaunal communities pooled from downward-looking images and forward-looking video. (a) Relative abundance of the 9 most important taxonomic groups across depths. (b) Vertical zonation of the 9 most important taxonomic groups based on their relative abundance among locations.

4.4.2.3 *Diversity*

We detected a total of 59 morphospecies of epibenthic megafauna along the transects. Morphospecies richness was much higher at the shallowest location (1095 m), and lowest at 2092 m (Fig. 4.9a). On average, the number of morphospecies detected was similar between the downward-looking images, and the forward-looking video. (Fig. 4.9a). Shannon-Wiener diversity (*H'*) and Pielou's evenness (*J'*) indices differed between cameras, but showed the same overall pattern as richness (Fig. 4.9b,c). For fauna recorded in the downward-looking images, diversity was highest at the shallowest location (1095 m), while in the forward-looking video, diversity was highest at the deepest location (2887 m). Lowest diversity indices were found at 2092 m in both the downward-looking images and forward-looking video.

Estimated morphospecies richness using individual-based rarefaction analysis for both cameras was higher at the shallowest (1095 m) and deepest (2887 m) locations than in locations at intermediate depths, although the pattern was not strong for downward-looking images (Fig. 4.9d,e). Morphospecies accumulated most rapidly at the shallowest location than to all other transects in both the forward-looking video and downward-looking images (Fig. 4.10). In the forward-looking video, the rate of accumulation of morphospecies at the deepest locations (2515 m and 2887 m) was similar to that in the shallowest transect, and remained higher than in other locations (Fig. 4.10a). An abrupt increase in morphospecies richness detected at 1458 m (Fig. 4.10b) was due to the presence of a large boulder along the transect (Fig. 4.5a,c).

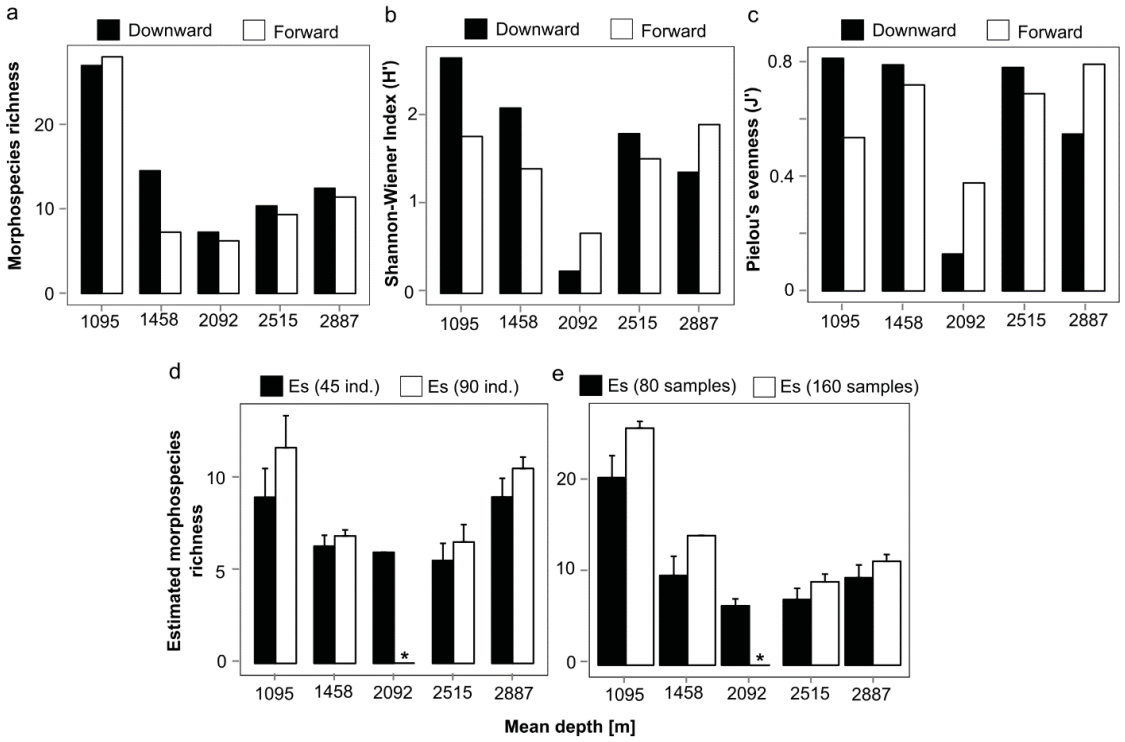

Figure 4.9: Top panels: diversity indices of epibenthic megafaunal communities across a depth gradient in the forward-looking and downward-looking cameras. (a) Morphospecies richness. (b) Shannon-Wiener diversity index (*H'*). (c) Pielou's evenness index (*J'*). Bottom panels: interpolated morphospecies richness using rarefaction. (d) Individual-based estimated morphospecies richness (+ SE) for 45 individuals (minimum surveyed) and 90 individuals in the forward-looking camera. (e) Sample-based morphospecies richness (+ SD) for 80 samples and 160 samples in the downward-looking images. * indicates no data. Mean depth of each dive is shown.

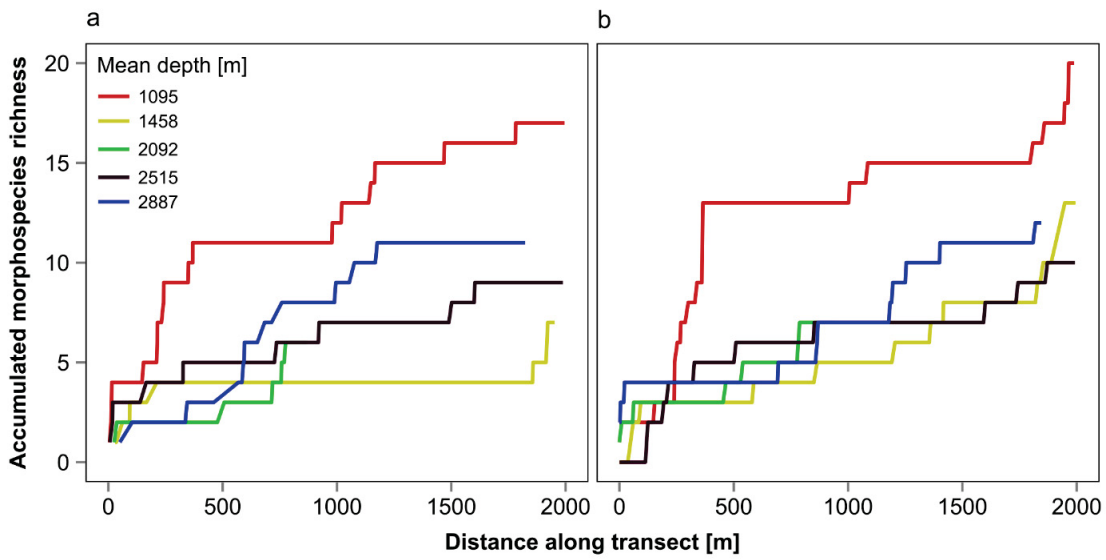

Figure 4.10: Morphospecies accumulation curves along the first 2000 m (when applicable) of transects for each dive. In dives R1358 (mean depth: 1458 m) and R1356 (mean depth: 2887 m), segments are treated as continuous. Distance along transect (m) represents real distance on the seafloor (i.e. including portions not used for analysis). (a) Forward-looking video. (b) Downward-looking images.

4.5 Discussion

Patterns in faunal communities on continental margins can be partially explained by environmental gradients, such as temperature, dissolved oxygen, substrate, magnitude of currents, and export of organic matter from the surface (Levin and Dayton 2009). In this study, a marked difference in abundance, community composition, and diversity was observed between the shallowest transect location at ~1100 m depth and the remaining transects, but variability within these deeper locations was also observed. Different environmental gradients may act at different scales to explain these patterns. In the study area, it is unlikely that either temperature or dissolved oxygen played a role in shaping these patterns since only weak gradients were observed across depths. Here, we focused on the role of substrate complexity in influencing megafaunal patterns, but given the wide

depth range, the input of particulate organic matter (POC) to the seafloor may also be important. POC input was not measured in our study, but indirect evidence leads us to speculate on its potential importance in shaping biological patterns in the Northeast Fan.

On a global scale, carbon flux to the deep ocean has been shown to decrease exponentially with depth (Pace et al. 1987), and this gradient in food supply is thought to influence benthic fauna (Rex et al. 2006). POC flux estimated from this depth-decay relationship was correlated with decreased biomass and abundance at depth, and changes in community composition of macrofauna in the North Atlantic (Johnson et al. 2007) and in the Gulf of Mexico (Wei et al. 2010). While a wide environmental gradient can be observed from the surface, the exponential nature of the curve leads to a theoretical plateau in POC flux at ~1,000 m, and predicts that only 1-2% of surface primary production would reach depths of 1150-3000 m (Pace et al. 1987). Further, even in the presence of inter-regional variability in flux, very little variability is empirically observed at depths greater than ~1,000 m in most regions (Lutz et al. 2002). In this study, megafaunal abundance was markedly different between the shallowest transect (~1100 m) and the remaining transects (~1450-3000 m), where abundance remained relatively constant, except at the intermediate depth of ~2095 m due to the high density of the brittle star *Ophiomusium lymani*. Based on this relationship alone, we speculate that it is likely that variability in POC could explain in part this abrupt change in megafaunal abundance, but may not have played a role at greater depths. However, since variability in sediment POC has been observed within this depth range (1200-4000 m) in the Mediterranean Sea, and has been shown to influence the composition of benthic

megafaunal communities (Tecchio et al. 2011), measurements are needed to confirm this hypothesis.

Food supply to the deep ocean can also come from sporadic sources from the surface ocean, such as pulses of phytodetritus (Billet et al. 1983, Sumida et al. 2014), whale falls (Smith and Baco 2003), and salp falls (Henschke et al. 2013). In addition to these vertical sources, large-scale geomorphological features can enhance export of organic matter to the deep ocean via lateral advection. Submarine canyons, in particular, modify local current regimes, and act as major conduits of particles from the continental shelf to the slope. This has been shown in the Mediterranean Sea with 'cascading events' of dense shelf water funneled through canyons, influencing deep-water benthic fauna (Canals et al. 2006, Company et al. 2008), and off the Californian coast, where megafauna was reported to be strongly associated with aggregates of macrophyte detritus (Vetter and Dayton 1999). Our study area lies downslope of 3 steep-walled submarine canyons cutting the shelf break at the mouth of Northeast Channel, a major water circulation pathway in the Gulf of Maine (Ramp et al. 1985). The circulation in these canyons is unknown, but currents are expected to be swift given the high density of cold-water corals reported in one of them, the Middle Canyon (Mortensen and Buhl-Mortensen 2004, Bryan and Metaxas 2006, Watanabe et al. 2009). Indirect evidence suggests that downwelling may occur in the area. Recruits of the cold-water coral *Primnoa resedaeformis* were reported deeper than its adult bathymetric range in the Middle Canyon (Lacharité and Metaxas 2013), and in the present study, we observed drift macroalgal debris at depths of ~2500 m. Further, the abundance of megafauna within the

depth range of the deeper dives in our study was higher than predicted by empirical data at a global scale (Rex et al. 2006), suggesting potential additional sources of organic matter. We conclude therefore that food supply in the area is likely influenced by the presence of canyons at the mouth of a major circulation pathway, and may influence overall megafaunal abundance. However, patterns in megafaunal abundance and diversity differed, which suggests that other environmental gradients may be important in determining diversity.

In the Northeast Fan, we showed that substrate complexity and its heterogeneity at local scales influences megafaunal community composition and diversity. A wider particle size spectrum was detected in both the shallowest and deepest locations, which was reflected with more outliers in image complexity. Outliers were also detected at depths of ~1450 m and ~2500 m, due to the sporadic presence of boulders. It is expected that the local diversity of megafauna increases with a wider range of substrate types at fine spatial scales, since specific adaptations are required for organisms to cement themselves to this substrate (Taylor and Wilson 2003). In this study, the most striking difference in megafaunal community composition and diversity was observed between the shallowest transect at ~1100 m and the remaining transects because of a distinct and diverse community of deep-water corals at the former. Within the deeper transects, areas where a wider particle size spectrum (pebbles, cobbles and boulders interspersed in a matrix of sand) was observed were correlated with higher diversity, in particular at the deepest location. In contrast, the location with the lowest mean substrate complexity was found at intermediate depths (~2095 m), and was associated with the lowest diversity. We

conclude therefore that within a broader hydrodynamic regime affecting the export of carbon organic matter to the study area, fine-scale variability in substrate complexity influences patterns in diversity, but seemingly not abundance.

We have shown here that the sporadic presence of hard substrate could be ecologically important in determining the distribution and local diversity of deep-water epibenthic megafaunal species. This suggests that the inclusion of fine-scale features in an otherwise relatively homogeneous environment is required in descriptions of habitat, given their potential spatially disproportionate influence on local diversity. This study also supports the contention that scale is critical in benthic habitat studies, and should be explicitly included in analyses (Lecours et al. 2015). Lastly, difficulties remain in quantifying the spatial distribution of hard substrate given its often sporadic presence. Qualitative observations and acoustic backscatter are often used, but the latter may be limited in the deeper ocean due to spatial resolution. We propose that optical imagery remains the most accurate tool to detect fine-scale features (e.g. < 10 m), and have shown here that substrate complexity can be described and quantified accurately when using this imagery to determine its ecological importance.

CHAPTER 5

DRIVERS OF EPIBENTHIC MEGAFAUNA ON A DEEP TEMPERATE SHELF: A MULTISCALE APPROACH

5.1 Abstract

The distribution of deep-water (> 75-100 m depth) epibenthic megafaunal communities is influenced by abiotic factors, in particularly those related to geological features (sediment properties, and geomorphometry), and oceanographic properties (hydrodynamics, hydrographic conditions). Given the disparity in the scale at which these factors operate, incorporating multiple spatial and temporal scales is necessary to determine the strength of these species-environment relationships, and at which scale the relationships are strongest. In this study, relationships between patterns of epibenthic megafauna with 3 environmental drivers acting at different scales (sediment properties, geomorphometry, and oceanographic properties) were determined on a deep temperate continental shelf in the eastern Gulf of Maine (northwest Atlantic), in 4 physiographic regions (Jordan Basin, Sewell Ridge, Browns Channel, and Georges Basin) with varying geological and oceanographic features. Twenty benthic photographic transects (length: 611 – 1021 m; total length surveyed: 18,902 m; 996 images) were performed in July and August 2009. Cover of epibenthic megafauna was recorded, and taxa identified at the lowest possible taxonomic level. Image complexity determined using computer vision was used as a proxy of substrate complexity (surficial geology). A bathymetric terrain model (grid cell size: 100 m) was used to derived bathymetric variability in the vicinity of transects (1 – 5 km). Oceanographic properties at the seafloor (temperature, salinity, current speed, current direction) over 10 years (1998-2009) were determined using

modelled data (Finite-Volume Community Ocean Model; 45 vertical layers; horizontal resolution: 1.7 – 9.5 km). Epibenthic megafaunal cover and diversity (sample-based expected richness) were influenced by bathymetric variability, with diversity being also influenced by substrate complexity. Community composition was influenced by substrate complexity and oceanographic properties. The use of the multiscale approach was proven necessary given the different environmental drivers influencing at different scales measures of megabenthic biological communities in deep waters.

5.2 Introduction

On deep continental margins (> 75-100 m depth), the distribution of epibenthic megafaunal communities is influenced by abiotic factors, including the geological features of the seafloor and the oceanographic properties of the water column (references therein). The relationship between benthic invertebrates and substrate type is broadly defined by a dichotomy of organisms dwelling on soft substrate (i.e., fine-grain sediment such as mud and clay), and on hard substrate (i.e., rocks and bedrock) - due in part to both the necessary adaptations to attach to the seafloor and the influence of feeding mode. This broad dichotomy also regulates the distribution of megafaunal communities in deep waters (Beaman et al. 2005; Jones et al. 2007; Robert et al. 2014). Bathymetric features, such as relative positioning (e.g., topographic high) and variability in terrain at multiple spatial scales (e.g., rugosity), can also influence the distribution of megafauna (Jones et al. 2013), and this relationship is particularly strong for certain megafauna, such as cold-water corals (Dolan et al. 2008; Rengstorf et al. 2012; Tong et al. 2012; Tong et al. 2016). The relationship of megafauna with bathymetric features is thought to be due in part to the influence of these features on local hydrodynamics, since fast currents have been

associated with steep bathymetry (Genin et al. 1986; White 2007), and in turn enhance the delivery of food particles, and regulate re-suspension and dispersal (Mosch et al. 2012; Mohn et al. 2014; Navas et al. 2014). Hydrographic conditions (temperature, salinity and water chemistry) also play a role in regulating benthic communities at regional scales (Williams et al. 2010; McCallum et al. 2013; Jørgensen et al. 2015), and at global scales (Tittensor et al. 2009).

Most deep-water benthic communities rely on the input of organic material from external sources (coastal and/or surface ocean), since *in-situ* primary productivity is restricted to the photic zone. The influence of coastal organic material to deep benthic communities has been observed in areas of steep bathymetry, where the presence of macroalgal debris is thought to enhance local megabenthic biomass, for example, in fjords on the West Antarctic Peninsula (Grange and Smith 2013), and in submarine canyons (Vetter and Dayton 1999). This latter coupling in particular suggests strong hydrodynamic pathways between coastal ecosystems and the deep ocean, with continental shelves acting as conduits. Concurrently, pelagic-benthic coupling with surface plankton is tighter on continental shelves than in deeper waters (Lin et al. 2014). This coupling is particularly strong in high-latitude shelf seas (Grebmeier and Barry 1991), where dense megafauna has been sporadically observed (Piepenburg et al. 1995; Renaud et al. 2007; Blicher and Sejr 2011), and large-scale patterns of benthic megafaunal abundance were linked to carbon supply from surface waters (Degen et al. 2016).

These species-environment relationships can act as proxies or abiotic surrogates for biological diversity, and hence potentially be used in conservation strategies (reviewed in McArthur et al. 2010; e.g. Anderson et al. 2011). Developing these proxies requires an understanding of the role of the physical environment in shaping communities, based on the relative strength of the relationships with environmental predictors and, due to spatial structuring in the environment (Wiens 1989), the scale (s) at which the relationships are strongest. The spatial scales of environmental predictors vary from fine-scale properties (e.g., the composition of the substrate), to local neighborhood analyses (e.g., bathymetric features – Wilson et al. 2007), to broader divisions of the marine environment into 'ecoregions' (Spalding et al. 2007) at regional to global scales. Temporal variability in environmental predictors also occurs due to water column dynamics, but its effect on deep-water benthic megafauna is unclear. Spatial patterns of megafauna are typically reported as snapshots based on the assumption that they are long-lived, slow-growing organisms 'integrating' environmental conditions over longer periods of time than in coastal ecosystems. Describing oceanographic properties over similarly long periods (e.g. years) may thus be needed to better assess their relationship with megafauna.

The accurate description of the scale(s) at which species-environment relationships occur leads to better predictions for the unexplored environments, which has obvious implications for building future sampling surveys and/or elaborating conservation strategies. The combination of geological features at multiple scales has proven powerful in explaining the distribution of megafaunal communities (Beaman et al.

2005; Buhl-Mortensen et al. 2009; Buhl-Mortensen et al. 2012; Robert et al. 2014), and useful in defining discrete habitats on the seafloor potentially influencing patterns of megafauna (Brown et al. 2011). Moreover, oceanographic properties (bottom currents and hydrographic properties) are increasingly incorporated into benthic habitat studies (Mosch et al. 2012; Pitcher et al. 2012; Henry et al. 2013; Murillo et al. 2016), and a hierarchical approach has been used to integrate these environmental factors (sediment properties, bathymetric features, and oceanography) at different scales (Williams et al. 2010; Huang et al. 2011).

Temperate continental shelves harbour complex benthic habitats. Glaciation has yielded diverse geomorphic features, such as deep basins, trenches and channels dug by subglacial flow. The retreat of glaciers left unconsolidated sediment or 'glacio-marine debris' on the seafloor, influencing the composition of the substrate typically described as coarser sediment, such as cobbles and boulders, co-occurring with fine-grain sediment (sand and mud) (Benn and Evans 2010). Additionally, seasonal patterns in water column dynamics lead to stratification in the summer, and deep convective mixing in the winter, and influence the delivery of food particles to the seafloor, thus potentially affecting spatial patterns of benthic biomass. This study aims to 1) determine substrate complexity (< 1 m) and heterogeneity (variability in complexity within 100s m), bathymetric features (1-5 km), and oceanographic properties of near-seafloor waters (1-10 km) on a temperate continental shelf in the Gulf of Maine (northwest Atlantic Ocean), and 2) determine the relative importance of these environmental factors acting at different scales in influencing the abundance, composition and diversity of epibenthic megafaunal communities.

5.3 Materials & Methods

5.3.1 Study area

The Gulf of Maine (northwest Atlantic Ocean) is a relic of the last glaciation event in northeastern North America, when the Laurentide ice sheet extended to the current continental break. The Gulf proper encompasses complex geomorphic features, in particular the presence of 3 deep basins (Jordan, Georges and Wilkinson), ridges and channels. In the eastern Gulf of Maine, 2 deep channels - Northeast Channel (between Browns Bank and Georges Bank) and Browns Channel (between German Bank and Browns Bank) - form connections to the open ocean and Scotian Shelf, respectively (Fig. 5.1a).

The surficial geology of the eastern Gulf of Maine was impacted by glaciation, being mainly composed of 'glacial till' or ice-contact sediment/moraine debris (Fader et al. 1971). Thus, a wide range of particle grain size is often observed at fine spatial scales (< 1 – 10 m) on the seafloor, as coarse sediment, such as cobbles and boulders, is interspersed in a matrix of sand and mud (this study, Edinger et al. 2011). However, differences between physiographic regions are apparent in the eastern Gulf of Maine. For example, while fine-grain sediment is dominant in Georges Basin, locations dominated by coarse sediment are found on the flanks of Browns Channel and Jordan Basin (this study).

The Gulf of Maine is a semi-enclosed basin dominated by a counter-clockwise surface circulation and influenced by seasonal variability. In the eastern Gulf of Maine,

the Labrador Current flows from the Scotian Shelf along the coast of Nova Scotia (Canada), feeding into the Eastern Maine Coastal Current southwest of the Bay of Fundy. Inflow into the Gulf is also observed on the northeast flank of Northeast Channel, with an outflow on the southwest flank. A deep flow also occurs in Northeast Channel, forming a connection to the deep open ocean. In addition to these broad circulation patterns, the seasonal formation of counter-clockwise gyres has been observed over Jordan and Georges Basins, and a strong eastward circulation from Northeast Channel through Browns Channel along Browns Bank (modelled in Xue et al. 2000, and supported by unpublished empirical observations).

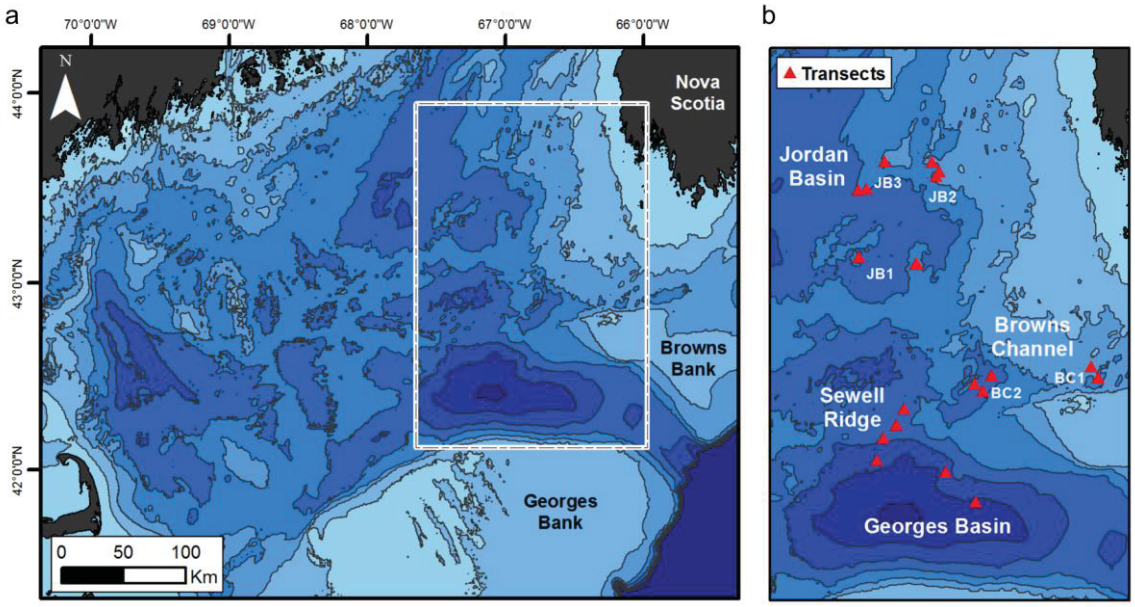

Figure 5.1: (a) Gulf of Maine (northwest Atlantic). 50-m depth contours are shown (50-400 m). Study area in the eastern Gulf of Maine is indicated with the rectangular box. (b) Locations of benthic video transects (n = 20) in 4 physiographic regions: Jordan Basin, Browns Channel, Sewell Ridge and Georges Basin.

5.3.2 Benthic photographic transects

Twenty benthic photographic transects were performed in 4 physiographic regions in the eastern Gulf of Maine (Jordan Basin, Georges Basin, Browns Channel, and Sewell Ridge) in July and August 2009 aboard the *CCGS Hudson* (Fig. 5.1; Table 5.1). In 2 physiographic regions (Browns Channel and Jordan Basin), transects were performed in 2 and 3 areas, respectively, as clusters, yielding 'subregions'. Thus, for simplicity, the term 'subregion' is used to describe the spatial distribution of all transects (7 subregions in total; Table 5.1). Transects were performed using Campod, an instrumented tripod equipped with video and still cameras (Gordon Jr. et al. 2007), and with an open profile and wide stance, which minimizes disturbance on the seafloor. The instrument was operated in near-seafloor drift mode, and landed on the seafloor to collect high-definition imagery with a downward-facing still camera (Nikon D300, resolution: > 12 megapixels). Images were taken ~every 1 minute along transect tracks, and the field of view could be determined using lasers 10 cm apart. Campod is equipped with an ultra-short baseline (USBL) navigation system (ORE Trackpoint II), which allows its precise positioning on the seafloor. Transect length varied from 611 m to 2979 m, with a total length of seafloor surveyed of 28,683 m and 2507 images collected.

Table 5.1: Benthic photographic transects performed using Campod in the eastern Gulf of Maine (northwest Atlantic) in 4 physiographic regions. The number of images and length surveyed used for analysis, and the geographic positions of the middle point of each transect are indicated.

Physiographic region	Subregion	Transect	Latitude	Longitude	Depth range [m]	Length surveyed [m]	Total # of images	# Images used for biological analysis
Georges Basin	GB1	1	42°33'59" N	66°52'57" W	260-265	1000	80	20
		2	42°27'29" N	66°44'18" W	316-318	1017	53	22
Sewell Ridge	SR1	1	42°47'27" N	67°05'00" W	217-220	1004	45	20
		2	42°43'51" N	67°07'14" W	209-215	1001	52	22
		3	42°41'17" N	67°11'01" W	221-230	1012	70	21
		4	42°36'33" N	67°12'59" W	263-266	974	40	18
Jordan Basin	JB1	1	43°18'11" N	67°01'21" W	131-177	942	47	16
		2	43°18'09" N	67°01'42" W	140-184	784	59	17
		3	43°19'36" N	67°18'10" W	144-190	953	17	12
	JB2	1	43°36'49" N	66°55'45" W	76-125	831	59	18
		2	43°39'45" N	66°56'56" W	119-140	957	43	21
		3	43°37'47" N	66°54'47" W	138-163	900	54	20
	JB3	1	43°39'55" N	67°10'45" W	137-144	611	43	14
		2	43°34'09" N	67°15'56" W	160-182	1017	29	20
		3	43°33'52" N	67°18'24" W	154-211	891	77	19
Browns Channel	BC1	1	42°56'25" N	66°10'36" W	116-152	1021	30	17
		2	42°53'57" N	66°08'37" W	140-160	997	63	20
	BC2	1	42°52'50" N	66°44'38" W	181-193	997	53	20
		2	42°51'21" N	66°42'08" W	198-225	996	29	16
		3	42°54'32" N	66°39'33" W	235-252	993	53	21

Some images were discarded due to the absence of lasers (outside of field of view), any obstruction of the field of view (such as the presence of large fish), and/or blurriness in the quality of the image. In total, 1464 images were retained. Given these constraints, distance between usable images varied. Images were cropped to a standard size of 75 cm (width) by 50 cm (height) of the most illuminated portion of the image. To minimize variability in the amount of seafloor surveyed between transects while retaining a sufficient resolution to infer physical and biological patterns within transects, a standard length of 1000 m was adopted. Thus, for transects longer than 1000 m, only a portion of the transect was used for analysis. This resulted in a final dataset of 996 images, transect length varying from 611 m to 1021 m on the seafloor, and a total length surveyed on the seafloor of 18,902 m (Table 5.1).

5.3.3 Epibenthic megafauna: abundance & community composition

Epifaunal abundance was determined as proportional cover in the image. This approach accounts for the diversity of organisms encountered in the survey (i.e., individuals and colonial organisms), and the limitations of the sampling tool (imagery). More detailed measures of abundance could be used to determine the distribution of individual species or taxonomic groups, but this was not the purpose of this study, which was to capture the distribution of communities. Cover was determined with a grid (cell size: 5 cm x 5 cm; 150 grid cells per image), and cells with >50% cover of epifauna were enumerated. This was considered adequate to capture epibenthic megafauna (> 2-3 cm). Faunal cover was determined for all images (n = 974) to determine their usability for measuring substrate complexity (see below '5.3.4.1 Substrate complexity').

For each transect, a subset of images was used to determine the abundance and composition of biological communities in the study area. One image was extracted for every 50 m of seafloor surveyed for describing potential differences in community composition between transects, resulting in 374 images used for biological analysis (Table 5.1). Given the length of transect, variability in distance between adjacent images, and observed spatial patterns of epibenthic fauna, this sampling frequency was considered adequate.

Epibenthic taxa were visually identified based on morphotype, and also recorded as presence/absence to infer community composition. Taxa were identified at the lowest possible taxonomic level. Given the lack of collected specimens, we refer to these taxa as 'morphospecies'. Diversity is reported as morphospecies richness (# of taxa detected in each transect) and expected morphospecies richness was calculated with sample-based rarefaction analysis to correct for the different number of images between transects based on the smallest sample size (n = 12 images).

5.3.4 Hierarchical description of the physical environment in the eastern Gulf of Maine

5.3.4.1 *Substrate complexity*

Image complexity was determined for all images along transects (n = 974) using object-based image analysis (Lacharité et al. 2015). Object-based image analysis decomposes a digital image (raster-based representation of pixels) into 'image-objects', relatively homogeneous regions in the image based on texture and/or colour. Here, image

complexity acts a proxy of substrate complexity, since the number of image-objects detected is highly correlated with the distribution of sediment particles on the seafloor (Lacharité et al. 2015). A continuous gradient of substrate complexity is thus created, with higher values of complexity indicating a dominance of coarse sediment (Fig. 5.2). To compute image complexity, 2 parameters are needed: minimum size of image-objects allowed and the amount of equally-sized bins dividing the luminosity axis in the HSV color space. In this study, we used the same parameters as in Lacharité et al. (2015): a minimum size of image-objects of 1 cm^2 on the seafloor, and 20 luminosity bins. Image complexity is reported as a dimensionless number, which is equivalent to the amount of image-objects detected in relation to the maximum amount of image-objects that could be detected in an image (based on the input parameters). Given the dimensions of the images used in this study, this equals to 3750 image-objects.

Mean complexity (± standard deviation) was calculated for each transect using images with less than 10% epifaunal cover (Table 5.2). This maximizes the use of the dataset, since most of the images (n = 803) displayed less than 10% epifaunal cover. Despite the presence of fauna, which has been shown to alter measures of complexity, image complexity remains highly correlated with mean particle grain size under these conditions (Lacharité et al. 2015).

Figure 5.2: Diversity of substrate types in the eastern Gulf of Maine with associated image complexity computed using object-based image analysis. (a) Complexity = 0.05; Georges Basin (GB1-1); depth: 265 m. (b) Complexity = 0.16; Sewell Ridge (SR1-2); depth: 213 m. (c) Complexity = 0.34; Jordan Basin (JB2-1); depth: 117 m. Scale bar: 10 cm.

Table 5.2: Environmental variables related to substrate complexity, geomorphometry and oceanographic properties at the seafloor. BPI = Bathymetric position index. For each variable, the mean and standard deviations are used as environmental variables in analyses. Units are indicated in brackets. Absence of unit indicates a dimensionless variable.

Category	Length scale measured	Variable
Substrate complexity	Transect	Image complexity
Geomorphometry	Transect	Deviation from mean depth – 1 km [m] Deviation from mean depth – 5 km [m] BPI 1 km [m] BPI 5 km [m]
Oceanographic properties at the seafloor	Subregion	Current speed [m/s] – 10 years Kappa parameter – 10 years Current speed [m/s] – Annual amplitude Kappa parameter – Annual amplitude Temperature [°C] – 10 years Temperature [°C] – Annual amplitude Salinity [PSU] – 10 years Salinity [PSU] – Annual amplitude

5.3.4.2 *Geomorphometry*

Patterns in geomorphometry in the eastern Gulf of Maine were determined using a digital bathymetric model (DBM) with a resolution of 3 arc-seconds (~90 m) developed by the United States Geological Survey (Twoney and Signell 2013). This DBM is a compilation of various datasets of bathymetry from both Canadian and US sources. Bathymetric data were gridded to a cell size of 100 m, and grids were extracted for all 7 subregions (Table 5.1). The extent of each subgrid was determined using the bounded extent of a 10-km buffer from the middle location of each transect.

Bathymetric variability within a radius *r* (1000 m and 5000 m) of the middle of each transect was computed using the mean deviation (absolute values; ± standard deviation) from the mean depth within each radius (for r = 1000 m, n = 304-313; for r= 5000 m, n = 7710-7739; Table 5.2). A minimum length of radius *r* of 1000 m was used to infer variability in terrain for the whole transect (middle point is for most transects 500 m away from start- and end-points). A maximum length of radius *r* of 5000 m to infer broader-scale variability. The bathymetric position index (BPI; Wilson et al. 2007) was also computed for each transect. The BPI is an index of the average position of a point in relation to a neighbourhood of grid cells. Positive values indicate bathymetric highs, while negative values indicate crests. BPI was calculated for each grid cell within subregions at 2 radii (1000 m and 5000 m). Mean BPI (absolute values; ± standard deviation; Table 5.2) was subsequently calculated within a 1-km circular zone of the middle point of each transect for each length of BPI radius (n = 304-313). BPI was calculated using the Benthic Terrain Modeller (Wright et al. 2012) in ArcGIS.

5.3.4.3 *Oceanography at the seafloor*

FVCOM (Finite-Volume Community Ocean Model; Chen et al. 2003) is an unstructured, terrain-following ocean circulation model with 45 vertical layers. Its unstructured grid is meant to account for the irregular coastal geometry and steep topographic features on continental margins. In the Gulf of Maine, the application of FVCOM is now in its 3rd generation, and hindcasts are available as monthly means of temperature, salinity and currents (u,v components) from 1978 to 2013.

In this study, monthly means were used over a 10-year period (January 1999 – December 2008) to reflect seasonal and inter-annual variability. Resolution at the scale of transects was not possible given the coarser resolution of the ocean circulation model in the deeper areas of the Gulf of Maine; consequently, modelled oceanographic data were extracted for each subregion. In each subregion, the extent of the area covered by modelled oceanographic data was determined with the prior geomorphometric analyses (i.e., a boundary box derived from a 10-km buffer from the middle points of each transect). Only the bottom layer of the ocean circulation model is considered in this study, which integrated conditions over a depth of < 1 m to 5 m off bottom. Sample sizes of locations where temperature and salinity are resolved ('rho' points) and where currents are resolved ('current' points), as well as the average distance between these points, are indicated in Table 5.3.

Time series of salinity, temperature and currents were constructed for each subregion. At each month, spatially-weighted means of temperature, salinity and current

speed were computed using Voronoi tessellation – which partitions the surface area into regions based on distance to resolved points – to account for variable spacing between model points. Environmental variables derived from ocean circulation for analysis represented 10-year mean (± standard deviation, n = 120; Table 5.2) of temperature (°C), salinity (PSU), current speed ($m \cdot s^{-1}$) and estimates of Kappa parameter (variability in the direction of currents). The Kappa parameter is a parameter of variability in the von Mises distribution for circular data (equivalent to a circular normal distribution). It is a measure of concentration of the direction of currents, and is reciprocal to a measure of dispersion. High estimates of Kappa parameters indicate low variability in current direction. Additionally, seasonal variability was calculated with annual amplitude (maximum – minimum; ± standard deviation; n = 10; Table 5.2) for temperature, salinity, current speed and current direction (estimates of Kappa parameter).

Table 5.3: Number of locations where temperature and salinity are resolved ('rho-points') and where the components of currents are resolved ('current points') in the ocean circulation model FVCOM in the eastern Gulf of Maine within each subregion. Average distance between points is indicated.

Physiographic region	Subregion	# of rho-points	Avg. distance [km]	# of current points	Avg. distance [km]
Browns	BC1	78	2.6	159	1.7
Channel	BC2	13	8.3	26	5.7
Georges Basin	GB1	41	5.6	74	3.6
Jordan Basin	JB1	15	9.5	27	6.0
	JB2	15	7.6	30	5.0
	JB3	23	7.4	44	4.9
Sewell Ridge	SR1	17	9.2	40	6.0

5.3.5 Statistical data analysis

Given the correlation between environmental variables related to oceanographic properties and geomorphometry, Principal Component Analysis (PCA) was used to reduce the dimensions of the variables. Mean temperature (°C) was removed from analysis given its lack of spatial variability among subregions (on average, within ~0.2°C). Principal components were retained when they explained more variance than the null model (i.e., eigenvalues > 1). Environmental variables were tested for normality prior to PCA using the Shapiro-Wilk tests, and were square-root- or log10-transformed, if needed. Environmental variables were standardized with zero mean and unit standard deviation.

Stepwise multiple regression was used to assess the relationship between principal components (related to oceanography and geomorphometry) and variables on substrate complexity, to mean epifaunal cover (%), maximum epifaunal cover (%) and expected morphospecies richness (based on sample-based rarefaction analysis with a sample of 12 images). The best model was determined using the Akaike information criterion. Epifaunal cover was log-transformed prior to analysis, and normality of residuals was tested using Shapiro-Wilk tests.

Differences in community composition between transect, and the potential environmental drivers of communities were assessed using ordination. Rare morphospecies (i.e., only 1 occurrence in the dataset; n = 11) were removed prior to analysis. Ordination of communities by transects was performed with non-metric

multidimensional scaling (nMDS). Biological distance between communities was assessed using the Jaccard Index for presence-absence of community data. Correlation between ordination scores and environmental variables was subsequently assessed by fitting environmental vectors in the ordination space. 'Significance' (pseudo) was tested with permutations (n = 999), and goodness-of-fit was determined with squared correlation coefficients (r^2). Analyses were performed in the R environment using the 'vegan' package (Oksanen et al. 2016).

5.4 Results

5.4.1 Abundance and community composition of epibenthic megafauna

Overall mean epifaunal cover across the 20 transects surveyed was 7.7 % (± 16.0% (SD); Fig. 5.3a). In only 13 images (4% of the dataset) was epifaunal cover > 50%, while only in 9 images (3% of the dataset) was it > 75%, and those were found in Browns Channel (3 in BC1, 2 in BC2), and Jordan Basin (4 in JB1). The highest mean epifaunal cover was found in BC1-1 (34.4 ± 33.9%; Fig. 5.3b), while the lowest was in BC2-2 (0.2 ± 0.6%; Fig. 5.3b). Intermediate values of epifaunal cover were found in JB1 (transect #1: 20.8 ± 31.0%; transect #2: 22.6 ± 23.2%; transect #3: 18.0 ± 24.3%) and BC2-3 (15.9 ± 25.8%). Between subregions, JB1 showed the highest mean epifaunal cover (20.8 ± 26.0%), while Sewell Ridge (SR1) showed the lowest mean epifaunal cover (1.4 ± 1.7%).

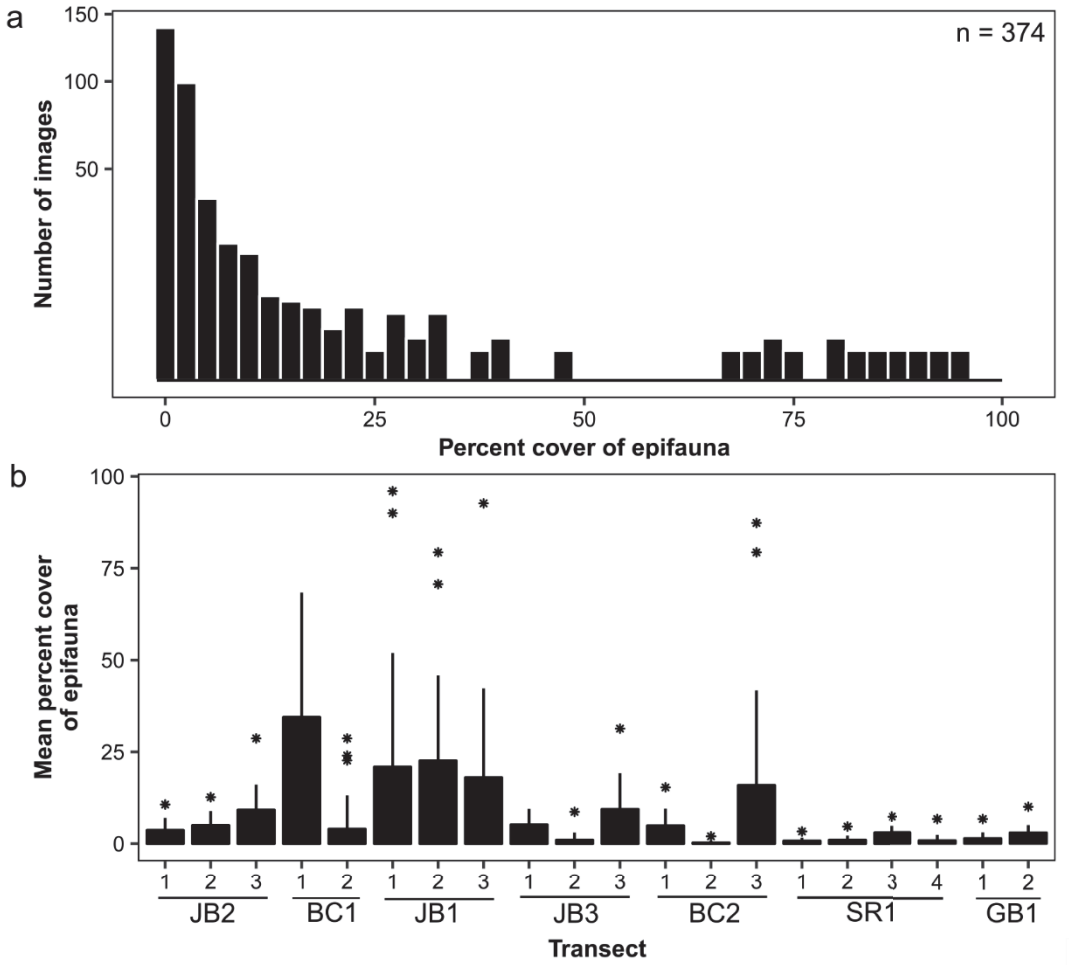

Figure 5.3: (a) Frequency distribution of epifaunal cover (%) among all transects (n = 374 images; shown on a square-root scale of frequency). (b) Mean percent cover (+ sd) between transects (each subregion is indicated below numbered transects). Outliers (i.e., more than 1.96 x standard deviation) are shown with '*'. The order of subregions reflects increasing depth.

Epibenthic megafaunal communities in Jordan Basin and Browns Channel were dominated by morphospecies dwelling on hard and/or mixed substrate, sporadically forming dense faunal mats (Fig. 5.4; Table 5.4). In Jordan Basin, a diverse community composed of sea stars (Fig. 5.5a), the brachiopod *Terebratulina septentrionalis* (Fig. 5.5b), 8 morphospecies of anemones (Fig. 5.5c), and sponges was recorded (Fig. 5.4b;

Table 5.4). The communities in Browns Channel were dominated by sponges, sea stars and dense cover of bryozoans (Fig. 5.4a; Table 5.4) in one subregion (BC1). In the other subregion (BC2), sporadic occurrences of high density of the brittle star *Ophiacantha* sp. were recorded (Fig. 5.4c; Table 5.4). In contrast, the communities in Georges Basin were dominated by soft-substrate morphospecies, with an high abundance of an unidentified brittle star (Ophiuroidea sp. 1), which was often half-buried in the sediment. A taxon of a stalked tunicate (Tunicata sp. 3) was also abundant in this region relative to other regions (Table 5.4). Overall, cnidarians (in particular anemones and *Epizoanthus* sp.) and poriferans dominated the communities recorded in the survey, both in terms of occurrences and morphospecies diversity (Table 5.4). Echinoderms – in particular sea stars – were diverse, but only sporadically observed for most morphospecies. Only the ophiuroid *Ophidomopholis aculeata* was more broadly distributed than other taxa. Among all morphospecies, the brachiopod *Terebratulina septentrionalis* was observed most often with 131 occurrences recorded in the survey (Fig. 5.5b; Table 5.4).

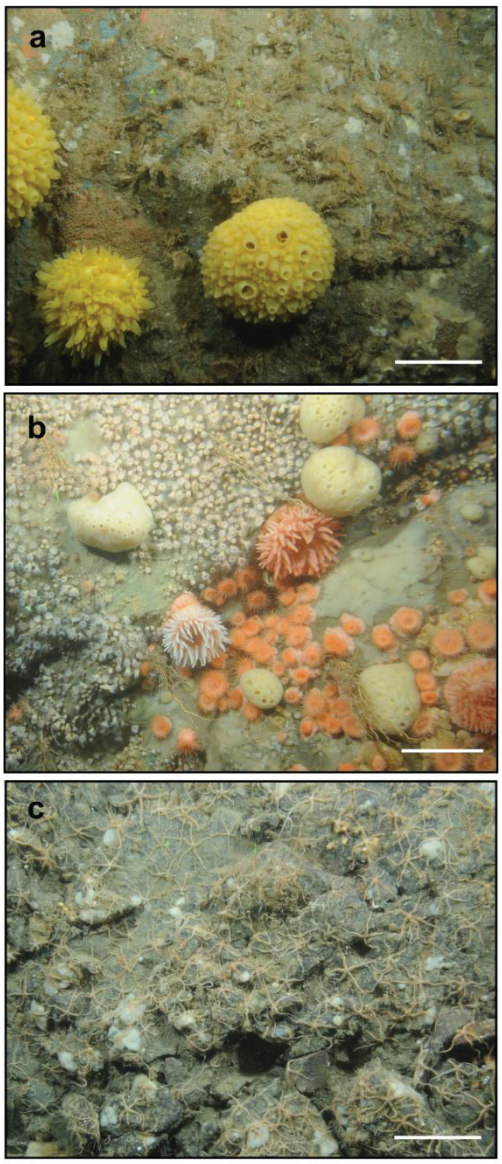

Figure 5.4: Occurrences of dense epifaunal cover in the eastern Gulf of Maine. (a) Browns Channel (BC1-1); depth: 119 m. (b) Jordan Basin (JB1-1); depth: 131 m. (c) Browns Channel (BC2-3); depth: 240 m. Scale bar: 10 cm.

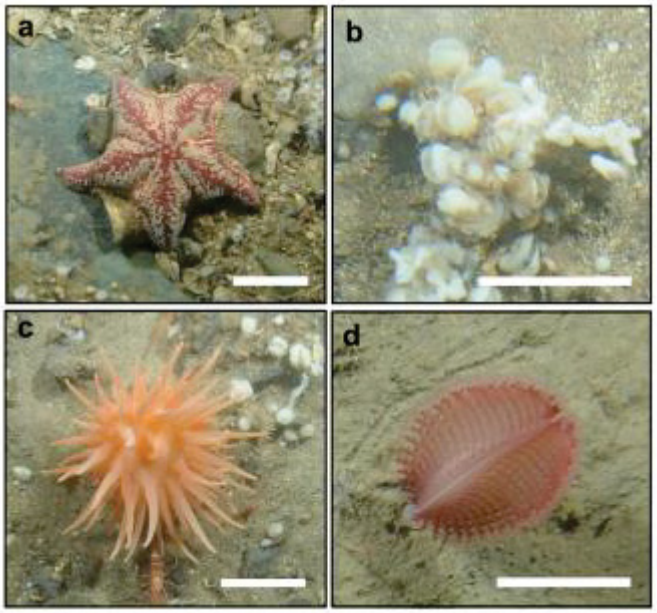

Figure 5.5: Benthic taxa found in the deep waters of the eastern Gulf of Maine. (a) *Porania* sp.; Jordan Basin (JB1-1); depth: 148 m. (b) *Terebratulina septentrionalis*; Jordan Basin (JB3-3); depth: 172 m. (c) *Urticina crassicornis*; Jordan Basin (JB3-3); depth: 198 m. (d) Pennatulacea. Sewell Ridge (SR1-3); depth: 224 m. Scale bar: 5 cm.

Table 5.4: Occurrences of epibenthic taxa recorded in the video transects in the eastern Gulf of Maine in 7 subregions of 5 physiographic regions. 'JB' = Jordan Basin; 'BC' = Browns Channels; 'SR' = Sewell Ridge; 'GB' = Georges Basin. Order of subregions reflects increasing depth.

Phylum	Taxa	JB2	BC1	JB1	JB3	BC2	SR1	GB1
Cnidaria	Octocorallia	0	0	0	0	0	1	0
	Pachycerianthus borealis	1	0	2	1	0	9	3
	Ceriantharia	0	0	0	0	0	0	3
	Urticina felina	1	2	3	3	0	0	0
	Urticina crassicornis	0	0	4	7	0	1	0
	Stomphia coccinea	5	1	1	0	0	0	0
	Antholoba achates	0	1	6	0	1	8	0
	Hormathia nodosa	0	1	12	0	0	0	0
	Solitary anemone 1	1	0	1	3	0	16	0
	Solitary anemone 2	0	0	1	0	0	1	0
	Epizoanthus sp.	0	1	25	8	11	0	0
	Pennatulacea	0	0	0	1	0	28	8
	Hydrozoa	4	3	1	2	2	4	0
Echinodermata	*Ophidomopholis aculeata*	1	2	7	3	1	3	1
	Ophiuroidea sp. 1	0	0	0	0	4	1	18
	Ophiura sp.	0	0	1	0	0	0	0
	Ophiacantha sp.	0	0	0	0	13	0	8
	Porania sp.	0	0	0	1	1	0	0
	Asteroidea sp. 1	2	2	7	1	0	1	0
	Asteroidea sp. 2	1	1	0	0	0	0	0
	Asteroidea sp. 3	1	0	0	0	0	3	0
	Asteroidea sp. 4	0	3	0	0	3	0	0
	Asteroidea sp. 5	0	5	0	0	0	0	0
	Asteroidea sp. 6	0	0	1	0	0	0	0
	Asteroidea sp. 7	0	0	2	0	0	0	1
	Asteroidea sp. 8	0	0	2	0	0	0	0
	Asteroidea sp. 9	1	0	0	0	0	0	0
	Crinoidea	1	0	4	5	8	0	17
Porifera	Encrusting porifera sp. 1	16	10	19	8	25	16	6
	Encrusting porifera sp. 2	3	3	3	0	3	1	0
	Encrusting porifera sp. 3	4	8	7	1	8	2	0
	Encrusting porifera sp. 4	8	4	1	0	1	0	0
	Encrusting porifera sp. 5	4	11	5	1	2	9	0
	Encrusting porifera sp. 6	0	5	5	0	0	0	0
	Encrusting porifera sp. 7	1	0	0	0	0	0	0
	Erect porifera sp. 1	17	3	0	21	0	7	0
	Erect porifera sp. 2	0	0	0	0	0	2	1
	Bulbous porifera sp. 1	12	0	8	2	0	0	0
	Bulbous porifera sp. 2	2	2	11	1	0	0	1
	Bulbous porifera sp. 3	0	0	0	0	0	0	1
	Bulbous porifera sp. 4	11	5	1	0	0	0	0
	Bulbous porifera sp. 5	0	9	3	0	1	2	0
	Bulbous porifera sp. 6	0	5	0	0	0	0	0
Brachiopoda	*Terebratulina septentrionalis*	53	1	33	27	0	13	4

Table 5.4 (continued)

Phylum	Taxa	JB2	BC1	JB1	JB3	BC2	SR1	GB1
Tunicata (subphylum)	Tunicata sp. 1	9	1	20	6	0	1	0
	Tunicata sp. 2	1	0	4	0	0	2	0
	Tunicata sp. 3	0	0	0	1	0	5	22
Arthropoda	Decapoda	2	0	0	1	0	0	0
	Pycnogonida	0	0	1	0	0	0	0
	Cirripedia	1	0	0	0	0	0	0
Mollusca	Bivalvia	2	2	0	0	0	0	0
	Flabellina sp.	1	1	0	1	0	0	0
	Cephalopoda	0	0	0	0	0	1	0
Bryozoa	*Caberea ellisii*	16	11	4	2	2	0	0
	Bryozoa sp. 1	4	4	3	1	14	2	0
Worms	Worm sp. 1	4	0	2	0	0	0	0
	Worm sp. 2	2	0	0	1	0	0	0
Undetermined	Und. sp. 1	0	0	2	0	0	0	0
	Und. sp. 2	1	0	0	0	0	2	0
	Und. sp. 3	0	0	0	0	0	0	1
	Und. sp. 4	0	1	0	0	0	0	0
	Und. sp. 5	3	0	0	0	0	0	0

In total, 62 morphospecies were observed in the survey, 11 of which occurred only once. Maximum richness per image was 13 morphospecies (JB1), while median richness was 2 morphospecies. Between subregions, the highest diversity was recorded in Jordan Basin (JB1: 36 morphospecies; JB2: 34 morphospecies) and Browns Channel (BC1: 29 morphospecies). The least diverse regions were also in Browns Channel (BC2: 17 morphospecies) and in Georges Basin (15 morphospecies). When standardized to a sample size of 12 images, expected morphospecies richness was highest in Jordan Basin

(JB1-3; Fig. 5.6) and Browns Channel (BC1-1; Fig 5.6), and lowest in one subregion of Browns Channel (BC2-2; Fig. 5.6).

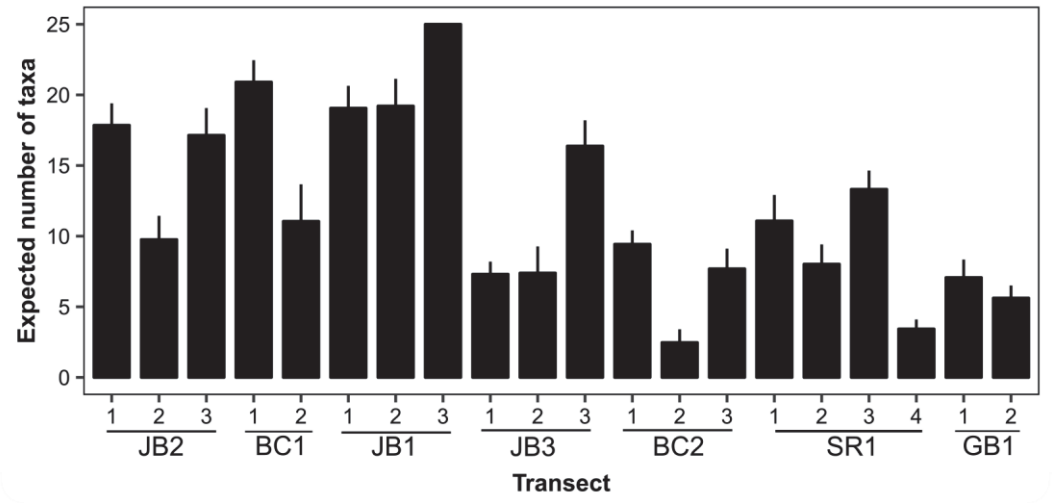

Figure 5.6: Expected taxa richness (+ sd) based on sample-based rarefaction analysis for each transect (n = 12 images). Subregion is indicated for the numbered transect. The order of subregions reflects increasing depth.

5.4.2 Patterns in substrate complexity, geomorphometry, and oceanographic properties

Browns Channel (BC1, BC2) and 2 subregions of Jordan Basin (JB1, JB2) had overall coarser substrate and more variable bathymetric features than the other subregions. A mixture of boulders, cobbles, and pebbles observed in these areas translated into high mean substrate complexity (e.g. BC1-1, JB2-1), and high variability in substrate complexity (JB1-1, BC1-1), due to the sporadic presence of finer-grain sediment (Fig. 5.7a). Maximum deviations from the average depth were observed in these

areas with radii of 1000 m (BC1-1: 57.8 m; BC2-3: 52.1 m) and 5000 m (BC2-3: 75.4 m; JB2-1: 63.0 m). Mean deviation from average depths was high in Jordan Basin (JB2-1; Fig. 5.7b) within a 1000-m radius. Minimums in BPI were observed in one subregion of Browns Channel (BC2-3) at scale lengths of 1000 m (-52 m) and 5000 m (-75 m), while maximums in BPI were observed in Jordan Basin (JB2-1) at scale lengths of 1000 m (28 m) and 5000 m (62 m). The highest mean BPI (in absolute values) were recorded in Jordan Basin (JB2-1 with both scale lengths; Fig. 5.7c) and in Browns Channel (BC1-1 with a scale length of 1000 m; BC2-3 with a scale length of 5000 m; Fig. 5.7c).

In contrast, transects in Sewell Ridge (in particular, SR1-1 and SR1-2) and transects in Georges Basin were dominated by fine-grain sediment, with the occasional presence of coarse sediment, and relatively flat relief on the seafloor. Mean substrate complexity (and variability) was low (Fig. 5.7a), mean deviations from average depths oscillated around 1 m within radii of both 1000 m and 5000 m (Fig. 5.7b), and the lowest BPI were near 0 in these areas (Fig. 5.7c).

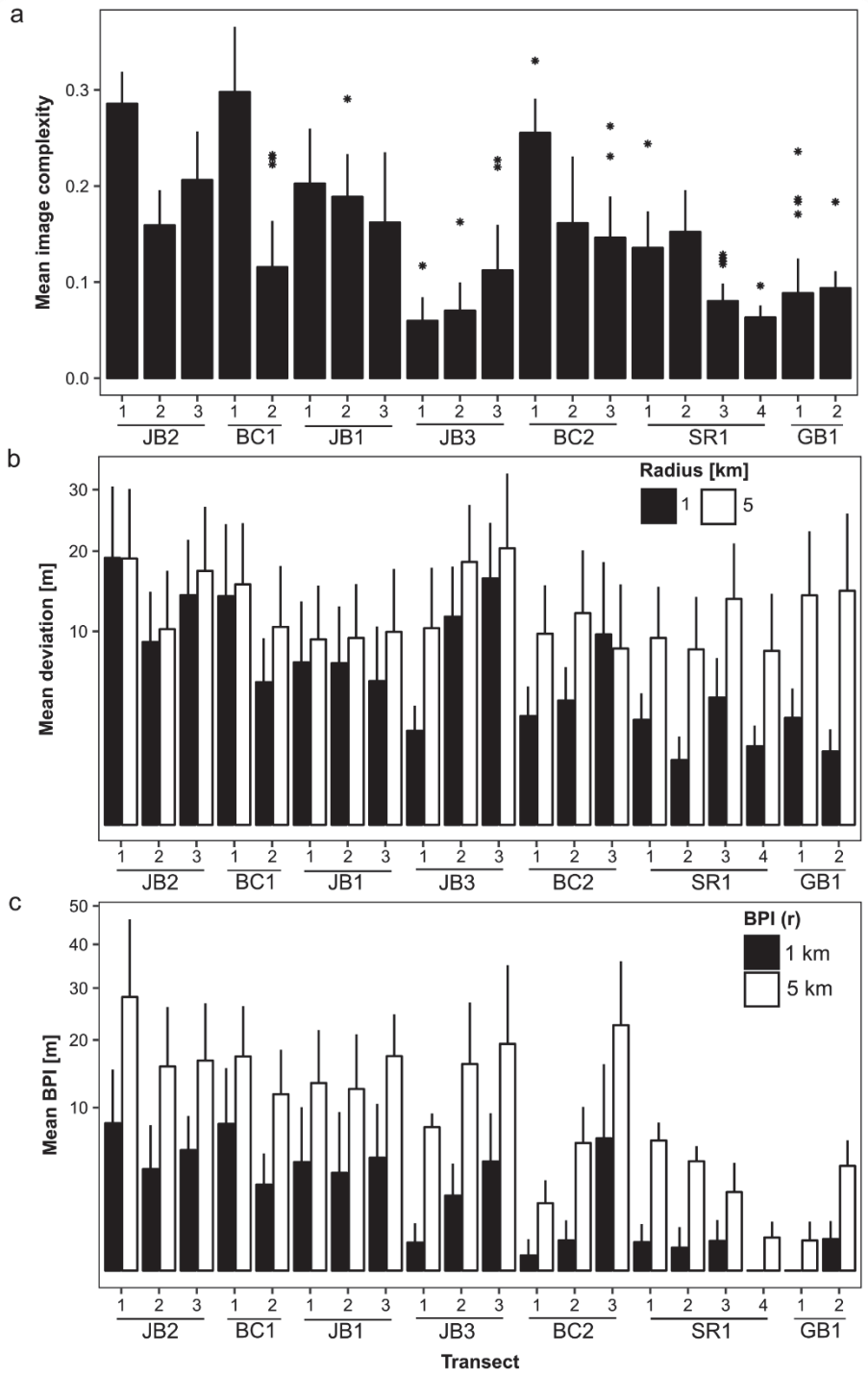

Figure 5.7: Geological features in 20 transects in 7 subregions in the eastern Gulf of Maine ('JB' = Jordan Basin, 'BC' = Browns Channel, 'SR' = Sewell Ridge, 'GB' = Georges Basin). The order of subregions reflects increasing depth. (a) Mean image complexity (+ SD). Outliers (> 1.96 * SD) are indicated with '*'. (b) Mean deviation from average depth within 2 radii (1 and 5 km). (c) Mean bathymetric position index (BPI) (+SD) using a radius of 1 km and 5 km.

Overall, a strong seasonal signal in flow and oceanographic properties was detected in one subregion of Browns Channel (BC1) relative to other subregions. Intermediate strength and directionality in flow was also detected in Jordan Basin (JB1) and the other subregion in Browns Channel (BC2). Current speed and estimates of Kappa parameter was highest in BC1 over the 10-year period, and intermediate values were found in JB1 and BC2 (Fig. 5.8a), reflecting strong, quasi-unidirectional currents in these areas. Mean temperature was relatively constant among subregions (7.9 – 8.1°C), with BC2 being slightly warmer and JB2, slightly cooler (Fig. 5.8b). Variability in temperature was widest in Browns Channel (BC1, BC2) and Jordan Basin (JB2) (Fig. 5.8b). In contrast, mean salinity varied between subregions, being lowest in BC1 with the largest variability, and highest in Georges Basin and Sewell Ridge with minimal variability (Fig. 5.8b). Patterns in seasonality were also detected with mean amplitude of temperature and salinity, being widest in one subregion of Browns Channel (BC1), with intermediate values in Jordan Basin and the other subregion of Browns Channel (Fig. 5.8d); Sewell Ridge and Georges showed the narrowest annual amplitude in these properties (Fig. 5.8d). One subregion of Browns Channel (BC1) also had strong annual amplitudes of mean current speed and Kappa parameters, but patterns were less clear in other subregions (Fig. 5.8c).

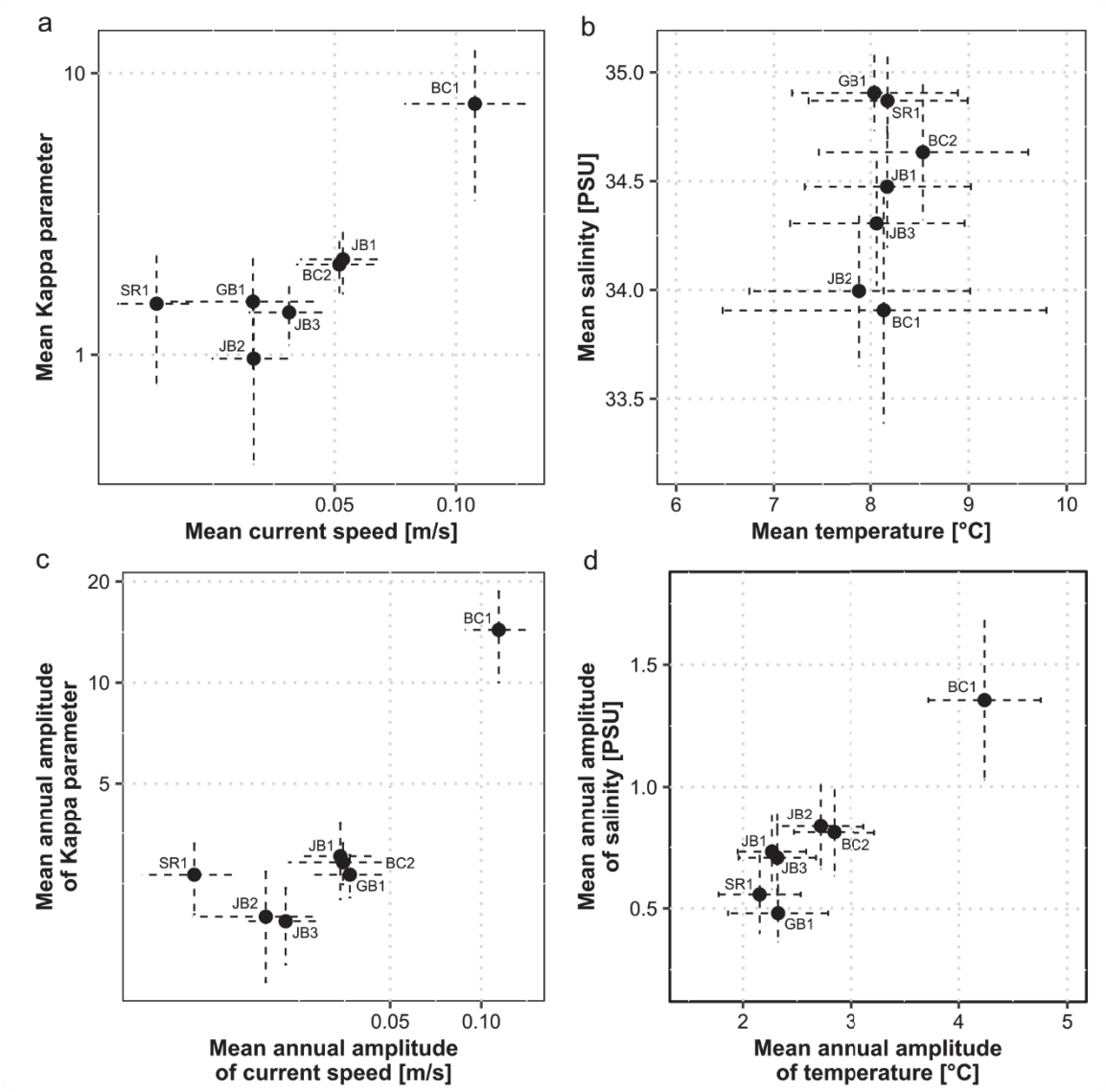

Figure 5.8: Oceanographic features in 7 subregions of the eastern Gulf of Maine over a 10-year period (1998-2008) recorded as monthly means (n = 120 for a,b; n = 10 for c,d). Variables are combined to describe hydrodynamic regimes (current speed and Kappa parameter) and hydrographic conditions (temperature, salinity). ('JB' = Jordan Basin, 'BC' = Browns Channel, 'SR' = Sewell Ridge, 'GB' = Georges Basin). (a) Mean current speed (± SD; m/s) and mean Kappa parameter (± SD), and (b) mean salinity (± SD; PSU) and mean temperature (± SD; °C). (c) Mean annual amplitude of current speed (± SD; m/s) and Kappa parameter (± SD), and (d) salinity (± SD; PSU) and temperature (± SD; °C).

5.4.3 Environmental drivers of epibenthic megafaunal communities

Two principal components were retained for both oceanographic variables (89% of the variance explained; Table 5.5) and geomorphometric variables (95% of the variance explained; Table 5.5). Environmental variables related to substrate complexity (mean and standard deviation) were uncorrelated. Six environmental variables were hence used in subsequent analyses: 2 principal components for each group of oceanographic and geomorphometric variables, and 2 variables related to substrate complexity.

Mean epifaunal cover (%) in each transect was best explained by geomorphometry (Table 5.6), in particular its first principal component, which was strongly correlated with variability in depth within a radius of 1000 m (Table 5.5). Geomorphometry and oceanography explained maximum epifaunal cover, although the contribution of oceanographic properties was negligible when controlling for other variables. A negative contribution to R^2 may indicate an interaction between these environmental variables.

Expected morphospecies richness was best explained by a combination of geomorphometric features (PC1) and variability in substrate complexity, although the latter was marginally significant (Table 5.6). Strong outliers in the relationship between variability in substrate complexity and expected richness might reduce the importance of this predictor variable, since correlation was significant ($r = 0.53$, $p = 0.008$, Fig. 5.9), but much stronger when removing the 4 outlier transects ($r = 0.92$, $p < 0.001$).

Table 5.5: Factor loadings of principal components derived from variables related to geomorphometry (n = 8) and oceanography at the seafloor (n = 15). 'sd' = standard deviation. 'AA' = annual amplitude. Proportion of variance explained is indicated with each principal component.

Geomorphometry	Variable	PC1 (76 %)	PC2 (19%)
	Deviation mean depth – 1 km (mean)	0.96	-0.07
	Deviation mean depth – 1 km (sd)	0.97	0.10
	Deviation mean depth – 5 km (mean)	0.56	-0.80
	Deviation mean depth – 5 km (sd)	0.58	-0.77
	BPI – 1 km (mean)	0.94	0.28
	BPI – 1 km (sd)	0.88	0.41
	BPI – 5 km (mean)	0.95	0.19
	BPI – 5 km (sd)	0.97	0.06
Oceanography		**PC1** (79 %)	**PC2** (9%)
	Current speed (mean)	-0.96	0.06
	Current speed (sd)	-0.86	0.35
	Current speed – AA (mean)	-0.88	0.35
	Current speed – AA (sd)	-0.88	0.26
	Kappa parameter (mean)	-0.90	0.27
	Kappa parameter (sd)	-0.88	0.18
	Kappa parameter – AA (mean)	-0.94	0.22
	Kappa parameter – AA (sd)	-0.91	-0.14
	Temperature (sd)	-0.94	-0.2
	Temperature – AA (mean)	-0.97	-0.07
	Temperature – AA (sd)	-0.70	0.37
	Salinity (mean)	0.69	0.64
	Salinity (sd)	-0.93	-0.36
	Salinity – AA (mean)	-0.96	-0.28
	Salinity – AA (sd)	-0.88	-0.37

Table 5.6: Results of stepwise multiple linear regression analyses of average and maximum cover of epifauna, and diversity (i.e. expected richness based on rarefaction analysis) in transects in the eastern Gulf of Maine (n = 20). Data were standardized prior to analyses. Only significant environmental predictors are included ($p < 0.05$). ('MS' = 0.05 $p < 0.10$)

Response variable	Relationship	R^2	Adj. R^2	*p* value	Contribution to R^2
Mean epifaunal cover (MeanEC)	MeanEC = 0.73*Geo.PC1 + 0.43*Geo.PC2	0.55	0.46	0.005	Geo.PC1 (0.42) Geo.PC2 (0.17)
Max epifaunal cover (MaxEC)	MaxEC = 0.77*Geo.PC1 + 0.53*Geo.PC2 + 0.41*Ocean.PC2	0.66	0.60	< 0.001	Geo.PC1 (0.44) Geo.PC2 (0.25) Ocean.PC2 (-0.02)
Expected richness (ER)	ER = 0.45*Geo.PC1 + 0.36*Complexity.sd$^{(MS)}$	0.46	0.40	0.005	Geo.PC1 (0.27) Complexity.sd (0.19)

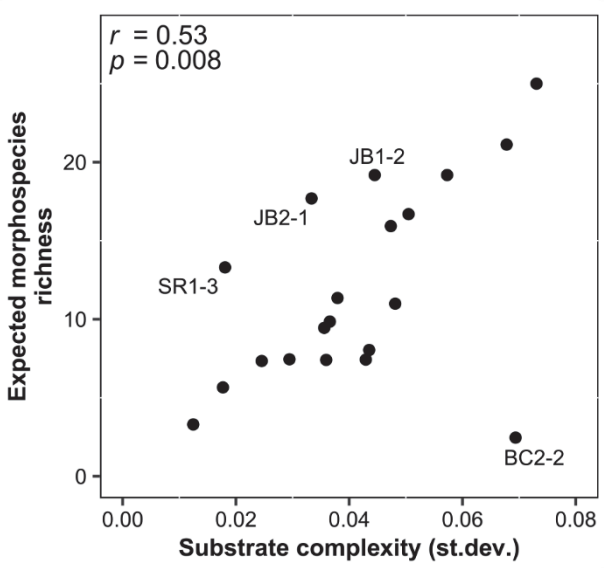

Figure 5.9: Relationship between variability in substrate complexity (computed with object-based image analysis) and expected morphospecies richness (sample-based rarefaction analysis, n = 12 images) for 20 transects in the eastern Gulf of Maine. Outliers are indicated ('BC' = Browns Channel, 'JB' = Jordan Basin, 'SR' = Sewell Ridge). Pearson's correlation coefficient (*r*) and *p* are indicated.

Ordination revealed no obvious clusters in community composition among transects (Fig 5.10). Transects within subregions in Jordan Basin were relatively closer to each other in the ordination space relative to other subregions, where transects were more distinct from one another, in particular transects in one subregion of Browns Channel (BC2) and Georges Basin (GB1) (Fig. 5.10). Overall, transects in deeper waters in habitats dominated by soft sediment had positive values of ordinations scores (both nMDS1 and nMDS2; Fig. 5.10). Communities thriving in shallower regions, with a more complex geomorphometry and greater variability in substrate complexity had negative values of ordination scores (Fig. 5.10). Differences in community composition were most

strongly related to gradients in substrate complexity, and the second principal component of the bottom oceanographic features (Table 5.7).

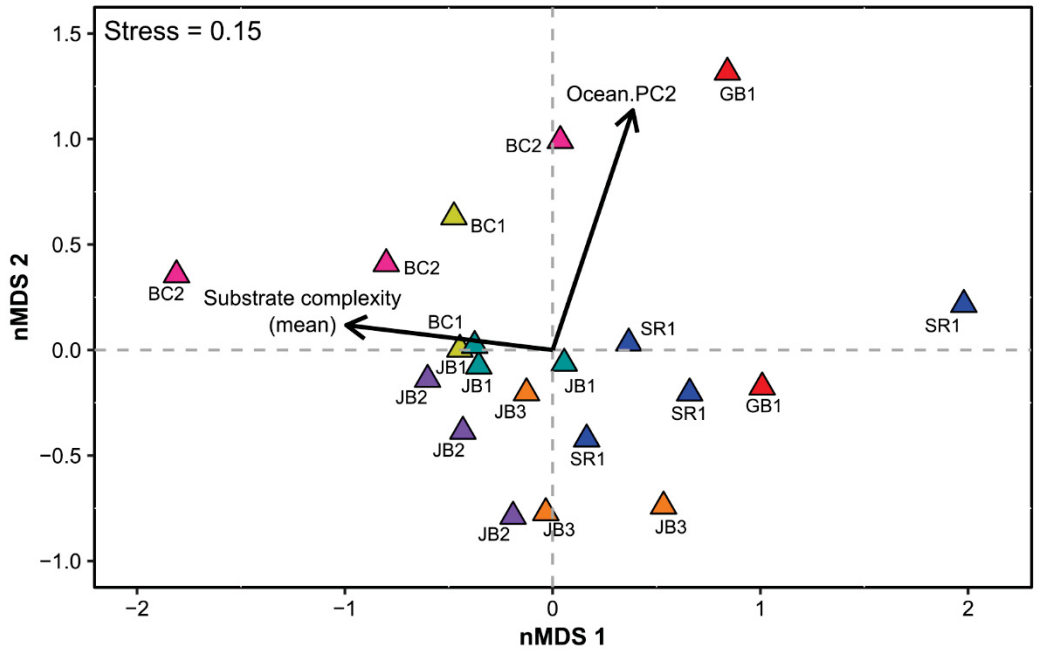

Figure 5.10: Ordination of communities among transects based on the Jaccard Index (presence/absence of taxa; 51 taxa were considered). Gradients in the 2 environmental factors best correlated with changes in communities are shown and their length is proportional to their relative squared correlation coefficient (mean substrate complexity and the second principal component of the bottom oceanographic features 'Ocean.PC2'). Subregions are indicated with labels and colours.

Table 5.7: Coefficients of determination and (pseudo) significance (i.e., proportion > *r*; 999 permutations, '*' indicates significance for $\alpha = 0.05$) of fitted environmental vectors (variables) to the ordination (nMDS) of epibenthic megafaunal communities among transects.

Environmental variable	r^2	Proportion > *r*
Substrate complexity (mean)	0.40	0.012*
Substrate complexity (sd)	0.47	0.004*
Geo.PC1	0.20	0.17
Geo.PC2	0.03	0.79
Ocean.PC1	0.24	0.10
Ocean.PC2	0.49	0.005*

5.5 Discussion

The composition and diversity (measured with rarefaction-based expected richness) of epibenthic megafaunal communities were correlated with the physical characteristics of the substrate, both through its complexity (and the spatial variability in complexity) and geomorphometric features. In offshore benthic habitats, the relationship between the sediment and diversity of megafauna depends on the range of particle grain size. In the deep ocean, variation in megabenthic assemblages was observed in the presence of coarser-grain fraction on the abyssal plains (Durden et al. 2015), and on the continental slope where higher diversity was correlated with an increased presence of hard substrate as ice-rafted drop stones (Jones et al. 2007). Enhanced species richness has also been recorded at shallower depths in areas with coarser sediment on a bank off the coast of Norway (Buhl-Mortensen et al. 2009), and in the Gulf of Maine on Browns Bank (Kostylev et al. 2001). Here, the use of computer vision allowed a clear quantification of substrate complexity as a proxy of substratum type – and its spatial

variability along transects – along a continuous scale. Although we cannot speculate outside of the environmental range observed in the study area, this approach demonstrates that the relationship between sediment properties (namely spatial variability at local scales of 10s to 100s m) and diversity in epibenthic megafauna could lack thresholds and/or discrete bounds, and hence be best described as a continuous relationship.

The influence of geomorphometry on benthic megafaunal communities is difficult to disentangle from the effect of sediment properties. On a shallow bank off the Australian coast, community composition was spatially correlated with discrete habitats (described as 'biotopes') that were derived from a combination of both seafloor geomorphology and substrate type (e.g. 'granite outcrop') (Beaman et al. 2005). 'Geomorphological zones' also influenced megafaunal community composition (but not diversity) on the Mauritian continental slope (Jones and Brewer 2012). In reality, the effect of variability in seafloor geomorphic features on the composition of megafaunal communities may depend on the diversity of feeding guilds. For example, rugosity, slope, and the bathymetric position index were significant drivers of spatial turnover in communities of sessile-suspension feeders on the Mingulay Reef off the coast of Scotland (Henry et al. 2010). On the Nigerian continental slope, enhanced diversity of suspension-feeding species was observed in steep-slope areas, but no clear pattern in richness of deposit-feeders was detected (Jones et al. 2013). This effect on suspension-feeding taxa was most likely due to the interaction between steep bathymetry and near-seafloor hydrodynamics, which can also influence the local abundance of epibenthic megafauna.

In this study, dense epifaunal cover was very sparse, and influenced by geomorphometry and oceanographic properties. In general, the role of oceanographic properties in influencing deep-water epifaunal abundance relates to food supply, either through their influence on surface primary productivity and subsequent export to the seafloor, or direct influence on particle encounter rate at depths. For example, enhanced megafaunal abundance off the coast of Brazil was related to organic enrichment through coastal upwelling (De Léo et al. 2006), while temperature-related changes in surface productivity affected megafaunal abundance in the deep ocean on relatively short (5 years) timescales (Bergmann et al. 2011). Alternatively, accelerated flow in areas of steep bathymetric features can influence the occurrence and abundance of cold-water corals along the continental break (Mohn et al. 2014), and at finer spatial scales between individual reefs (Duineveld et al. 2012). Dense assemblages of epifaunal filter-feeders were also observed on scarcely-distributed vertical walls and over-hangs in a submarine canyon, and were attributed to local interactions with internal waves (Johnson et al. 2013; Robert et al. 2015).

In the Gulf of Maine, currents did not explain a significant amount of variability in epifaunal cover. However, high epifaunal cover (i.e., > 75%) was recorded sporadically in areas of distinct hydrodynamic regimes, namely in Browns Channel (BC1), where swift, focused currents dominated, and in Jordan Basin (JB1) and the other subregion of Browns Channel (BC2), where intermediate values of mean current speed and Kappa parameters occurred. Broader-scale oceanographic features might be driving fast currents in these areas. In Jordan Basin, a cyclonic (counterclockwise) gyre forms

seasonally in surface waters, and this gyre extends to the seafloor (Aretxabaleta et al. 2014). The potential for re-suspension is high within the basin: the benthic nepheloid layer is thick relative to areas closer to shore, particularly in the middle of the basin, where it can reach upwards of 55 m above the seafloor (Pilskaln et al. 2014). One subregion of Jordan Basin (JB1) lies at the periphery of this gyre, where the thickness of the benthic nepheloid layer is estimated at 27-28 m (Pilskaln et al. 2014), potentially explaining both the presence of faster currents relative to other regions, and the enhanced potential for particle delivery to suspension-feeders. Fast near-bottom (i.e. at depths > 100 m) currents also occur in the eastern Gulf of Maine flowing north in Northeast Channel along Browns Bank, with a seasonal eastward flow around the bank into Browns Channel (Xue et al. 2000). One subregion in Browns Channel (BC2) lies within this flow pattern, whereas the other (BC1) is also potentially influenced by the seasonal inflow of Scotian Shelf Water. However, this latter current seems to dominate on the northern flank of Browns Channel, near German Bank, rather than on the southern flank where the study was conducted. These inflow patterns in the Gulf of Maine not only affect current speed and directionality, but also oceanographic properties near the seafloor.

At larger spatial scales (10s – 100s km), oceanographic properties may also influence the composition of benthic megafaunal communities, but sharp discontinuities in conditions may be required to discern their effect. The effect of oceanographic 'regimes' on benthic megafauna at these scales has been reported in submarine canyons off the coast of Australia, where strong vertical zonation in communities coincided with discontinuities in the vertical structure of water masses (although the effect of depth

cannot be disregarded entirely) (Beaman et al. 2005). Similarly, depth-corrected temperature was found to be strong indicator of spatial turnover of communities on the Chatham Rise, east of New Zealand (Compton et al. 2013). In the Gulf of Maine, oceanographic properties (e.g., satellite-derived sea surface temperature, summer surface stratification) were amongst the most important predictors of compositional change of benthic fauna (Pitcher et al. 2012). However, in the eastern Gulf of Maine in particular, the continuous progression of water properties near the seafloor might explain the overall lack of sharp demarcation in community composition.

Three processes are thought to control properties of bottom waters in the Gulf proper (reviewed in Mountain & Jessen 1987). First, inflow is observed at 2 locations. Most of the inflow consists of warm and salty (salinity > 34.0) slope water into the deep layer from Northeast Channel, which forms the only deep connection of the Gulf to the open ocean (Ramp et al. 1985). This inflow subsequently spills into all deep basins, and is considered to cause in part the formation of gyres in Jordan and Georges Basin (Brooks 1985). An additional seasonal inflow of Scotian Shelf Water, which is relatively colder and fresher, flows around the coast of Nova Scotia, northwestward into Jordan Basin and the mouth of the Bay of Fundy (Smith 1983). Second, density-driven vertical convection (mostly in winter) mixes the upper layers of the water column, and is thought to be limited to 100 m from the surface, thus isolating bottom waters, however deep convection has been observed occasionally in Jordan Basin. Third, turbulent mixing enhanced by strong tidal currents and irregular bottom topography creates spatial gradients in bottom water properties, with salinity generally decreasing from Northeast Channel onto Georges

Basin, and subsequently, Jordan Basin (shown in Mountain & Jessen 1987). These broad oceanographic features of the eastern Gulf of Maine were reproduced well by the ocean circulation model used in this study, particularly the spatial gradient in salinity. Large variability in temperature and salinity in the shallowest areas (i.e., one subregion of Browns Channel, and of Jordan Basin) are hypothetically attributed to vertical mixing where tidal currents are strongest, while the low annual variability in other regions would indicate the decoupling of bottom oceanographic features from seasonal variability in water column dynamics. Under these conditions, Georges Basin, Sewell Ridge, and some areas of the second subregion of Browns Channel could be influenced by a similar oceanographic regime, distinct from the one influencing both Jordan Basin and Browns Channel. This could have an effect on community composition, but large differences should not be expected given the connectivity of the area.

This study has shown that different descriptors of biological communities interact with spatial scale differently, justifying the use of a multiscale approach to detect differences in environmental drivers. The effect of fine- to local-scale features was apparent for diversity, but epifaunal abundance was best explained by local- to meso-scale features. Concurrently, a multiscale approach could be used used for community composition, since it was affected in this study by both fine- to local-scales factors (i.e., substrate complexity), and mesoscale oceanographic properties. Uncertainties remain, however, on the most appropriate scale driving the distribution of these communities. Local-scale variability in geomorphometry (10s m) could reveal important features that influence megafaunal communities, particularly in areas of greater variability in terrain

(i.e., Jordan Basin and Browns Channel), which could only be captured by acoustic surveys. Similarly, fine-scale current features could best explain patterns in epifaunal abundance, but such measurements are unavailable for the study area. The influence of water column dynamics, and not only bottom water properties, could also reveal important patterns in the spatial structure of the oceanography in the area, which could be important indicators of the distribution of epibenthic megafaunal communities on deep continental shelves.

CHAPTER 6

DELIMITING OCEANOGRAPHIC PROVINCES TO DETERMINE DRIVERS OF MESOSCALE PATTERNS IN BENTHIC MEGAFAUNA: A CASE STUDY IN THE BARENTS SEA[4]

6.1 Abstract

Communities of benthic megafauna in the deep waters of continental shelves (> 100 m) are important components of marine ecosystems. In high-latitude ecosystems, this fauna is increasingly impacted by human activities and climate variability. In this study, we provide baseline knowledge on the oceanographic conditions affecting its distribution in the Barents Sea in the vicinity of the Polar Front - an oceanic front occurring at the transition zone between the Atlantic and Arctic water masses. We used fields of temperature and currents from an ocean circulation model (Regional Ocean Modelling System - ROMS) to derive variables divided into 3 groups relevant to bottom fauna (temperature, water column structure and bottom currents) expressing either mean conditions or temporal variability over 10 years (2001-2010). Benthic megafauna was surveyed in summer 2011 at 139 sites. To analyze the relationship between spatial variability in the composition of benthic megafauna (i.e., β-diversity) and oceanographic conditions, we: 1) used generalized dissimilarity modelling (GDM), and 2) delimited

[4] Lacharité, M., L.L. Jørgensen, A. Metaxas, V.S. Lien, and H.R. Skjoldal. Submitted to Progress in Oceanography [first submission: January 2016; revised submission: June 2016].

My coauthors Drs. L.L. Jørgensen and V.S. Lien (Institute of Marine Research, Norway) provided guidance and data in the form of epibenthic trawling surveys and outputs of an ocean circulation model, respectively. My coauthor Dr. A. Metaxas supervised the development of the study and analyses. My coauthor Dr. H.R. Skjoldal (Institute of Marine Research, Norway) provided guidance in the development of the study. All coauthors edited the manuscript.

oceanographic provinces (i.e., regions of similar conditions) for each group of variables using principal component analysis (PCA) followed by cluster analysis. Turnover in benthic megafauna was explained by 7 oceanographic variables (temperature: 4, water column structure: 2, bottom currents: 1), depth and geographic distance (56.5% of total deviance explained). Concurrently, patterns in oceanographic provinces among the 3 groups of variables coincided with results from the GDM, where provinces derived from temperature were sharply delimited relative to the other groups. We concluded that the spatial structure of the environment is important in the relationship between spatial variability of benthic megafauna and oceanographic conditions in shelf deep waters. Ocean models are powerful tools to study this relationship, but the way in which their inherent uncertainty affects the conclusions of ecological models should be assessed more thoroughly.

6.2 Introduction

Oceanic fronts occur at the transition between water masses, creating strong horizontal gradients in water properties (e.g. temperature, nutrients). Fronts play a major role in marine ecosystems, since they have a significant impact on their physical, chemical and biological properties, for example by elevating and/or concentrating surface primary production (Tett 1981; Franks 1992), which can in turn impact biological communities on the seafloor through enhanced export of organic matter (Josefson and Conley 1997). Fronts are considered 'hotspots' of marine life because they shape patterns in pelagic and benthic communities by determining biogeographical boundaries (van Aken et al. 1991; Carroll et al. 2008), and by promoting an accumulation of biomass at

several trophic levels near or at frontal boundaries (Bluhm et al. 2007; Landry et al. 2012). On a global scale, the frequency and magnitude of fronts are considered meaningful characteristics to distinguish the various regimes within 'large marine ecosystems' – regions of ocean space on continental shelves, enclosed and semi-enclosed seas with distinct bathymetry, hydrography, productivity and trophic dynamics (Belkin et al. 2009).

The Barents Sea is a continental shelf sea and a transition zone between the Atlantic and Arctic Oceans. The warmer and more saline Atlantic waters meet the colder and less saline Arctic waters at the 'Polar Front', a key oceanographic feature influencing biological communities in the region (Loeng and Drinkwater 2007). The oceanographic properties of the Barents Sea are influenced by the inflow of Atlantic water, which varies monthly and seasonally, and inter-annually (Furevik 2001; Ingvaldsen et al. 2004). The region has recently undergone significant environmental change, which is anticipated to continue in the future. Between the late 1990s and 2010, the surface area occupied by Arctic waters decreased by roughly 50% (Johannesen et al. 2012b). These changes in water mass dynamics are thought to be partially responsible for the decrease in seasonal ice cover (Årthun et al. 2012), although other factors, such as atmospheric conditions (e.g., pressure anomalies and wind patterns), influence sea-ice thickness, extent and import from the Arctic Ocean from year to year (Herbaut et al. 2015). The seasonal ice cover in the Barents Sea, which has a minimum in September and a maximum in April, shows inter-annual to decadal oscillations; however, a significant decrease in cover has been observed since the start of the industrial revolution (Shapiro et al. 2001), and more

acutely in recent decades (Cavalieri and Parkinson 2012). Moderate increases in net surface primary production (NPP) have also been reported in the Barents Sea during the period 1998-2011, with the largest annual NPP reported from the western region of the sea (Dalpadado et al. 2014). Given these recent environmental changes in the Barents Sea, a quantification of baseline patterns of biological communities and the physical factors driving their distribution is needed to better anticipate the magnitude of the impact of future climate variability on these communities.

Deep waters on continental margins (> 100 m depth) harbour abundant and diverse benthic megafaunal communities, particularly in topographically complex habitats (Buhl-Mortensen et al. 2012; Compton et al. 2013; Jørgensen et al. 2015). 'Megafauna' include organisms large enough to be seen in images of the seafloor (> centimetres) or to be caught by fishing trawling gear (e.g. sponges, corals, and brittle stars), and provide an ecologically significant link with pelagic ecosystems, particularly through benthic carbon respiration (Piepenburg et al. 1995). These organisms are heavily impacted by human activities, such as bottom fishing (Mangano et al. 2013; Jørgensen et al. 2016). On a global scale, climate variability can impact deep-water benthic communities, either by altering the magnitude and frequency of food supply (Jones et al. 2014), or by warming near-bottom temperature (Somero, 2012). Therefore, there is a need to include this fauna in an ecosystem approach to marine management, which aims to provide a holistic view of the overall state of an ecosystem.

It is well established that the composition of benthic megafaunal communities on continental margins is influenced by variability in the morphology of the seabed at multiple spatial scales, and the composition of the sediment (Williams et al. 2010; Buhl-Mortensen et al. 2012). However, less is known about the influence of oceanographic conditions – water properties (e.g., temperature, salinity) and hydrodynamics (i.e., the magnitude and direction of currents) – on the composition of these communities. Some evidence points to bottom temperature as a driver of changes in composition at mesoscales (10s – 100s km) (Piepenburg et al. 1997; Compton et al. 2013; Murillo et al. 2015). While hydrodynamics influence the local (10s -100s m) distribution of individual deep-water megafaunal species or groups of species, such as deep-water corals (Mohn et al. 2014), their effect on variability in community composition has so far been found to be minimal (Compton et al. 2013). In the Barents Sea, baseline monitoring of benthic megafaunal communities revealed a spatial structure in community composition with two types of communities segregated in the southern and northern regions of the sea, and this structure was correlated with depth, bottom temperature, salinity and ice-days (Jørgensen et al. 2015). However, this biogeographic boundary (the 'benthic Polar Front') overlaps only partially with the general location of the Polar Front, indicating that other oceanographic features of the Barents Sea may also be important drivers of the observed spatial structure of these biological communities among other environmental gradients.

Deep-water benthic communities are directly affected by food supply, which in turn is influenced by the dynamics of surface primary productivity, and subsequent export to the seafloor. In polar shelf ecosystems, the relationship between surface primary

productivity and benthic biomass is considered to be particularly tight, and in the Barents Sea, this coupling is responsible for high benthic standing stocks relative to other Arctic continental shelf seas (Grebmeier and Barry 1991). However, the influence of food supply on community composition is unclear, and may be best assessed at broader spatial and temporal scales than with point observations. Benthic community structure in the Barents Sea was hypothesized to reflect long-term trends in the export of carbon to the seafloor (Renaud et al. 2008). On the Greenland shelf, on an intermediate spatial scale (100 km), benthic zones based on community composition correlated with changes in pelagic regimes, which differed in surface hydrography and productivity, and ice cover (Piepenburg et al. 1997). In general, export of organic matter to the seafloor is partially affected by physical processes governing the transport of zooplankton and the downward flux of particulate organic matter (Greibmeier and Barry 1991; Wassmann et al. 1996). Documenting physical processes occurring in the water column can provide insights on how surface primary production and its export to the seafloor can influence benthic communities.

In temperate and polar waters, water column structure (defined here as the vertical variability in the magnitude and direction of currents and hydrographic properties, such as temperature and salinity) varies seasonally (Mann and Lazier 1996). In winter, wind-driven turbulence and/or convection brings nutrients from deeper waters to the surface, while in spring, the stratification due to warming of surface waters, coupled with the availability of nutrients, triggers blooms of surface primary production. In polar waters covered by seasonal ice, such as the northern Barents Sea, the presence of melt water

from retreating sea ice also contributes to the stratification of the water column, and hence surface production (Perrette et al. 2011).

Environmental drivers of benthic communities, such as geomorphometry and oceanographic conditions, operate at various spatial and temporal scales, but the importance of defining scale(s) in benthic habitat modelling studies is only briefly acknowledged (reviewed in Lecours et al. 2015). The difficulty lies in determining the scale at which each environmental driver is operating. In addition to spatial variability, oceanographic conditions display temporal variability (from seconds to decades) that is difficult to integrate in benthic habitat models because of sporadic empirical observations, especially in remote areas, such as polar waters. Further, the temporal scale most relevant to patterns of benthic megafaunal communities is unclear. These large, long-lived organisms are often described as 'environmental integrators', and a relatively longer temporal resolution may be needed to explain their distribution (Wassmann et al. 1996). Ocean circulation models, despite their associated uncertainty, represent an opportunity to incorporate oceanographic conditions in benthic habitat modelling. These models are flexible in terms of the temporal resolution they offer, which can span seconds to decades depending on the availability of hindcast modelled data. Coupled with enhanced spatial coverage, they increase dramatically the potential of using oceanographic conditions to understand the environmental drivers of benthic communities in deep waters on continental shelves.

In our study, we firstly derived environmental variables describing the temporal variability of oceanographic features in the Barents Sea over 10 years (2001-2010), with a particular focus on the western region where the influence of the Atlantic inflow and the ecological impacts of the Polar Front are most pronounced. Secondly, we identified the oceanographic variables best correlated with spatial variability in the composition of benthic megafaunal communities (i.e., β-diversity) at mesoscales (10s – 100s km). Thirdly, we determined the spatial structure of three groups of variables relevant to benthic megafauna (temperature, bottom currents, and water column structure) to estimate the spatial scale at which these groups could be appropriate in determining variability in the composition of benthic megafaunal communities. Overall, we aimed to estimate the relative importance of oceanographic conditions in shaping benthic megafaunal communities at mesoscales in the high-latitude, dynamic ecosystem of the western Barents Sea, and identify how the spatial structure of key oceanographic drivers could explain their significance.

6.3 Materials & Methods

6.3.1 Study area

The Barents Sea is situated on the Arctic continental shelf between 70°N and >80°N, and is bordered to the south by Norway and Russia, and to the west by the Norwegian Sea. Its surface area covers ~1.6 million km^2, and it has an average depth of 230 m. The Barents Sea has a complex geomorphology, with deep basins and trenches (300-400 m) separating shallow banks (50-200 m).

The Barents Sea is a transition zone between the warm and saline Atlantic water in the southwest, and the cold and less saline Arctic water, dominating the northern Barents Sea. The Atlantic inflow in the western Barents Sea through the opening (between Bear Island and the Norwegian coast) - commonly termed the Barents Sea Opening - divides into 2 branches: one flowing east along the Norwegian coast and one flowing north toward Hopen Deep. The magnitude of this inflow varies seasonally – being strongest in winter – and inter-annually (Furevik 2001; Ingvaldsen et al. 2004; Fig. 6.1). The volume and hydrographic properties of the Atlantic inflow into the Barents Sea strongly influence the temperature in the southern region of the sea (Loeng 1991). The relatively warm and less saline Norwegian Coastal Current flows eastward along the Norwegian coast and adds fresh water to the Barents Sea (Skagseth et al. 2011). Arctic waters enter in the northern Barents Sea from the east between Franz Joseph Land and Novaya Zemlya, and from the north between Franz Joseph Land and Svalbard, flow toward Spitsbergen Bank and exit into the Norwegian Sea south of Bear Island (Loeng 1991; Pfirman et al. 1994). The 'Polar Front' is where Atlantic and Arctic waters meet, the location of which varies, but typically circles Spitsbergen Bank, continuing north of Hopen Deep, and west of Central Bank (Fig. 6.1).

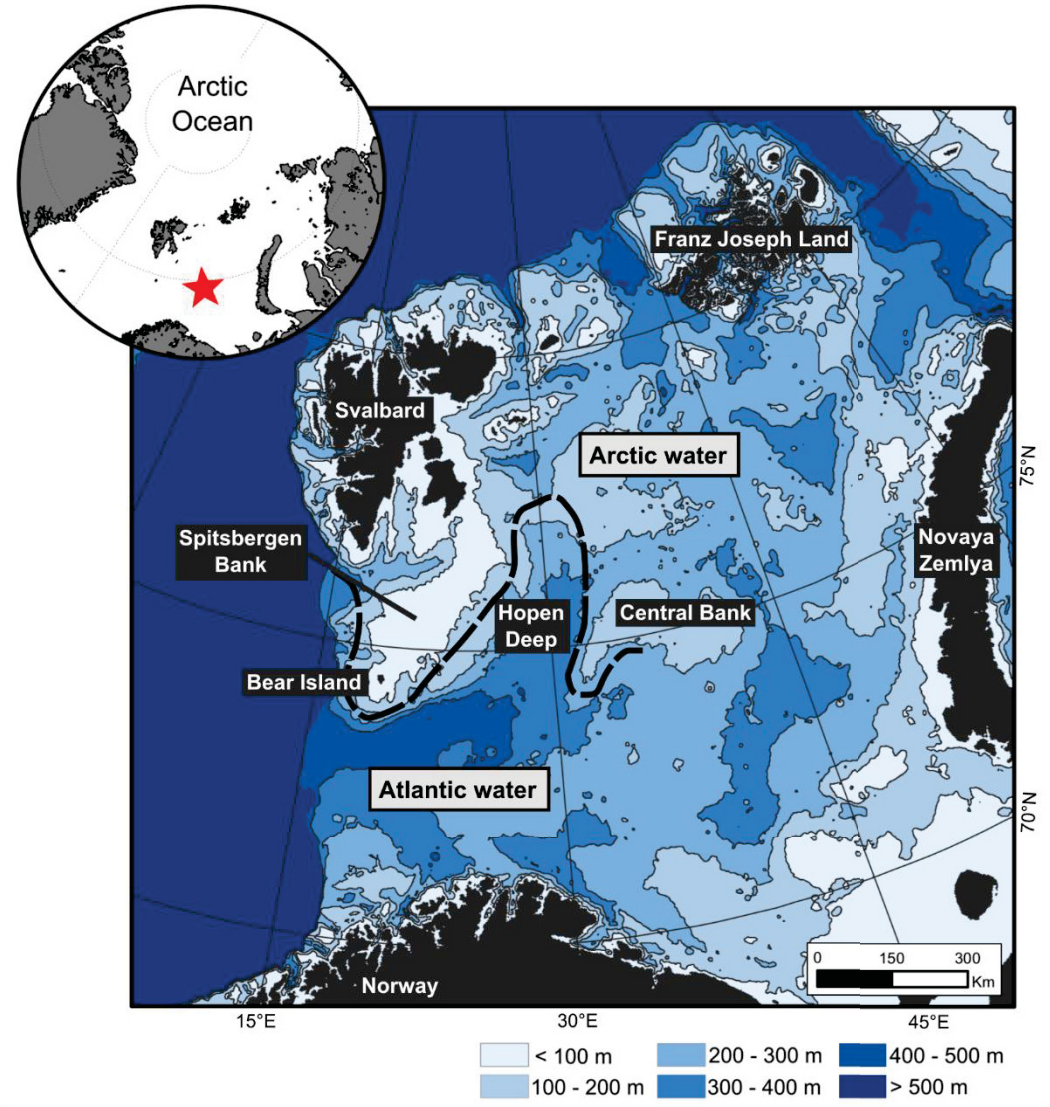

Figure 6.1: Bathymetry and general hydrographic pattern of the Barents Sea (its location is indicated by a red star in the inset showing the Arctic Ocean). The average location of the Polar Front is delimited with a dashed line (Ozhigin and Iyshin 1999).

6.3.2 Ocean circulation model

The Regional Ocean Modelling System (ROMS) is a 3-dimensional ocean general circulation model that uses normalized, terrain-following, stretched coordinates in the vertical dimension (Shchepetkin and McWilliams 2005). The model domain covers the Nordic Seas, the Barents Sea, the Kara Sea, and parts of the Arctic Ocean. It has 32 layers in the vertical and a minimum water depth of 10 m. Terrain-following vertical coordinates have the advantage of mapping all layers in each grid cell of the model domain, but the depth and thickness of each layer vary depending on the bottom depth. Moreover, in this model, surface layers are more densely packed than bottom layers to better resolve surface oceanographic processes. The horizontal grid cell size is 4 x 4 km. Thus, only processes that occur on scales > ~10 km in horizontal extent (based on the Nyquist criterion) are represented in the model, and processes > 25 km in horizontal extent are resolved, since at least 7 points are required to resolve features adequately. The model includes a module simulating ice dynamics (Budgell 2005) and tides are imposed as surface elevation and corresponding barotropic velocity components at open lateral boundaries. Monthly means of hydrographic properties and currents are available for the period 1960-2014. The model has been shown to reproduce well the oceanographic conditions of the Barents Sea (Lien et al. 2013b). More details on the model (i.e., atmospheric and open lateral boundary forcing, and tidal constituents) can be found in Lien et al. (2013a,b). In the present study, we used a subset of the model domain covering the western Barents Sea (Fig. 6.2).

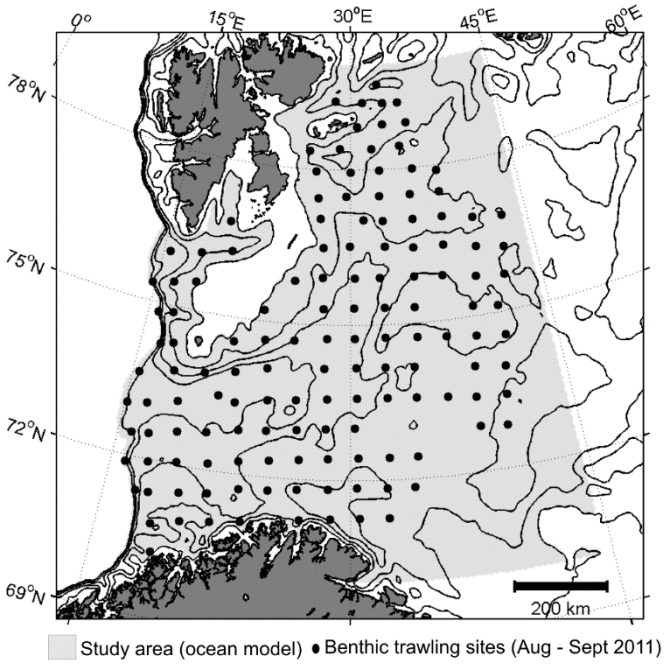

Figure 6.2: Study area (shaded in grey) in the western Barents Sea and benthic megafaunal trawling sites in waters > 100 m from surveys in August – September 2011 (black dots; n = 139 sites).

6.3.2.1 *Oceanographic variables derived from the ocean circulation model*

Eighty-four oceanographic variables were derived from the ocean circulation model (Table 6.1), which captured seasonal and inter-annual variability by integrating conditions over 10 years (2001-2010). For each variable, a value was derived for every grid cell of the model domain in the western Barents Sea (Fig. 6.2), generating a 2-dimensional environmental layer. Oceanographic variables were segregated into 3 groups that are relevant to benthic habitats in deep waters on continental shelves: temperature, bottom currents, and water column structure.

Table 6.1: Oceanographic variables (n = 84) derived from the ocean circulation model in the western Barents Sea, organized in three categories: temperature (25 variables), bottom currents (19 variables), water column structure (40 variables). Precision for measures of entropy: surface/bottom temperature, 0.01 °C; vertical velocity gradient, 0.0001 s^{-1}; vertical direction gradient, 0.1°·m^{-1}; vertical portion with negative N^2, 0.01; vertical portion Ri < 0.25, 0.01; bottom current speed, 0.001 m·s^{-1}; bottom current direction, 10°. Time lags are defined for sample autocorrelation coefficients (SAC).

Category	Variable [units]	Measure
Temperature	Surface temperature (10 m) [°C] Bottom temperature (10 m) [°C]	mean, stdev, max, min SAC (3,6,12,60 months) Annual amplitude (mean, stdev) Permutation entropy (3 consecutive months) Entropy (over 10 years)
	Bottom water masses	Entropy (over 10 years)
Bottom currents	Bottom current speed [m·s^{-1}]	mean, stdev, max SAC (3,6,12,60 months) Annual amplitude (mean, stdev) Permutation entropy (3 consecutive months) Entropy (over 10 years)
	Bottom current direction [-180°,180°]	Component mean (north-south; east-west) Circular stdev SAC (3,6,12,60 months) Entropy (over 10 years)
Water column	Vertical current speed gradient [s^{-1}] Vertical current direction gradient [° ·m^{-1}] Vertical portion with negative N^2 Vertical Portion Ri < 0.25	mean, stdev SAC (3,6,12,60 months) Annual amplitude (mean, stdev) Permutation entropy (3 consecutive months) Entropy (over 10 years)

Oceanographic variables related to temperature included mean, maximum and minimum values, and temporal variability of surface temperature (range = -1.90°C – 13.35°C) and bottom temperature (range = -2.03 °C – 10.84°C) (Table 6.1). Discrete bottom water masses (defined by temperature only) were identified to derive a single oceanographic variable that described them (Atlantic waters = $T \geq 3$°C; Arctic waters = $T \leq 0$°C; mixed waters = $0 < T < 3$°C; Dalpadado et al. 2012). Oceanographic variables related to bottom currents included mean and maximum values, and temporal variability

of current speed (range = 0 $m \cdot s^{-1}$ – 0.52 $m \cdot s^{-1}$), and mean values and temporal variability in current direction (segregated into its north-south and east-west components) (Table 6.1). Variables at the surface represented average values in the upper 10 m of the water column. Variables at the bottom were affected by the thickness of the bottom layer, which varies in our study area. In grid cells where the bottom layer was less than 10 m thick (16% of all grid cells), average values over the deepest 10 m of the water column were used for temperature-related variables and values at 10 m off the seafloor were used for variables related to bottom currents. Alternatively, values in the bottom layer of the model were used. Overall, the bottom layer was thinner than 20 m in 86% of grid cells in our study area.

Water column structure was assessed with measures of water column stratification through dynamic and static instability. Dynamic instability is measured with vertical gradients in current speed (i.e., shear, s^{-1}) and direction ($° \cdot m^{-1}$). Static instability is a measure of the degree to which water density changes with depth. In a stable water column, less dense water overlays denser water, reducing mixing and increasing stability. To measure static stability, we used: 1) the Brunt-Väisälä frequency (buoyancy frequency; N^2; s^{-2}; see Appendix I for calculations), which indicates the vertical gradient in density; and 2) the dimensionless Richardson number (Ri; see Appendix I), which compares the stabilizing effect of stratification (measured with N^2) against the destabilizing effect of changes in flow (vertical gradient in current speed). Negative values of N^2 indicate instability, leading to convection and/or overturning, while Ri values < 0.25 indicates turbulent flow and high mixing rates.

Temporal variability in oceanographic variables was measured as the standard deviation of the mean, temporal correlation, entropy, and annual amplitude (see Appendix I for calculations) (Table 6.1). Sample correlation coefficients (SAC) measure the correlation (-1, 1) between observations in a time series at given time lags and were used to quantify seasonal (3 and 6 months), inter-annual (12 months) and multi-year (60 months) variability. Entropy is a measure of the uncertainty associated with a set of observations, and increases with increasing unpredictability in the observations. Shannon entropy (base 2; bits) was calculated for the entire series (120 observations; 2001-2010) and permutation entropy (Bandt and Pompe 2002) was calculated for sets of observations (3 consecutive months; 40 observations). Entropy was measured on detrended time series (trend and seasonal components) using the X-11 method (US Census Bureau), which decomposes time series in trend, seasonal and irregular components (original algorithm modified by Pezulli et al. 2005). The X-11 method allows the inclusion of inter-annual variability in the seasonal component. For measures of entropy using continuous data, a measure of precision is required since values are compared as discrete values, specified in Table 6.1. Annual amplitude was derived as the range in values (maximum – minimum) over each calendar year. Mean and standard deviations of the mean of annual amplitudes were calculated over the entire study period.

6.3.3 Spatial turnover of benthic megafaunal communities

6.3.3.1 *Benthic megafaunal trawling surveys*

Benthic megafaunal trawling surveys were performed from August to September 2011 in the western Barents Sea on the Norwegian research vessels *Johan Hjort* and

Helmer Hanssen, using a Campelen 1800 bottom trawl with a mesh size of 80 mm (stretched) (16-22 mm in the cod end). Given our focus on benthic habitats in deep waters, we only considered sites deeper than 100 m, situated on the western continental shelf (n = 139) (Fig. 6.2). The sites were selected on a regular grid, with a standard distance between them of ~65 km (35 nautical miles). Data were standardized to a 15-min tow duration on the seafloor after initial contact, which, with a towing speed of 3 knots, represented a distance of ~1.4 km. Benthic megafauna was sorted to the lowest possible taxonomic level, but lumped according to genus (i.e., 'sp') when identification to the species level was not possible, or in the presence of an unknown species. Some specimens could only be identified at a higher taxonomic level, and hence were lumped into broader groups (e.g. Porifera). Individuals were wet-weighed for biomass and counted aboard the vessels. In the present study, community composition was defined as presence-absence of taxa. A total of 238 taxa were recorded in the survey (see Appendix II for list of taxa). Taxonomic names were verified with the World Register of Marine Species (www.marinespecies.org).

6.3.3.2 *Generalized dissimilarity modelling*

Dissimilarity in community composition between sites (i.e., spatial turnover) was calculated with Bray-Curtis dissimilarity values adapted for presence-absence data. This measure of biological distance (d_{ij}, between site i and site j; Eq. (6.1)) is constrained at 0 and 1, with 1 representing maximal dissimilarity.

$$d_{ij} = 1 - \frac{2A}{2A + B + C}$$

A = number of taxa common to both sites *i* and *j*

B = number of taxa present only at site *i* (6.1)

C = number of taxa present only at site *j*

Generalized dissimilarity modelling (GDM; Ferrier et al. 2007) is a statistical technique designed to analyze the environmental drivers of turnover of community composition across large regions. This technique models a curvilinear relationship between ecological distance (i.e., dissimilarity in environmental conditions) and compositional dissimilarity, the latter often reaching maximal values in large study areas. Total ecological distance between sites is modelled as a linear combination of partial ecological distances contributed by each environmental variable *x* (here described as gradients). Each environmental gradient is expressed as a function built from a linear set of non-linear monotonic I-splines functions (analogous to terms in polynomial regression). Along each environmental gradient, partial ecological distance between any 2 sites can therefore be non-linear, which allows the rate of compositional turnover to vary. These approximated functions are fitted to best explain compositional dissimilarity between sites. Summing the coefficients of the I-spline functions (constrained to be positive in monotonically-increasing functions) represents the maximum partial ecological distance contributed by the gradient, and indicates the relative importance of each gradient in explaining compositional dissimilarity. In the present study, we used the default of 3 I-splines functions to model each environmental gradient (Ferrier et al. 2007). Compositional dissimilarity is fitted against predicted ecological distance with generalized linear modelling, which uses a link function between the predicted response and the set of linear predictors, and a variance function describing the relationship of the

variance with the predicted mean response. Model fit is assessed by the proportion of deviance explained. Analyses were performed in the R environment with the 'gdm' package.

In our study, the full GDM included the 84 oceanographic variables in addition to depth (since this is often a strong predictor of variability in benthic community composition) and geographic distance. The number of environmental variables was reduced before fitting the final GDM as follows. Pearson's correlation coefficient (r) calculated for each pair of oceanographic variables revealed clusters of correlated variables ($r > 0.8$). For each cluster, one oceanographic variable was retained based on its potential ecological significance. Subsequently, a 2-step backward-elimination procedure was used (Fitzpatrick et al. 2013): (1) all variables that generated a reduction in overall model deviance < 0.5% were excluded; and (2) Monte Carlo permutations were used to test the significance of removing each variable from the model (999 permutations). The p-value indicated the proportion of permutations that generated a greater reduction in model deviance than is achieved by removing the variable from the original model. We used a threshold p-value of 0.05 to determine statistical significance of each variable. The first step to the backward-elimination procedure identified 9 oceanographic variables. Two of these variables were only marginally significant (p-value < 0.10) and were hence removed in the second-step of elimination procedure (Table 6.2). The final generalized model included 7 oceanographic variables (Table 6.2).

Table 6.2: Environmental variables included in the final generalized dissimilarity model (seven oceanographic variables, depth, and geographic distance). The sum of coefficients of the I-splines functions indicates the maximum partial ecological distance reached by each environmental gradient when all other gradients are held constant; it indicates the relative importance of each gradient in explaining compositional dissimilarity of megabenthic communities in the western Barents Sea. Marginally-significant (p-value < 0.10) not included in the final generalized model are indicated with (*).

Environmental variable	Sum I-splines coefficients
Surface Temperature [mean]	1.25
Surface Temperature [Annual amplitude; stdev]	0.60
Geographic distance	0.51
Bottom current speed [SAC; 60 months]	0.49
Depth	0.41
Vertical Portion Ri [0 - 0.25] [SAC; 6 months]	0.40
Surface Temperature [SAC; 3 months]	0.36
Surface Temperature [SAC; 6 months]	0.24
Vertical portion with neg. N^2 [SAC; 12 months]	0.19
Bottom Temperature [Annual amplitude; stdev]*	--
Bottom current speed [SAC; 12 months]*	--

We used deviance partitioning (based on variance partitioning, Borcard et al., 1992) to segregate model deviance associated with the environment only, space only (distribution due to biological processes governed by species' traits such as dispersal and differences in growth), and the interaction of space and environment (distribution due to separate relationships of biological communities and environment to similar space-structuring processes).

6.3.3.3 *Spatial structure in the oceanography of the western Barents Sea*

Multivariate statistical analysis was used to determine oceanographic provinces, i.e. regions of homogeneous oceanographic conditions integrated over a 10-year period (2001-2010). Sets of oceanographic provinces were derived separately for the three

groups of oceanographic variables (temperature, bottom currents, and water column structure) to compare their spatial structure.

Principal component analysis (PCA) was used to reduce the dimensions of the initial set of 84 oceanographic variables. PCA transforms a correlated set of environmental variables into a set of linearly-independent variables (principal components). Whenever necessary, variables were transformed (logarithmic or arcsin) to reduce skewness in their distribution. Data were normalized to zero-mean and unit variance. Principal components are ordered according to the proportion of the overall variance they explain. For further analyses, we retained the principal components with eigenvalues > 1 since they explain more variance than is contained in the individual variables (i.e. Kaiser-Guttman criterion; Legendre and Legendre 1998). Scores of principal components were then subjected to a k-means clustering algorithm to identify oceanographic provinces in the study area. The optimal number of clusters was determined by minimizing the total error (within-clusters) sums of squares obtained when 1 to 25 clusters were used (Legendre and Legendre 1998). The final number of clusters was determined subjectively using a criterion inspired by the 'elbow criterion' (determining the number of clusters beyond which the marginal decrease in total error is reduced). For simplicity in our analysis, we used the smallest amount of clusters for each group of variables, i.e. where the error initially levels off. We have not tested whether our conclusions are affected by this clustering. Each observation was assigned to a cluster, and each cluster represented an oceanographic province: an ensemble of locations in the study area where oceanographic conditions are similar. A confusion index assessing the

strength of the clustering was also derived for each observation by comparing the distance to its assigned cluster centroid against the distance to all other centroids (Ismail et al. 2015 modified from Lucieer and Lucieer, 2009, see Appendix III). Roughly equal distances to all centroids indicate indecisive assignments reflected in higher values of the confusion index.

6.4 Results

6.4.1 Spatial patterns of benthic communities – Generalized dissimilarity modelling

The final generalized model included eight environmental variables (seven oceanographic variables and depth) and geographic distance as predictors (Table 6.2). Among the oceanographic variables, four were related to temperature, two to water column structure, and one to bottom currents. The model overall explained 56.7% of the total deviance (Fig. 6.3), with 27.3% solely due to the relationship with the environment, 2.5% due to space, and 26.9% due to the interaction between space and the environment. The most important predictor (defined by summing the coefficients of the I-spline functions) was mean surface temperature over the study period (2001-2010) (Table 6.2). For each predictor, the rate of compositional turnover varied along the environmental gradients (Fig. 6.4).

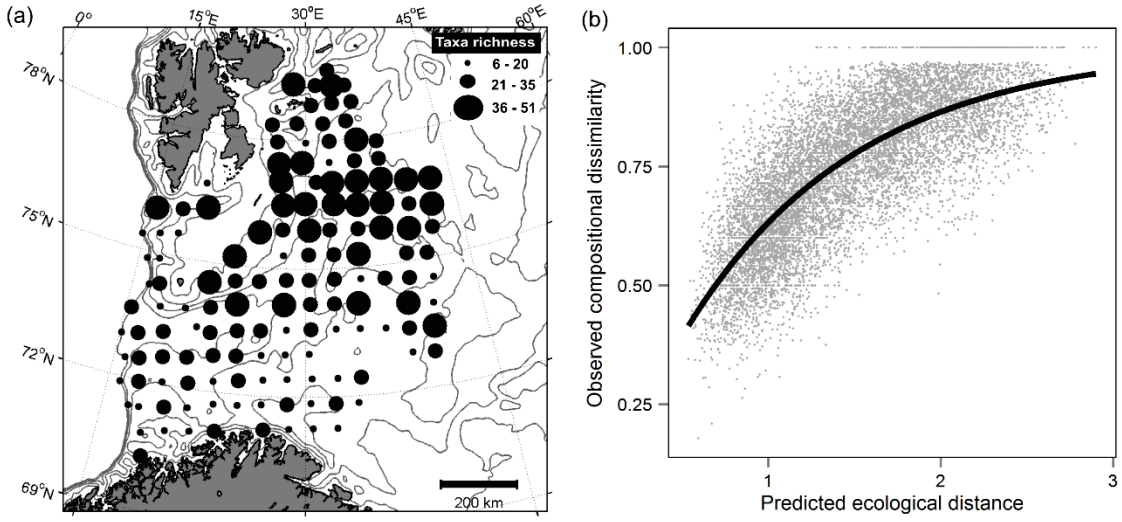

Figure 6.3: Communities of benthic megafauna. (a) Benthic megafauna species richness sampled in August-September 2011 with the Norwegian Ecosystem trawling surveys (n = 139 sites). All sampling sites are at depths > 100 m. (b) Observed compositional dissimilarity (calculated with Bray-Curtis distance adapted for presence-absence data) against predicted ecological distance from the final generalized dissimilarity model (GDM; n = 9591). The GDM explained 56.7% of the total deviance (line of best fit is shown in bold).

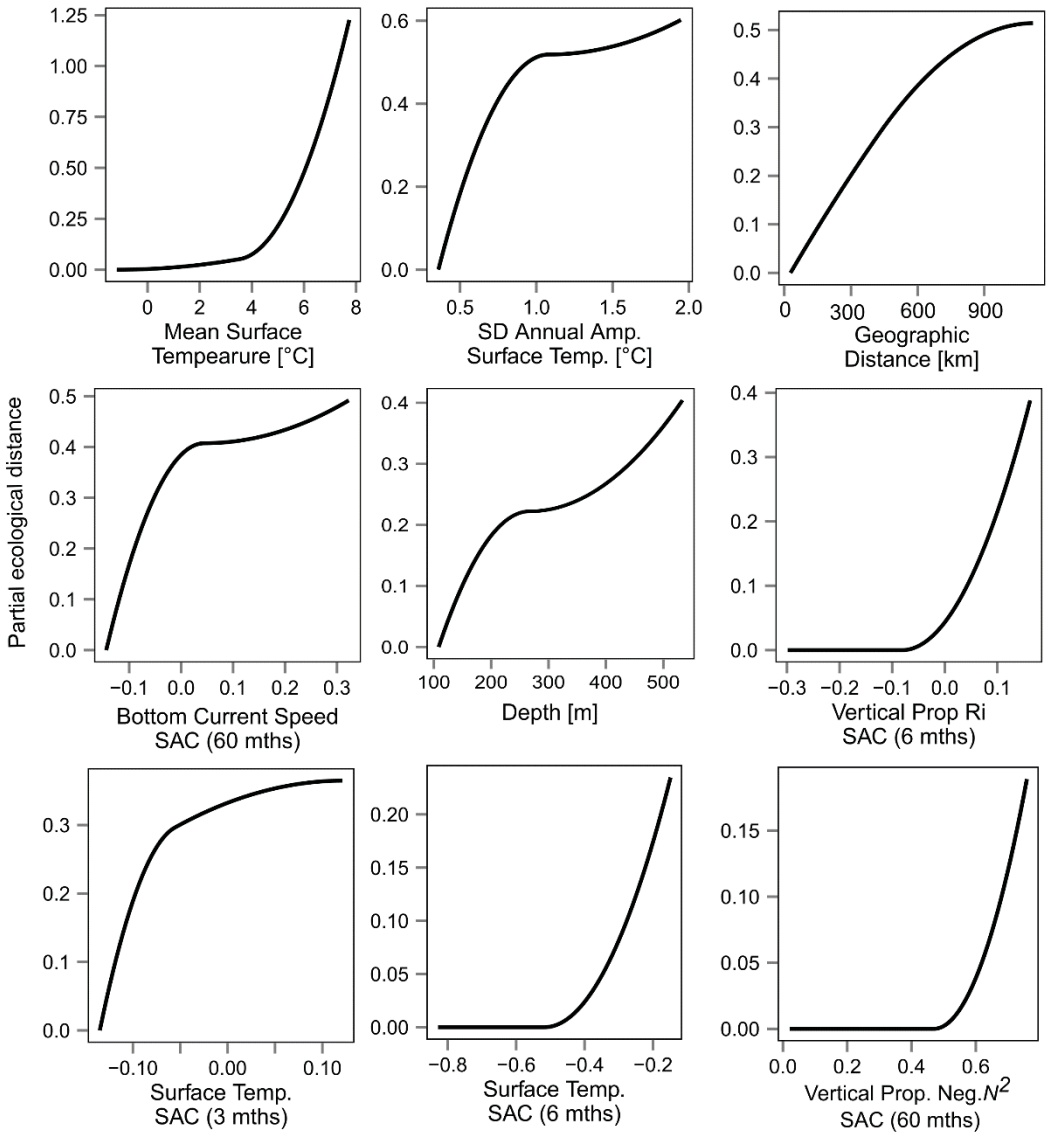

Figure 6.4: Partial ecological distance predicted along each environmental gradient. Maximum height of each curve represents the total amount of compositional turnover explained by the environmental gradient (holding all others constant). The shape of each curve indicates the varying rate of compositional turnover along each gradient.

6.4.2 Spatial structure in the oceanography of the western Barents Sea

Five significant principal components (eigenvalue > 1) were derived from oceanographic variables related to temperature (n = 25) and to bottom currents (n = 19). Nine significant principal components were derived from oceanographic variables related to water column structure (n = 40). Factor loadings are shown in Appendix IV. Seven clusters ('oceanographic provinces') were determined for oceanographic variables related to temperature and bottom currents, while nine clusters were determined for oceanographic variables related to water column structure (Fig. 6.5). Oceanographic variables related to temperature yielded the most homogeneous provinces (Fig. 6.6a) with sharp boundaries reflected in the lowest mean confusion index (CI = 0.39 ± 0.25; Fig. 6.6b). Provinces derived from variables related to water column structure were defined at a similar spatial scale than those derived from temperature (Fig. 6.6c), but were less homogeneous with fuzzy boundaries (CI = 0.65 ± 0.22; Fig. 6.6d). Homogeneity in provinces derived from variables related to bottom currents was apparent at a finer spatial scale (Fig. 6.6e). However, these provinces were also less homogeneous with no clear boundaries (CI = 0.57 ± 0.25; Fig. 6.6f).

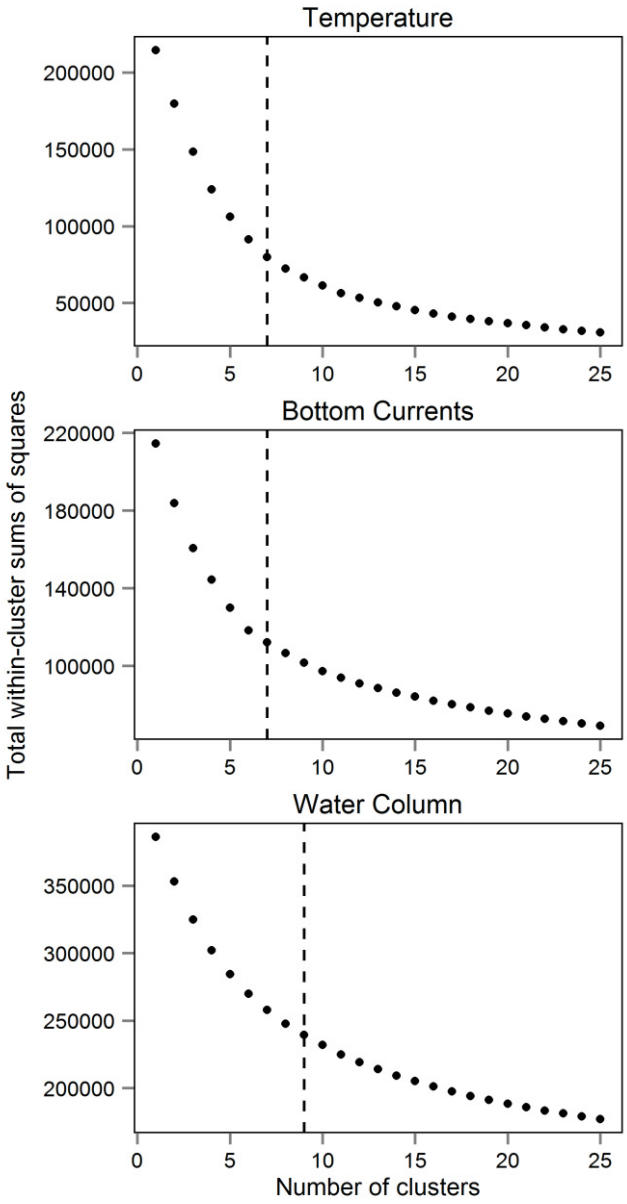

Figure 6.5: Total within-cluster sums of squares (Euclidean distance between each observation and their assigned cluster centroid) from k-mean clustering using variables related to temperature, water column structure and bottom currents. Vertical dashed lines indicate the number of clusters determined subjectively (i.e., the number where the rate of decreases of sums of squares begins to level off) for each group of variable.

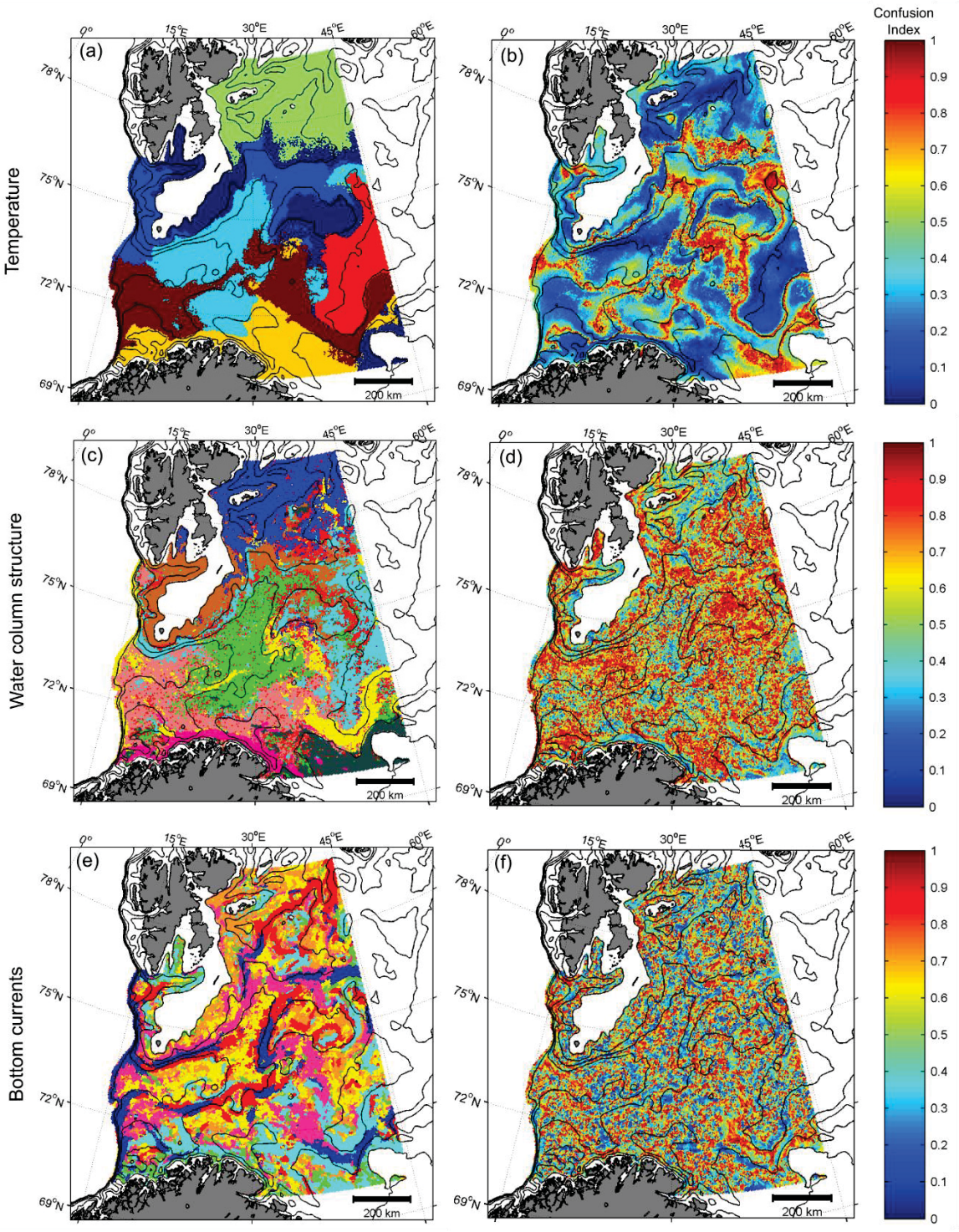

Figure 6.6: Oceanographic provinces identified with principal component analysis and k-means clustering for 3 categories of oceanographic variables: (a) temperature, 7 provinces; (c) water column structure, 9 provinces; (e) bottom currents, 7 provinces. Each color represents a province. Confusion indices are shown for the 3 categories: (b), (d), (f) – see Appendix III for details.

6.5 Discussion

We provided a baseline understanding of the relative importance of oceanographic conditions in shaping deep-water benthic megafaunal communities at mesoscales (10s-100s kms) in the western Barents Sea, which could be used in assessing and predicting impacts of environmental change. In the generalized dissimilarity model, 56.5% of the total deviance in composition dissimilarity was explained by 7 oceanographic variables, depth and geographic distance between sites. The unexplained deviance in this model is due to other environmental factors not included in our analysis - such as those related to surficial geology and geomorphology, and to random variation due to historical dynamics of community development. However, the underlying dynamics driving changes in community composition remain elusive because of the effect of spatial structure (i.e. the non-random organization of communities in space), which was as important in determining spatial variability of benthic communities as the direct relationship with the environment. Therefore, changes in the spatial structure of the environment over time likely are as important as direct relationships with environmental gradients in predicting variability in community composition.

6.5.1 Spatial structure in the oceanographic provinces

Spatial structure varied among the 3 groups of oceanographic variables (temperature, water column structure and bottom currents). Patterns in oceanographic provinces correlated with the significant oceanographic variables identified with the generalized dissimilarity model. While 4 significant variables were related to temperature, only 1 significant variable was related to bottom currents. The disparity in

spatial structure between the groups of environmental variables derived from temperature and bottom currents may explain why variables associated with temperature are stronger predictors of variability in community composition at mesoscales. In the Barents Sea, spatial patterns in temperature have been shown to influence demersal fish communities (Johannesen et al. 2012a; Fossheim et al. 2015). Spatial structure in bottom currents was detected at a fine spatial scale, which might overlap only partially with spatial structure in communities. This may explain why bottom currents are generally not reported as important drivers of benthic megafaunal communities at regional and multi-year scales (Compton et al. 2013; Jørgensen et al. 2015) despite their importance in shaping the distribution of individual species or communities at finer spatial and temporal scales (Henry et al. 2013; Mohn et al. 2014). Our results highlight the importance of recognizing that different environmental factors act at different scales (e.g. Williams et al. 2010), making it difficult to obtain a holistic view of the ecosystem by focusing at a single scale.

6.5.2 Scale of currents

Currents may be significant in habitat models at different scales than the one used in our study. 'Neighborhood' analyses of oceanographic features at multiple spatial and temporal scales could be useful for estimating the effect of the structure of hydrodynamics in shaping benthic communities, similarly to deriving terrain variables based on the geomorphology of the seafloor at increasing spatial scales (Wilson et al. 2007). Capturing the temporal and spatial variability of the oceanographic features of a region on multiple scales is challenging given the changes in current speed and direction,

and the 3-dimensionality of the water column. Akin to fronts, other oceanographic features (such as eddies) may be important in determining spatial patterns in megabenthic fauna, through their influence on dispersal (Harrison et al. 2013) and sedimentation of surface primary productivity (Lathuilière et al. 2010). A temporal multiscale approach to currents may also be important in determining their effect on benthic megafauna. In our study, 6 of 7 significant oceanographic variables were measures of variability (i.e. standard deviation of the mean, sample autocorrelation coefficient) rather than mean values. However, sporadic events were not accounted for in our study, but could also be important in determining the composition of benthic communities. This has been shown in shallow waters (e.g. Dayton 1971), but the frequency and magnitude of sporadic disturbance in deeper waters on shelves is unresolved.

6.5.3 Water column structure and carbon export

In our study, water column structure had intermediate significance in driving spatial turnover in benthic megafaunal communities. Since the structure of the water column (i.e. degree of stratification) influences the productivity regime in an area, the dynamics of surface productivity and its export to the seafloor plays a key role in shaping the communities in our study. Patterns in oceanographic provinces can help elucidate the spatial scale at which surface primary productivity correlates with biomass, abundance and composition of benthic communities. In the Barents Sea, modelled primary productivity positively correlates with infaunal abundance and richness (Cochrane et al. 2009), and it has been suggested that food availability and benthic community structure are linked, especially at or near the Polar Front (Carroll et al. 2008). While this

relationship between surface chlorophyll *a* and benthic biomass has also been observed in the Chukchi Sea, no relationship was detected in the Beaufort Sea, highlighting the potential importance of physical advective processes in determining carbon export to the seafloor (Dunton et al. 2005). In our study, the spatial patterns of provinces derived from these oceanographic variables broadly matched our current understanding of conditions in the western Barents Sea. The Polar Front created a homogeneous region circling Spitsbergen Bank, running north of the Hopen Deep, and circling Central Bank. Water column structure in the northern region is influenced by the dominance of Arctic waters and seasonal ice cover. The central portion where the Atlantic and Arctic waters meet was also delimited by the influence of the cold, dense water flowing from adjacent banks (Årthun et al. 2011; Lien and Ådlandsvik 2014). Lastly, near-coastal conditions were delimited by the influence of the Norwegian Coastal Current. These patterns illustrate a spatial scale at which the export of surface primary productivity could be correlated with turnover in benthic megafaunal communities.

6.5.4 Potential mesoscale dispersal barriers

In our study, only 2.3% of total deviance was due to purely spatial components, possibly because of unlimited dispersal leading to spatially homogeneous communities (Borcard et al. 1992). However, there may be differences in dispersal abilities between taxonomic groups not resolved here. It has been proposed that few dispersal barriers occur in marine systems at the regional scale and the composition of local communities is influenced by local propagules (see Cornell and Harrison 2013 for review). However, in deep waters off the coast of New Zealand, space was estimated to account for 26% of the

variability in the composition of nematode communities at mesoscales (Leduc et al. 2012). In contrast, off the Scottish west coast, space explained only 5.1% of the variability in the composition of sessile suspension-feeding megafaunal communities associated with *Lophelia pertusa* reefs at scale of 100s of meters (Henry et al. 2010). Overall, ~30% of the turnover in benthic megafaunal communities in the western Barents Sea was explained by the geographic distance between sites, but most of this variability (27.1%) was due to induced spatial dependence. Concurrently, we also detected rapid changes in community composition along environmental gradients with the generalized dissimilarity model, which may indicate the presence of strong spatial boundaries delimiting oceanographic regimes. Therefore, we suggest that turnover in the communities in our study may be partially explained by the presence of dispersal barriers at mesoscales, such as the interaction between distinct water masses at the Polar Front or in other areas, which would influence both the turnover in community composition and the spatial structure of the environment, but may not be detected at the regional scale.

6.5.5 The role of latitude

Assessing the effect of the environment on spatial turnover in benthic communities at broad spatial scales can be confounded by the role of latitude. At the scale of the deep North Atlantic (500-4,000 m depth), a decrease in species richness of bivalves, gastropods and isopods was observed with increasing latitude (Rex et al. 2000). However, there was no evidence of a latitudinal gradient in soft-sediment macrobenthic species richness along the Norwegian continental shelf (65 – 434 m depth) spanning ~15° of latitude (Ellingsen and Gray 2002). In our study, benthic megafaunal species richness

seemingly *increased* with latitude, with richness being higher on the seafloor overlaid by Arctic rather than Atlantic waters. However, this could have been biased by the taxonomic breadth of the communities (see Appendix II) (Hillebrand 2004), and the influence of bottom fishing in the southern region (Jørgensen et al. 2016). In high-latitude ecosystems, the effects of latitude and temperature can be confounded, since these factors tend to be correlated (Yesson et al. 2015). In our study, the mean, maximum and minimum of both surface and bottom temperature correlated with latitude (data not shown), which was expected given the oceanography of the region (i.e. the presence of the Polar Front). However, the spatial structure of the oceanography in the Barents Sea cannot be solely explained by latitude, as we have shown with the pattern of distinct oceanographic provinces derived from variables related to temperature.

6.5.6 Using ocean models in habitat mapping

Ocean circulation models are valuable tools to study the properties of dynamic marine ecosystems at appropriate scales – such as the western Barents Sea and in other areas where oceanic fronts are present – making it possible to assess and/or predict the impacts of future environmental change in a timely manner. However, the outputs of these models, akin to those of digital bathymetric models and atmospheric models, include inherent uncertainty arising from the discretization of the set of underlying equations and associated assumptions, and the numerical methods applied to solve these equations. Moreover, the usefulness of the results of numerical models is limited by the resolution in both space and time. In our study, as an example, it is likely that our calculation of the Brunt-Väisälä frequency (N^2) is underestimated due to time-averaging

when using monthly means and the smoothing of the horizontal velocity gradient given the model resolution. However, since the ocean circulation model applied here has been shown to represent well the mean oceanographic features of the Barents Sea as well as their temporal variability (Lien et al. 2013b), we consider it unlikely that our overall conclusions are sensitive to the errors within the model, given our spatial and temporal scale of interest. How uncertainty in the outputs of a physical model affects conclusions drawn from ecological models using these outputs is unclear, and this can prevent the use of physical models in habitat modelling. While the need to consider uncertainty has already been recognized in digital bathymetric models of the seafloor (Dolan and Lucieer 2014), analyzing the magnitude of and scale-specific impacts of uncertainty in oceanographic modelled data on habitat models would promote their use, especially in areas difficult to monitor with empirical observations, such as the deep polar ocean.

6.6 Conclusions

In our study, we have provided a baseline knowledge of the oceanographic conditions influencing spatial turnover in deep-water benthic megafaunal communities at mesoscales. We have shown that temperature is an important driver of turnover, most likely because of the sharp spatial structure of the oceanographic provinces they induce at the scale under study. Establishing how changes in the spatial structure of the environment could affect these biological communities may be an important avenue of research to anticipate the impacts of climate variability, especially in high-latitude ecosystems. We have also shown that coupling physical models and ecological models can help us better resolve the relevant scale of physical drivers of benthic megafaunal

communities, but the inherent uncertainty associated with physical models need to be addressed more thoroughly.

CHAPTER 7

CONCLUSION

This thesis aimed to increase our understanding of how the physical environment influences the abundance, composition, and diversity of epibenthic megafaunal communities in deep waters. Key findings are summarized below, namely the necessity to explicitly incorporate scale into habitat studies, and the validity of developing new approaches and tools to study deep benthic ecosystems, which aided in describing the importance of fine-scale substrate features and oceanographic properties.

This thesis aided in the development of new approaches and tools to maximize information on remote ecosystems that are logistically difficult to sample, such as deep-water benthic ecosystems. In **Chapter 3**, I developed an approach adapted from algorithms in the computer vision literature to quantify substrate complexity at fine spatial scale (< 1 m) and its heterogeneity at broader spatial scales (10 – 100s m). I have subsequently shown the usefulness of this approach at the base of the continental slope by detecting sporadic substrate features as potential key ecological features influencing megafaunal diversity (**Chapter 4**), and in deep waters on a continental shelf, where a continuous relationship between variability in substrate complexity (heterogeneity) and epibenthic megafaunal diversity was clearly defined (**Chapter 5**). In **Chapter 6**, I showed that deriving 'oceanographic provinces', which was inspired by methods widely used in benthic habitat mapping, can act as a diagnostic tool to understand the scale at which oceanographic properties – given their spatiotemporal variability that is difficult to

resolve – may be important drivers of composition in epibenthic megafaunal communities.

The work presented in this thesis supports the contention that fine-scale substrate features influence benthic megafauna in deep waters, in particular the (often sporadic) presence of hard substrate (e.g. bedrock, coarse sediment). In **Chapter 2**, deep-water corals recruited almost exclusively on hard substrate, which was not restricted to geological features *per se,* since abundant recruits were also collected on the surfaces of the collectors. Interestingly, other recruits were also found on consolidated grains of sand and pebbles, a type of substrate that is not typically suitable for adult colonies, but did represent suitable 'hard' substrate for recruits. In **Chapter 4**, I showed that differences in local-scale substrate type at the base of the continental slope enhanced local megafaunal diversity. The sporadic presence of glacio-marine debris (e.g. large boulders) in an otherwise homogeneous environment dominated by fine-grain sediment and/or 'patches' of coarser sediment (pebbles, cobbles and boulders) provided habitat heterogeneity at great depths, hence influencing diversity. A similar relationship was observed in **Chapter 5** in shallower habitats on the continental shelf, where variability in substrate complexity at local scales (10s m – 1 km) influenced the composition of megafaunal communities and enhanced diversity.

Oceanographic properties were found to be important drivers of epibenthic megafaunal communities, either at the seafloor or in the water column. The incorporation of these properties in advanced deep-water benthic habitat modelling is becoming more

prominent, and is a promising future avenue of research. In **Chapter 2**, coral recruits were often found on vertical surfaces of the larval settlement collectors, either hanging sideways or upside down. This could indicate the importance of shelter for recruits from biological disturbance, especially since a dense cover of suspension-feeding brittle stars was observed. Concurrently, the interaction between the complexity of the seafloor and water currents is also possible, enhancing turbulence and potential larval and food supply at a very fine scale. In **Chapter 5**, areas of dense epifaunal cover were associated with strong, quasi-unidirectional currents, and differences in the composition of megafaunal communities were partially explained by oceanographic properties. I suggested that highly divergent communities should not be expected, given the overall connectivity of the region, which underscores the potential role of strong oceanographic features yielding distinct benthic megafaunal communities. In **Chapter 6**, the development of spatially-coherent regions of similar conditions (i.e. 'oceanographic provinces'), the boundaries of which were particularly sharp for temperature, explained the relative importance of groups of variables in determining the composition of benthic megafaunal communities.

Lastly, this thesis provides evidence for the importance of identifying the relevant scale at which environmental factors operate. In **Chapter 2**, coral recruits were observed on any hard substrate that satisfied their immediate habitat requirements (for example, consolidated grains of sand), but this patterns also suggested ontogenetic habitat shifts, since fine-grain sediment do not typically harbour juvenile and adult colonies of these species. These different habitat requirements for recruits and adult colonies may partially explain the post-recruitment mortality suggested in this study, and hence elucidate the

role of the physical environment in influencing life-history processes in deep-water corals. In **Chapter 4**, diversity in epibenthic megafauna was correlated with variability in fine-scale substrate features (< 1 m to a few meters), in particular the presence of highly sporadic large boulders which are difficult to detect from ship-based surveys, and to quantify to characterize the benthic environment. In **Chapter 5**, the relationship between megafaunal community composition and diversity was again detected in shallower habitats, but abundance of megafauna was driven by environmental factors acting at larger spatial scales: the shape of seafloor (100-1000 m) and oceanographic properties (1-10 km). In **Chapter 6**, in the dynamic area of the western Barents Sea (10s – 100s km), disparity in the spatial structure of the 3 different groups of properties I examined (temperature, bottom currents and water column structure) highlighted the relevance of determining the spatial structure of the ocean to understand patterns in biological communities. An important conclusion from this chapter is that monitoring changes in the spatial structure of the environment could help us both identify the underlying physical drivers of environmental change and more accurately predict their impact on biological communities.

Lastly, by studying species-environment relationships in the deep benthic ocean, this thesis highlighted the complexity and heterogeneity of a physical environment that was once thought to be highly homogeneous. Describing the deep-water physical environment - and its linkages with pelagic and shallow-water environments – remains an important challenge for ecological studies, with obvious dependencies on other sub-disciplines of ocean sciences, such as ocean dynamics and biogeochemistry. To

understand the current state of the deep ocean ecosystem, and anticipate the impacts of future environmental change, a holistic approach that incorporates different aspects of ocean sciences should thus be encouraged.

Future work

Approaches to describe deep-water benthic ecosystems should be developed further, in particular the use of ocean circulation models to better resolve the role of hydrodynamics and water properties in shaping biological communities on the seafloor. For example, integrating time and space in oceanographic properties in statistical benthic habitat modelling remains challenging, and could be coupled with a Lagrangian approach that complements the typical Eularian perspective. Additionally, combining physical properties across multiple scales is necessary, and in particular across different groups of environmental predictors. For example, the relative role of local-scale heterogeneity in sediment properties within broader-scale oceanographic properties need to be better resolved in order to accurately predict the distribution of megafauna in unsurveyed areas. Accurate predictions would also benefit from developing approaches to incorporate uncertainty in physical data in statistical benthic habitat modelling. This is particularly needed when deriving higher-level metrics of deep-water benthic ecosystems - such as those used in the budding field of 'seascape ecology' - and when informing resource management strategies.

References

Abelson, A., T. Miloh, and Y. Loya. 1993. Flow patterns induced by substrata and body morphologies of benthic organisms, and their roles in determining availability of food particles. Limnology and Oceanography **38**:1116–1124.

Aguzzi, J., C. Costa, Y. Fujiwara, R. Iwase, E. Ramirez-Llodra, and P. Menesatti. 2009. A novel morphometry-based protocol of automated video-image analysis for species recognition and activity rhythms monitoring in deep-sea fauna. Sensors **9**: 8438–55.

Aguzzi, J., C. Costa, K. Robert, M. Matabos, F. Antonucci, S. K. Juniper, and P. Menesatti. 2011. Automated image analysis for the detection of benthic crustaceans and bacterial mat coverage using the VENUS undersea cabled network. Sensors **11**:10534–56.

Anderson, T. J., S.L. Nichol, C. Syms, R. Przeslawski, and P.T. Harris. 2011. Deep-sea bio-physical variables as surrogates for biological assemblages, an example from the Lord Howe Rise. Deep-Sea Research Part II: Topical Studies in Oceanography **58**: 979–991.

Andrews, A.H., E.E. Cordes, M.M. Mahoney, K. Munk, K.H. Coale, G.M. Cailliet, and J. Heifetz. 2002. Age, growth and radiometric age validation of a deep-sea, habitat-forming gorgonian (*Primnoa resedaeformis*) from the Gulf of Alaska. Hydrobiologia **471**: 101–110.

Aretxabaleta, A. L., B. Butman, R.P. Signell, P.S. Dalyander, C.R. Sherwood, V.A. Sheremet, and D.J. McGillicuddy. 2014. Near-bottom circulation and dispersion of sediment containing *Alexandrium fundyense* cysts in the Gulf of Maine during 2010-2011. Deep-Sea Research Part II: Topical Studies in Oceanography **103**: 96–111.

Årthun, M., T. Eldevik, L.H. Smedsrud, Ø Skagseth, and R.B. Ingvaldsen. 2012. Quantifying the Influence of Atlantic Heat on Barents Sea Ice Variability and Retreat. Journal of Climate **25**: 4736–4743.

Årthun, M., R.B. Ingvaldsen, L.H. Smedsrud, and C. Schrum. 2011. Dense water formation and circulation in the Barents Sea. Deep Sea Research Part I: Oceanographic Research Papers **58**: 801–817.

Auster, P.J. 2005. Are deep-water corals important habitats for fishes? In: Freiwald, A., and J.M. Roberts [eds]. Cold-water Corals and Ecosystems. Berlin Heidelberg: Springer-Verlag. pp. 747–760.

Ayre, D.J., and T.P. Hughes. 2000. Genotypic diversity and gene flow in brooding and spawning corals along the Great Barrier Reef, Australia. Evolution **54**: 1590–1605.

Bandt, C., and B. Pompe. 2002. Permutation entropy: a natural complexity measure for time series. Physics Review Letters **88**: 174102.

Barnard, P. L., D. M. Rubin, J. Harney, and N. Mustain. 2007. Field test comparison of an autocorrelation technique for determining grain size using a digital "beachball" camera versus traditional methods. Sedimentary Geology **201**:180–195.

Barnes, N. 2010. Publish your computer code: it is good enough. Nature **467**: 753.

Beaman, R. J., J.J. Daniell, and P.T. & Harris. 2005. Geology-benthos relationships on a temperate rocky bank, eastern Bass Strait, Australia. Marine and Freshwater Research **56**: 943–958.

Belkin, I.M., P.C. Cornillon, and K. Sherman. 2009. Fronts in Large Marine Ecosystems. Progress in Oceanography **81**: 223–236.

Benn, D.I., and Evans, D.J.A. 2010. Glaciers & Glaciation, 2nd edition. Hodder Education, United Kingdom.

Bergmann, M., N. Langwald, J. Ontrup, T. Soltwedel, I. Schewe, M. Klages, and T.W. Nattkemper. 2011. Megafaunal assemblages from two shelf stations west of Svalbard. Marine Biology Research **7**: 525–539.

Bergmann, M., T. Soltwedel, and M. & Klages. 2011. The interannual variability of megafaunal assemblages in the Arctic deep sea: Preliminary results from the HAUSGARTEN observatory (79°N). Deep-Sea Research Part I: Oceanographic Research Papers **58**: 711–723.

Billett, D.S.M., R.S. Lampitt, A.L. Rice, and R.F.C. Mantoura. 1983. Seasonal sedimentation of phytoplankton to the deep-sea benthos. Nature **302**: 520-522.

Blaschke, T. 2010. Object based image analysis for remote sensing. ISPRS Journal of Photogrammetry and Remote Sensing **65**: 2–16.

Blicher, M. E., and M.K. Sejr. 2011. Abundance, oxygen consumption and carbon demand of brittle stars in young sound and the NE Greenland shelf. Marine Ecology Progress Series **422**: 139–144.

Bluhm, B. A., K.O. Coyle, B. Konar, and R. Highsmith. 2007. High gray whale relative abundances associated with an oceanographic front in the south-central Chukchi Sea. Deep Sea Research Part II: Topical Studies in Oceanography **54**: 2919–2933.

Bongiorni, L., M. Mea, C. Gambi, A. Pusceddu, M. Taviani, and R. Danovaro. 2010. Deep-water scleractinian corals promote higher biodiversity in deep-sea meiofaunal assemblages along continental margins. Biological Conservation **143**: 1687–1700.

Borcard, D., P. Legendre, and P. Drapeau. 1992. Partialling out the spatial component of ecological variation. Ecology **7**: 1045–1055.

Breiman, L. 2001. Random Forests. Machine Learning **45**: 5-32.

Breeze, H., D.S. Davis, M. Butler, and V.E. Kostylev. 1997. Distribution and Status of Deep Sea Corals off Nova Scotia. Halifax: Ecology Action Centre. 64 pp.

Brooks, D.A. 1985. Vernal circulation in the Gulf of Maine. Journal of Geophysial Research **90**: 4687-4705.

Brown, C. J., S. J. Smith, P. Lawton, and J. T. Anderson. 2011. Benthic habitat mapping: A review of progress towards improved understanding of the spatial ecology of the seafloor using acoustic techniques. Estuarine and Coastal Shelf Science **92**: 502–520.

Bryan, T.L., and A. Metaxas. 2006. Distribution of deep-water corals along the North American continental margins: Relationships with environmental factors. Deep-Sea Research I **53**: 1865–1879.

Budgell, W.P., 2005. Numerical simulation of ice-ocean variability in the Barents Sea region. Ocean Dynamics **55**: 370–387.

Buhl-Mortensen, L., and P.B. Mortensen. 2004. Crustaceans associated with the deep-water gorgonian corals *Paragorgia arborea* (L., 1758) and *Primnoa resedaeformis* (Gunn., 1763). Journal of Natural History **38**: 1233–1247.

Buhl-Mortensen, L., and P.B. Mortensen. 2005. Distribution and diversity of species associated with deep-sea gorgonian corals off Atlantic Canada. In: Freiwald, A., and J.M. Roberts [eds]. Cold-water Corals and Ecosystems. Berlin Heidelberg: Springer-Verlag. pp. 849–879.

Buhl-Mortensen, P., M. Dolan, and L. Buhl-Mortensen. 2009. Prediction of benthic biotopes on a Norwegian offshore bank using a combination of multivariate analysis and GIS classification. ICES Journal of Marine Science **66**: 2026–2032.

Buhl-Mortensen, L., A. Vanreusel, A.J. Gooday, L.A. Levin, I.G. Priede, P. Buhl-Mortensen, H. Gheerardyn, N.J. King, and M. Raes. 2010. Biological structures as a source of habitat heterogeneity and biodiversity on the deep ocean margins. Marine Ecology **31**: 21–50.

Buhl-Mortensen, L., P. Buhl-Mortensen, M. F. J. Dolan, J. Dannheim, V. Bellec, and B. Holte. 2012. Habitat complexity and bottom fauna composition at different scales on the continental shelf and slope of northern Norway. Hydrobiologia **685**: 191–219.

Buscombe, D. 2008. Estimation of grain-size distributions and associated parameters from digital images of sediment. Sedimentary Geology **210**: 1–10.

Canals, M., P. Puig, X.D. de Madron, S. Heussner, A. Palanques, and J. Fabres. 2006. Flushing submarine canyons. Nature **444**: 354–357.

Carney, R.S. 2005. Zonation of deep biota on continental margins. Oceanography and Marine Biology: An Annual Review **43**: 211–278

Carroll, M.L., S.G. Denisenko, P.E. Renaud, and W.G. Ambrose. 2008. Benthic infauna of the seasonally ice-covered western Barents Sea: Patterns and relationships to environmental forcing. Deep Sea Research Part II: Topcial Studies in Oceanography **55**: 2340–2351.

Cavalieri, D. J., and C.L. Parkinson. 2012. Arctic sea ice variability and trends, 1979-2010. The Cryosphere **6**: 881-889.

Chen, C., H. Liu, and R.C. Beardsley. 2003. An unstructured grid, finite-volume, three-dimensional, primitive equations ocean model: Application to coastal ocean and estuaries. Journal of Atmospheric and Oceanic Technology **20**: 159–186.

Cochrane, S.K.J., S.G. Denisenko, P.E. Renaud, C.S. Emblow, W.G. Ambrose, I.H. Ellingsen, and J. Skarðhamar. 2009. Benthic macrofauna and productivity regimes in the Barents Sea — Ecological implications in a changing Arctic. Journal of Sea Research **61**: 222–233.

Company, J.B., P. Puig, F. Sardà, A. Palanques, M. Latasa, and R. Scharek. 2008. Climate influence on deep sea populations. PLoS ONE **3**: e1431.

Compton, T.J., D.A. Bowden, C.R. Pitcher, J.E. Hewitt, and N. Ellis. 2013. Biophysical patterns in benthic assemblage composition across contrasting continental margins off New Zealand. Journal of Biogeography **40**: 75–89.

Cordes, E.E., J.W. Nybakken, and G. VanDykhuizen. 2001. Reproduction and growth of *Anthomastus ritteri* (Octocorallia: Alcyonacea) from Monterey Bay, California, USA. Marine Biology **138**: 491–501.

Cornell, H. V., and S.P. Harrison. 2013. Regional effects as important determinants of local diversity in both marine and terrestrial systems. Oikos **122**: 288–297.

Currie, D.R., and S.J. Sorokin. 2014. Megabenthic biodiversity in two contrasting submarine canyons on Australia's southern continental margin. Marine Biology Research **10**: 97-110.

Cusson, M., and E. Bourget. 1997. Influence of topographic heterogeneity and spatial scales on the structure of the neighboring intertidal endobenthic macrofaunal community. Marine Ecology Progress Series **150**: 181–193.

Dalpadado, P., K.R. Arrigo, S.S. Hjøllo, F. Rey, R.B. Ingvaldsen, E. Sperfeld, G.L. van Dijken, L.C. Stige, A. Olsen, and G. Ottersen. 2014. Productivity in the Barents Sea--response to recent climate variability. PLoS ONE **9**: e95273.

Dalpadado, P., R.B. Ingvaldsen, L.C. Stige, B. Bogstad, T. Knutsen, G. Ottersen, and B. Ellertsen. 2012. Climate effects on Barents Sea ecosystem dynamics. ICES Journal of Marine Sciences **69**: 1303–1316.

Dayton, P.K., 1971. Competition, disturbance, and community organization: The provision and subsequent utilization of space in a rocky intertidal community. Ecological Monographs **41**: 351-389.

Dayton, P.K. and R.R. Hessler. 1972. Role of biological disturbance in maintaining diversity in the deep sea. Deep-Sea Research **19**: 199-208.

Degen, R., L.L. Jørgensen, P. Ljubin, I.H. Ellingsen, H. Pehlke, and T. Brey. 2016. Patterns and drivers of megabenthic secondary production on the Barents Sea shelf. Marine Ecology Progress Series **546**: 1–16.

De Leo, F. C., and A.M.S. Pires-Vanin. 2006. Benthic megafauna communities under the influence of the South Atlantic Central Water intrusion onto the Brazilian SE shelf: A comparison between an upwelling and a non-upwelling ecosystem. Journal of Marine Systems **60**: 268–284.

De Leo, F.C., E.W. Vetter, C.R. Smith, A.A. Rowden, and M. McGranaghan. 2014. Spatial scale-dependent habitat heterogeneity influences submarine canyon macrofaunal abundance and diversity off the Main and Northwest Hawaiian Islands. Deep-Sea Research Part II: Topical Studies in Oceanography **104**: 267–290.

Diesing, M., S.L. Green, D. Stephens, R.M. Lark, H.A. Stewart, and D. Dove. 2014. Mapping seabed sediments: Comparison of manual, geostatistical, object-based image analysis and machine learning approaches. Continental Shelf Research **84**: 107-119.

Dolan, M. F. J., A.J. Grehan, J.C. Guinan, and C. Brown. 2008. Modelling the local distribution of cold-water corals in relation to bathymetric variables: Adding spatial context to deep-sea video data. Deep-Sea Research Part I: Oceanographic Research Papers **55**: 1564–1579.

Dolan, M.F.J., and V.L. Lucieer. 2014. Variation and Uncertainty in Bathymetric Slope Calculations Using Geographic Information Systems. Marine Geodesy **37**: 187–219.

Duineveld, G. C. A., R.M. Jeffreys, M.S.S. Lavaleye, A.J. Davies, M.J.N. Bergman, T. Watmough, and R. Witbaard. 2012. Spatial and tidal variation in food supply to shallow cold-water coral reefs of the Mingulay Reef complex (Outer Hebrides, Scotland). Marine Ecology Progress Series **444**: 97–115.

Dunton, K.H., J.L. Goodall, S.V. Schonberg, J.M. Grebmeier, and D.R. Maidment. 2005. Multi-decadal synthesis of benthic–pelagic coupling in the western arctic: Role of cross-shelf advective processes. Deep Sea Research Part II Topical Studies in Oceanography **52**: 3462–3477.

Durden, J.M., B.J. Bett, D.O.B. Jones, V.A.I. Huvenne, and H.A. Ruhl. 2015. Abyssal hills - hidden source of increased habitat heterogeneity, benthic megafaunal biomass and diversity in the deep sea. Progress in Oceanography **137**: 209–218.

Du Preez, C., and V. Tunnicliffe. 2011. Shortspine thornyhead and rockfish (Scorpaenidae) distribution in response to substratum, biogenic structures and trawling. Marine Ecology Progress Series **425**: 217–231.

Edinger, E.N., O.A. Sherwood, D.J.W. Piper, V.E. Wareham, K.D. Baker, K.D. Gilkinson, and D.B. Scott. 2011. Geological features supporting deep-sea coral habitat in Atlantic Canada. Continental Shelf Research **31**: S69–S84.

Ellingsen, K.E., and J.S. Gray. 2002. Spatial patterns of benthic diversity : is there a latitudinal gradient along the Norwegian continental shelf ? Journal of Animal Ecology **71**: 373–389.

ESSIM Planning Office. 2006. Coral conservation plan Maritimes region (2006-2010). Oceans and Coastal Management Report 2006-01. 59 pp.

Etter, R., and F. Grassle. 1992. Patterns of species diversity in the deep sea as a function of sediment particle size diversity. Nature **360**: 576-578.

Etnoyer, P., and L.E. Morgan. 2005. Habitat-forming deep-sea corals in the Northeast Pacific Ocean. In: Freiwald, A., and J.M. Roberts [eds]. Cold-water Corals and Ecosystems. Berlin Heidelberg: Springer-Verlag. pp. 331–343.

Fader, G.B., L.H. King, and B. MacClean. 1977. Surficial geology of the eastern Gulf of Maine and Bay of Fundy. Geological Survey of Canada Pap. 76-17. 23 pp.

Ferrier, S., G. Manion, J. Elith, and K. Richardson. 2007. Using generalized dissimilarity modelling to analyse and predict patterns of beta diversity in regional biodiversity assessment. Diversity and Distributions **13**: 252–264.

Fitzpatrick, M.C., N.J. Sanders, S. Normand, J.-C. Svenning, S. Ferrier, A.D. Gove, and R.R. Dunn. 2013. Environmental and historical imprints on beta diversity: insights from variation in rates of species turnover along gradients. Proceedings of the Royal Society – Biological Sciences **280**: 20131201.

Fossheim, M., R. Primicerio, E. Johannesen, R.B. Ingvaldsen, M.M. Aschan, and A.V. Dolgov. 2015. Recent warming leads to a rapid borealization of fish communities in the Arctic. Nature Climate Change **5**: 1–6.

Franks, P. 1992. Sink or swim, accumulation of biomass at fronts. Marine Ecology Progress Series **82**: 1–12.

Furevik, T. 2001. Annual and interannual variability of Atlantic Water temperatures in the Norwegian and Barents Seas: 1980–1996. Deep Sea Research Part I: Oceanographic Research Papers **48**: 383–404.

Gage, J.D., and P.A. Tyler. 1991. Deep-sea biology: A natural history of organisms at the deep-sea floor. Cambridge University Press, 504 p.

Gallucci, F., G. Fonseca and T. Soltwedel. 2008. Effects of megafauna exclusion on nematode assemblages at a deep-sea site. Deep-Sea Research Part I: Oceanographic Research Papers **55**: 332–349.

Ganesan, P., V. Rajini, and R. I. Rajkumar. 2010. Segmentation and edge detection of color images using CIELAB color space and edge detectors. Emerging Trends in Robotics and Communications Technologies. IEEE. 393–397.

García-Sanz, S., F. Tuya, P. G. Navarro, C. Angulo-Preckler, and R. J. Haroun. 2012. Post larval, short-term, colonization patterns: The effect of substratum complexity across subtidal, adjacent, habitats. Estuarine and Coastal Shelf Science **112**: 183–191.

Gardiner, F. P., and R.L. Haedrich. 1978. Zonation in the deep benthic megafauna. Oecologia **317**: 311–317.

Gass, S.E., and J.H.M. Willison. 2005. An assessment of the distribution of deep-sea corals in Atlantic Canada by using both scientific and local forms of knowledge. In: Freiwald, A., J.M. Roberts [eds]. Cold-water Corals and Ecosystems. Berlin Heidelberg: Springer-Verlag. pp. 223–245.

Gass, S.E., and J.M. Roberts. 2006. The occurrence of the cold-water coral *Lophelia pertusa* (Scleractinia) on oil and gas platforms in the North Sea: Colony growth, recruitment and environmental controls on distribution. Marine Pollution Bulletin **52**: 549–559.

Genin, A., P.K. Dayton, P.F. Lonsdale, and F.N. Spiess. 1986. Corals on seamount peaks provide evidence of current acceleration over deep-sea topography. Nature **322**: 1–3.

Genin, A. C.K. Paull, W.P. Dillon. 1992. Anomalous abundances of deep-sea fauna on a rocky bottom exposed to strong currents. Deep Sea Research Part A. Oceanographic Research Papers **39**: 293-302.

Gordon Jr., D. C., D. L. McKeown, G. Steeves, W. P. Vass, K. Bentham, and M. Chin-Yee. 2007. Canadian imaging and sampling technology for studying benthic habitat and biological communities, p. 29–37. In B.J. Todd and H.G. Greene [eds.], Mapping the Seafloor for Habitat Characterization: Geological Association of Canada, Special Paper 47.

Gosselin, L. A., and P.Y. Qian. 1997. Juvenile mortality in benthic marine invertebrates. Marine Ecology Progress Series **146**: 265–282.

Gotelli, N.J., and R.K. Colwell. 2010. Estimating species richness. p. 39-54. In Magurran, A.E., and B.J. McGill [eds]. Biological diversity: frontiers in measurement and assessment. Oxford University Press.

Grabowski, J. H. 2004. Habitat complexity disrupts predator-prey interactions but not the trophic cascade on oyster reefs. Ecology **85**: 995–1004.

Grange, L. J., and C.R. Smith. 2013. Megafaunal communities in rapidly warming fjords along the West Antarctic Peninsula: Hotspots of abundance and beta diversity. PLoS ONE 8(11): e77917.

Grassle, J.F., and H.L. Sanders. 1973. Life histories and the role of disturbance. Deep-Sea Research **20**: 643-659.

Grassle, J.F., H.L. Sanders, R.R. Hessler, G.T. Rowe, and T. McLellan. 1975. Pattern and zonation: a study of the bathyal megafauna using the research submersible *Alvin*. Deep-Sea Research **22**: 457-481.

Grassle, J.F. 1977. Slow recolonisation of deep-sea sediment. Nature **265**: 618–619.

Gray, J.S. 1974. Animal-sediment relationships. Oceanography and Marine Biology: An Annual Review **12**: 223-261.

Grebmeier, J.M., and J.P. Barry. 1991. The influence of oceanographic processes on pelagic-benthic coupling in polar regions: A benthic perspective. Journal of Marine Systems **2**: 495–518.

Grigg, R.W. 1988. Recruitment limitation of a deep benthic hard-bottom octocoral population in the Hawaiian Islands. Marine Ecology Progress Series **45**: 121–126.

Haris, K., S.N. Efstratiadis, N. Maglaveras, and A.K. Katsaggelos. 1998. Hybrid image segmentation using watersheds and fast region merging. IEEE Trans. Image Processing **7(12)**: 1684-1699.

Harris, P. T., and T. Whiteway. 2011. Global distribution of large submarine canyons: Geomorphic differences between active and passive continental margins. Marine Geology **285**: 69–86.

Harrison, P.L., C.C. Wallace. 1990. Reproduction, dispersal and recruitment of scleractinian corals. In: Dubinsky, Z. [ed]. Coral Reefs: Ecosystems of the World. New York: Elsevier. pp. 133–207.

Harrison, C.S., D.A Siegel, and S. Mitarai. 2013. Filamentation and eddy-eddy interactions in marine larval accumulation and transport. Marine Ecology Progress Series **472**: 27–44.

Heifetz, J., R.P. Stone, and S.K. Shotwell. 2009. Damage and disturbance to coral and sponge habitat of the Aleutian Archipelago. Marine Ecology Progress Series **397**: 295–303.

Henry, L.-A., A.J. Davies, and J.M. Roberts. 2010. Beta diversity of cold-water coral reef communities off western Scotland. Coral Reefs **29**: 427–436.

Henry, L.-A., J. Moreno Navas, and J.M. Roberts. 2013. Multi-scale interactions between local hydrography, seabed topography, and community assembly on cold-water coral reefs. Biogeosciences **10**, 2737–2746.

Henschke, N., D.A. Bowden, J.D. Everett, S.P. Holmes, R.J. Kloser, R.W. Lee, and I.M. Suthers. 2013. Salp-falls in the Tasman Sea: A major food input to deep-sea benthos. Marine Ecology Progress Series **491**: 165–175.

Herbaut, C., M.-N. Houssais, S. Close, and A.-C. Blaizot. 2015. Two wind-driven modes of winter sea ice variability in the Barents Sea. Deep Sea Research Part I: Oceanography Research Papers **106**: 97–115.

Hillebrand, H. 2004. Strength, slope and variability of marine latitudinal gradients. Marine Ecology Progress Series **273**: 251–267.

Huang, Z., B. P. Brooke, and P. T. Harris. 2011. A new approach to mapping marine benthic habitats using physical environmental data. Continental Shelf Research **31**:S4–S16.

Hughes, T.P., A.H. Baird, E.A. Dinsdale, A. Moltschanniwskyj, M.S. Pratchett. J.E. Tanner, and B.L. Willis. 2000. Supply-side ecology works both ways: The link between benthic adults, fecundity, and larval recruits. Ecology **81**: 2241–2249.

Hunt, H.L., and R.E. Scheibling. 1997. Role of early post-settlement mortality in recruitment of benthic marine invertebrates. Marine Ecology Progress Series **155**: 269–301.

Huvenne, V. A. I., P. Blondel, and J.-P. Henriet. 2002. Textural analyses of sidescan sonar imagery from two mound provinces in the Porcupine Seabight. Marine Geology **189**: 323–341.

Huvenne, V.A.I., P.A. Tyler, D.G. Masson, E.H. Fisher, C. Hauton, V. Hühnerbach, T.P. Le Bas, and G.A. Wolff. 2011. A picture on the wall: Innovative mapping reveals cold-water coral refuge in submarine canyon. PLoS ONE **6**: e28755.

Ingvaldsen, R.B., L. Asplin, and H. Loeng. 2004. The seasonal cycle in the Atlantic transport to the Barents Sea during the years 1997–2001. Continental Shelf Research **24**: 1015–1032.

Incze, L. S., P. Lawton, S. L. Ellis, and N. H. Wolff. 2010. Biodiversity knowledge and its application in the Gulf of Maine Area, p. 43–63. In A.D. McIntyre [ed.], Life in the World's Oceans: Diversity, Distribution, and Abundance. Wiley-Blackwell.

Ismail, K., V.A.I. Huvenne, and D.G. Masson. 2015. Objective automated classification technique for marine landscape mapping in submarine canyons. Marine Geology **362**: 17– 32.

Jacquez, G. M., S. Maruca, and M.-J. Fortin. 2000. From fields to objects: A review of geographic boundary analysis. Journal of Geographical Systems **2**: 221–241.

Johannesen, E., Å.S. Høines, A.V. Dolgov, and M. Fossheim. 2012a. Demersal fish assemblages and spatial diversity patterns in the arctic-atlantic transition zone in the Barents Sea. PLoS ONE **7**:e34924.

Johannesen, E., R.B. Ingvaldsen, B. Bogstad, P. Dalpadado, E. Eriksen, H. Gjøsaeter, T. Knutsen, M. Skern-Mauritzen, J.E. Stiansen. 2012b. Changes in Barents Sea ecosystem state, 1970-2009: climate fluctuations, human impact, and trophic interactions. ICES Journal of Marine Sciences **69**: 880-889.

Johnson, M.P., M. White, A. Wilson, L. Würzberg, E. Schwabe, H. Folch, and A.L. Allcock. 2013. A vertical wall dominated by *Acesta excavata* and *Neopycnodonte zibrowii*, part of an undersampled group of deep-sea habitats. PLoS ONE **8**: e79917.

Johnson, N.A., J.W. Campbell, T.S. Moore, M.A. Rex, R.J. Etter, C.R. McClain, and M.D. Dowell. 2007. The relationship between the standing stock of deep-sea macrobenthos and surface production in the western North Atlantic. Deep-Sea Research Part I: Oceanographic Research Papers **54**: 1350–1360.

Jones, D.O.B., B.J. Bett, and P.A. Tyler. 2007. Megabenthic ecology of the deep Faroe-Shetland channel: A photographic study. Deep-Sea Research Part I: Oceanographic Research Papers **54**: 1111–1128.

Jones, D.O.B., A. Yool, C.-L. Wei, S.A. Henson, H.A. Ruhl, R.A. Watson, and M. Gehlen. 2014. Global reductions in seafloor biomass in response to climate change. Global Change Biology **20**: 1861–72.

Jones, D. O. B., and M.E. Brewer. 2012. Response of megabenthic assemblages to different scales of habitat heterogeneity on the Mauritanian slope. Deep-Sea Research Part I: Oceanographic Research Papers **67**: 98–110.

Jones, D. O. B., C.O. Mrabure, and A.R. Gates. 2013. Changes in deep-water epibenthic megafaunal assemblages in relation to seabed slope on the Nigerian margin. Deep-Sea Research Part I: Oceanographic Research Papers **78**: 49–57.

Jørgensen, L.L., P. Ljubin, H.R. Skjoldal, R.B. Ingvaldsen, N. Anisimova, and I. Manushin. 2015. Distribution of benthic megafauna in the Barents Sea: baseline for an ecosystem approach to management. ICES Journal of Marine Sciences **72**: 595–613.

Jørgensen L.L, B. Planque, T.H. Thangstad, and G. Certain. 2016. Vulnerability of megabenthic species to trawling in the Barents Sea**.** ICES Journal of Marine Sciences **73 (suppl 1)**: i84-i97.

Josefson, A., and D. Conley. 1997. Benthic response to a pelagic front. Marine Ecology Progress Series **147**: 49–62.

Jumars, P. 1975. Environmental grain and polychaete species' diversity in a bathyal benthic community. Marine Biology **30**: 253-266.

Kahng, S.E., Y. Benayahu, and H.R. Lasker. 2011. Sexual reproduction in octocorals. Marine Ecology Progress Series **443**: 265–283.

Kaskela, A. M., A. T. Kotilainen, Z. Al-Hamdani, J. O. Leth, and J. Reker. 2012. Seabed geomorphic features in a glaciated shelf of the Baltic Sea. Estuarine and Coastal Shelf Science **100**:150–161.

Kelly, N., A. Metaxas, and D. Butterfield. 2007. Spatial and temporal patterns of colonization by deep-sea hydrothermal vent invertebrates on the Juan de Fuca Ridge, NE Pacific. Aquatic Biology **1**: 1–16.

Kettig, R. L., and D. A. Landgrebe. 1976. Classification of multispectral image data by extraction and classification of homogeneous objects. IEEE Transactions on Geoscience and Remote Sensing **GE-14**: 19–26.

Kitchell, J.A., J.F. Kitchell, G.L. Johnson, and K.L. Hunkins. 1978. Abyssal traces and megafauna: Comparison of productivity, diversity and density in the Arctic and Antarctic. Paleobiology **4**: 171-180

Klitgaard, A. B., and O.S. Tendal. 2004. Distribution and species composition of mass occurrences of large-sized sponges in the northeast Atlantic. Progress in Oceanography **61**: 57–98.

Kostylev, V. E., J. Erlandsson, M. Y. Ming, and G. A. Williams. 2005. The relative importance of habitat complexity and surface area in assessing biodiversity: Fractal application on rocky shores. Ecological Complexity **2**: 272–286.

Kostylev, V. E., B. J. Todd, G. B. J. Fader, R. C. Courtney, G. D. M. Cameron, and R. A. Pickrill. 2001. Benthic habitat mapping on the Scotian Shelf based on multibeam bathymetry, surficial geology and seafloor photographs. Marine Ecology Progress Series **219**:121–137.

Kovalenko, K.E., S.M. Thomaz, D.M. Warfe. 2011. Habitat complexity: approaches and future directions. Hydrobiologia **685**: 1–17.

Krieger, K.J. 2001. Coral (*Primnoa*) impacted by fishing gear in the Gulf of Alaska. In: Willison, J.H.M., S.E. Gass, E. Kenchington, M. Butler, and P. Doherty [eds]. Proceedings of the First International Symposium on Deep-Sea Corals, pp. 106-116. Halifax, NS: Ecology Action Centre and Nova Scotia Museum.

Lacharité, M., and A. Metaxas. 2013. Early life history of deep-water gorgonian corals may limit their abundance. PLoS ONE **8**: e65394.

Lacharité, M., A. Metaxas, and P. Lawton. 2015. Using object-based image analysis to determine seafloor fine-scale features and complexity. Limnology and Oceanography: Methods **13**: 553–567.

Lambert, G. I., S. Jennings, H. Hinz, L. G. Murray, L. Parrott, M. J. Kaiser, and J. G. Hiddink. 2013. A comparison of two techniques for the rapid assessment of marine habitat complexity. Methods in Ecology and Evolution **4**: 226–235.

Landry, M.R., M.D. Ohman, R. Goericke, M.R. Stukel, K.A. Barbeau, R. Bundy, and M. Kahru. 2012. Pelagic community responses to a deep-water front in the California Current Ecosystem: overview of the A-Front Study. Journal of Plankton Research **34**: 739–748.

Lathuilière, C., V. Echevin, M. Lévy, and G. Madec. 2010. On the role of the mesoscale circulation on an idealized coastal upwelling ecosystem. Journal of Geophysical Research Oceans **115**: 1–14.

Lecours, V., R. Devillers, D.C. Schneider, V.L. Lucieer, C.J. Brown, and E.N. Edinger. 2015. Spatial scale and geographic context in benthic habitat mapping: review and future directions. Marine Ecology Progress Series **535**: 259–284.

Leduc, D., A.A. Rowden, D.A. Bowden, S.D. Nodder, P.K. Probert, C.A. Pilditch, G.C.A. Duineveld, and R. Witbaard. 2012. Nematode beta diversity on the continental slope of New Zealand: spatial patterns and environmental drivers. Marine Ecology Progress Series **454**: 37–52.

Leduc, D., A.A. Rowden, P.K. Probert, C.A. Pilditch, S.D. Nodder, A. Vanreusel, G.C.A. Duineveld, and R. Witbaard. 2012. Further evidence for the effect of particle-size diversity on deep-sea benthic biodiversity. Deep-Sea Research Part I: Oceanographic Research Papers **63**: 164–169.

Legendre, P., and L. Legendre. 1998. Numerical Ecology, 2nd Edition. Elsevier Science.

Levin, L.A., C.L. Huggett, and K.F. Wishner. 1991. Control of deep-sea benthic community structure by oxygen and organic-matter gradients in the eastern Pacific Ocean. Journal of Marine Research **49**: 763–800.

Levin, L.A., R.J. Etter, M.A. Rex, A.J. Gooday, C.R. Smith, J. Pineda, C.T. Stuart, R.R. Hessler, and D. Pawson. 2001. Environmental influence on regional deep-sea species diversity. Annual Review of Ecological Systematics **32**: 51-93.

Levin, L.A., and P.K. Dayton. 2009. Ecological theory and continental margins: where shallow meets deep. Trends in Ecology & Evolution **24**: 606–17.

Levin, L.A., and M. Sibuet. 2012. Understanding continental margin biodiversity: A new imperative. Annual Review of Marine Science **4**: 79–112.

Lien, V.S., and B. Ådlandsvik. 2014. Bottom water formation as a primer for spring-blooms on Spitsbergenbanken? Journal of Marine Systems **130**: 241–247.

Lien, V.S., Y. Gusdal, J. Albretsen, A. Melsom, and F.B. Vikebø. 2013a. Evaluation of a Nordic Seas 4 km numerical ocean model hindcast archive (SVIM), 1960-2011 (Report No. 7-2013). Retrieved from Institute of Marine Research: www.imr.no.

Lien, V.S., F.B. Vikebø, and O. Skagseth. 2013b. One mechanism contributing to co-variability of the Atlantic inflow branches to the Arctic. Nature Communications **4**, 1488.

Lin, H. Y., P.Y Lin, N.N. Chang, J.C. Shiao, and S.J. Kao. 2014. Trophic structure of megabenthic food webs along depth gradients in the South China Sea and off northeastern Taiwan. Marine Ecology Progress Series **501**: 53–66.

Loeng, H. 1991. Features of the physical oceanographic conditions of the Barents Sea. Polar Research **10**: 5–18.

Loeng, H., and K. Drinkwater. 2007. An overview of the ecosystems of the Barents and Norwegian Seas and their response to climate variability. Deep Sea Research Part II Topical Studies in Oceanography **54**: 2478–2500.

Lucieer, V., and A. Lucieer. 2009. Fuzzy clustering for seafloor classification. Marine Geology **264**: 230–241.

Lucieer, V., N. A. Hill, N. S. Barrett, and S. Nichol. 2013. Do marine substrates "look" and "sound" the same? Supervised classification of multibeam acoustic data using autonomous underwater vehicle images. Estuarine and Coastal Shelf Science **117**:94–106.

Lucieer, V. L. 2008. Object-oriented classification of sidescan sonar data for mapping benthic marine habitats. International Journal of Remote Sensing **29**: 905–921.

Lucieer, V., and G. Lamarche. 2011. Unsupervised fuzzy classification and object-based image analysis of multibeam data to map deep water substrates, Cook Strait, New Zealand. Continental Shelf Research **31**: 1236–1247.

Lutz, M., R. Dunbar, and K. Caldeira. 2002. Regional variability in the vertical flux of particulate organic carbon in the ocean interior. Global biogeochemical cycles **16**: 11–18.

Mangano, M., M. Kaiser, E. Porporato, and N. Spanò. 2013. Evidence of trawl disturbance on mega-epibenthic communities in the Southern Tyrrhenian Sea. Marine Ecology Progress Series **475**: 101–117.

Mann, K.H. and J.R.N. Lazier. 1996. Dynamics of Marine Ecosystems: Biological-Physical Interactions in the Oceans, 2nd edition. Blackwell Science, Cambridge.

Matias, M. G., A. J. Underwood, D. F. Hochuli, and R. A. Coleman. 2010. Independent effects of patch size and structural complexity on diversity of benthic macroinvertebrates. Ecology **91**: 1908–1915.

McArthur, M. A., B.P. Brooke, R. Przeslawski, D.A. Ryan, V.L. Lucieer, S. Nichol, A.W. McCallum, C. Melin, I.D. Cresswell, and L.C. Radke. 2010. On the use of abiotic surrogates to describe marine benthic biodiversity. Estuarine, Coastal and Shelf Science **88**: 21–32.

McCallum, A. W., G.C.B. Poore, A. Williams, F. Althaus, and T. O'Hara. 2013. Environmental predictors of decapod species richness and turnover along an extensive Australian continental margin (13-35° S). Marine Ecology **34**: 298–312.

McCoy, E. D., and S. S. Bell. 1991. Habitat structure: The evolution and diversification of a complex topic, p. 3–22. In S.S. Bell, E.D. McCoy, and H.R. Mushinsky [eds.], Habitat Structure: The physical arrangement of objects in space. Chapman & Hall.

Mercier, A., and J.-F. Hamel. 2011. Contrasting reproductive strategies in three deep-sea octocorals from eastern Canada: *Primnoa resedaeformis*, *Keratoisis ornata*, and *Anthomastus grandiflorus*. Coral Reefs **30**: 337–350.

Metaxas, A., and B. Giffin. 2004. Dense beds of the ophiuroid *Ophiacantha abyssicola* on the continental slope off Nova Scotia, Canada. Deep-Sea Research Part I **51**: 1307–1317.

Meyer, K.S., T. Soltwedel, and M. Bergmann. 2014. High biodiversity on a deep-water reef in the eastern Fram Strait. PLoS ONE **9**: e105424.

Meyer, K.S., A.K. Sweetman, C.M. Young, and P.E. Renaud. 2015. Environmental factors structuring Arctic megabenthos – a case study from a shelf and two fjords. Frontiers in Marine Science **2**: 22.

Miller, K., A. Williams, A.A. Rowden, C. Knowles, and G. Dunshea. 2010. Conflicting estimates of connectivity among deep-sea coral populations. Marine Ecology **31**: 144–157.

Mohn, C., A. Rengstorf, M. White, G. Duineveld, F. Mienis, K. Soetaert, and A. Grehan. 2014. Linking benthic hydrodynamics and cold-water coral occurrences: A high-resolution model study at three cold-water coral provinces in the NE Atlantic. Progress in Oceanography **122**: 92–104.

Morin, A., J. Urban, P. D. Adams, I. Foster, A. Sali, D. Baker, and P. Sliz. 2012. Shining light into black boxes. Science. **336(6078)**: 159–160.

Mortensen, P.B., and L. Buhl-Mortensen. 2004. Distribution of deep-water gorgonian corals in relation to benthic habitat features in the Northeast Channel (Atlantic Canada). Marine Biology **144**: 1223–1238.

Mortensen, P.B., and L. Buhl-Mortensen. 2005. Morphology and growth of the deep-water gorgonians *Primnoa resedaeformis* and *Paragorgia arborea*. Marine Biology **147**: 775–788.

Mosch, T., S. Sommer, M. Dengler, A. Noffke, L. Bohlen, O. Pfannkuche, V. Liebetrau, and K. Wallmann. 2012. Factors influencing the distribution of epibenthic megafauna across the Peruvian oxygen minimum zone. Deep-Sea Research Part I: Oceanographic Research Papers **68**: 123–135.

Mountain, D. G., and P.F. Jessen. 1987. Bottom waters of the Gulf of Maine, 1978—1983. Journal of Marine Research **45**: 319–345.

Mullineaux, L.S., S.W. Mills, E. Goldman. 1998. Recruitment variation during a pilot colonization study of hydrothermal vents (9°50′N, East Pacific Rise). Deep Sea Research Part II: Topical Studies in Oceanography **45**: 441–464.

Murillo, F.J., P. Duran Munoz, A. Altuna, and A. Serrano. 2011. Distribution of deep-water corals of the Flemish Cap, Flemish Pass, and the Grand Banks of Newfoundland (Northwest Atlantic Ocean): interaction with fishing activities. ICES Journal of Marine Science **68**: 319–332.

Murillo, F.J., A. Serrano, E. Kenchington, J. Mora. 2016. Epibenthic assemblages of the tail of the grand bank and Flemish cap (northwest Atlantic) in relation to environmental parameters and trawling intensity. Deep Sea Research Part I: Oceanographic Research Papers **109**: 99-122.

Navas, J.M., P.L. Miller, L.-A. Henry, S.J. Henniger, and J.M. Roberts. 2014. Ecohydrodynamics of Cold-Water Corals Reefs: A case study of the Mingulay Reef Complex (Western Scotland). PLoS ONE 9(5): e98218.

Netto, S.A., F. Gallucci, and G.F.C Fonseca. 2005. Meiofauna communities of continental slope and deep-sea sites off SE Brazil. Deep-Sea Research Part I: Oceanographic Research Papers **52**: 845–859.

Nishikawa, A., M. Katoh, K. Sakai. 2003. Larval settlement rates and gene flow of broadcast-spawning (*Acropora tenuis*) and planula-brooding (*Stylophora pistillata*) corals. Marine Ecology Progress Series **256**: 87–97.

Oksanen, J., F.G. Blanchet, R. Kindt, P. Legendre, P.R. Minchin, R.B. O'Hara, G.L. Simpson, P. Solymos, M. Henry, H. Stevens, and H. Wagner. 2016. Vegan: Community Ecology Package. R package version 2.3-5.

Ojala, T., M. Pietikäinen, and T. Mäenpää. 2002. Multiresolution gray-scale and rotation invariant texture classification with local binary patterns. IEEE Transactions on Pattern Analysis and Machine Intelligence **24**: 971–987.

Orejas, C., P.J. Lopez-Gonzalez, J.M. Gili, N. Teixido, J. Gutt, and W.E. Arntz. 2002. Distribution and reproductive ecology of the Antarctic octocoral *Ainigmaptilon antarcticum* in the Weddell Sea. Marine Ecology Progress Series **231**: 101–114.

Ozhigin, V.K., and V.A. Ivshin. 1999. Water masses of the Barents Sea. Knipowich Polar Research Institute of Marine Fisheries and Oceanography, Murmansk (Russia).

Pace, M.L., G.A. Knauer, D.M. Karl, and J.H. Martin. 1987. Primary production, new production and vertical flux in the Eastern Pacific-Ocean. Nature **325**: 803-804.

Pal, N. R., and S. K. Pal. 1993. A review of image segmentation techniques. Pattern Recognition **26**: 1277–1294.

Peng, R. D. 2011. Reproducible research in computational science. Science. **334(6060)**: 1226–1227.

Perona, P., and J. Malik. 1990. Scale-space and edge-detection using anisotropic diffusion. IEEE Transactions on Pattern Analysis and Machine Intelligence **12**:629–639.

Perrette, M., A. Yool, G.D. Quartly, and E.E. Popova. 2011. Near-ubiquity of ice-edge blooms in the Arctic. Biogeosciences **8**: 515–524.

Pezzulli, S., D.B. Stephenson, and A. Hannachi. 2005. The variability of seasonality. Journal of Climate **18**: 71–88.

Pfirman, S. L., D. Bauch, and T. Gammelsrød. 1994. The northern Barents Sea: water mass distribution and modification. In: Johannessen, O.M., R.D. Muench, and J.E. Overland [eds]. The polar oceans and their role in shaping the global environment. Washington, DC: American Geophysical Union. pp 77-94.

Piepenburg, D., T.H. Blackburn, C.F. von Dorrien, J. Gutt, P.O.J. Hall, S. Hulth, M.A. Kendall, K.W. Opalinski, E. Rachor, and M.K. Schmid. 1995. Partitioning of benthic community respiration in the Arctic northwestern Barents Sea. Marine Ecology Progress Series **118**: 199–213.

Piepenburg, D., W.G. Ambrose Jr., A. Brandt, P.E. Renaud, M.J. Ahrens, and P. Jensen. 1997. Benthic community patterns reflect water column processes in the Northeast Water polynya (Greenland). Journal of Marine Systems **10**: 467–482.

Pilskaln, C. H., K. Hayashi, B.A. Keafer, D.M. Anderson, and D.J. McGillicuddy. 2014. Benthic nepheloid layers in the Gulf of Maine and *Alexandrium* cyst inventories. Deep-Sea Research Part II: Topical Studies in Oceanography **103**: 55–65.

Pitcher, C.R., P. Lawton, N. Ellis, S. J. Smith, L. S. Incze, C.-L. Wei, M. E. Greenlaw, N. H. Wolff, J. A. Sameoto, P. V. R. Snelgrove, and M. Cadotte. 2012. Exploring the role of environmental variables in shaping patterns of seabed biodiversity composition in regional-scale ecosystems. Journal of Applied Ecology **49**: 670–679.

Ramp, S.R., S.J. Schlitz, and W.R. Wright. 1985. The deep flow through the Northeast Channel, Gulf of Maine. Journal of Physical Oceanography **15**: 1790–1808.

Renaud, P.E., N. Morata, M.L. Carroll, S.G. Denisenko, and M. Reigstad. 2008. Pelagic–benthic coupling in the western Barents Sea: Processes and time scales. Deep Sea Research Part II: Topical Studies in Oceanography **55**: 2372–2380.

Rengstorf, A. M., A. Grehan, C. Yesson, and C. Brown. 2012. Towards High-Resolution Habitat Suitability Modeling of Vulnerable Marine Ecosystems in the Deep-Sea: Resolving Terrain Attribute Dependencies. Marine Geodesy **35**: 343–361.

Rex, M. A., C.T. Stuart, and G. Coyne. 2000. Latitudinal gradients of species richness in the deep-sea benthos of the North Atlantic. Proceedings of the National Academy of Science of the United States of America **97**: 4082–4085.

Rex, M.A., R. Etter, J. Morris, J. Crouse, C. McClain, N. Johnson, C. Stuart, J. Deming, R. Thies, and R. Avery. 2006. Global bathymetric patterns of standing stock and body size in the deep-sea benthos. Marine Ecology Progress Series **317**: 1–8.

Rice, A.L., M.H. Thurston, and A.L. New. 1990. Dense aggregations of a hexactinellid sponge, *Pheronema carpenter*i, in the Porcupine Seabight (northeast Atlantic Ocean), and possible causes. Progress in Oceanography **24**: 179-196.

Richmond, R.H. 1997. Reproduction and Recruitment in Corals: Critical Links in the Persistence of Reefs. In: Birkeland, C. [ed]. Life and Death of Coral Reefs. Springer. pp. 1–23.

Risk, M. J. 1972. Fish diversity on a coral reef in the Virgin Islands. Atoll Research Bulletin **193**: 1–6.

Roark, E. B., T.P. Guilderson, R.B. Dunbar, S.J. Fallon, and D.A. Mucciarone. 2009. Extreme longevity in proteinaceous deep-sea corals. Proceedings of the National Academy of Sciences of the United States of America **106**: 5204–8.

Robert, K., D. Jones, and V.A.I. Huvenne. 2014. Megafaunal distribution and biodiversity in a heterogeneous landscape: the iceberg-scoured Rockall Bank, NE Atlantic. Marine Ecology Progress Series **501**: 67–88.

Robert, K., D.O.B. Jones, P.A. Tyler, D. Van Rooij, and V.A.I. Huvenne. 2015. Finding the hotspots within a biodiversity hotspot: Fine-scale biological predictions within a submarine canyon using high-resolution acoustic mapping techniques. Marine Ecology **36**: 1256–1276.

Roberts, J.M., A.J. Wheeler, and A. Freiwald. 2006. Reefs of the Deep: The Biology and Geology of Cold-Water Coral Ecosystems. Science **312**: 543–547.

Robison, B., B. Seibel, and J. Drazen. 2014. Deep-sea octopus (*Graneledone boreopacifica*) conducts the longest-known egg-brooding period of any animal. PLoS ONE **9**: e103437.

Rogers, A. D. 2000. The role of the oceanic oxygen minima in generating biodiversity in the deep sea. Deep-Sea Research Part II: Topical Studies in Oceanography **47**: 119–148.

Rowden, A.A., T.A. Schlacher, A. Williams, M.R. Clark, R. Stewart, F. Althaus, D.A. Bowden, M. Consalvey, W. Robinson, and J. Dowdney. 2010. A test of the seamount oasis hypothesis: seamounts support higher epibenthic megafaunal biomass than adjacent slopes. Marine Ecology **31**: 95–106.

Roy, V., K. Iken, and P. Archambault. 2014. Environmental drivers of the Canadian Arctic megabenthic communities. PLoS ONE **9**: e100900.

Rubin, D. M. 2004. A Simple autocorrelation algorithm for determining grain size from digital images of sediment. Journal of Sedimentary Research **74**:160–165.

Sameoto, J. A., P. Lawton, and M. B. Strong. 2008. An approach to the development of a relational database and GIS applicable scheme for the analysis of video-based surveys of benthic habitats. Canadian Technical Report of Fisheries and Aquatic Sciences 2818. 39 pp.

Sanders, H.L. 1968. Marine benthic diversity: a comparative study. The American Naturalist **102**: 243-281.

Sanders, H.L. 1979. Evolutionary ecology and life-history patterns in the deep sea. Sarsia **64**: 1–7.

Schlacher, T.A., M.A. Schlacher-Hoenlinger, A. Williams, F. Althaus, J.N.A. Hooper, and R. Kloser. 2007. Richness and distribution of sponge megabenthos in continental margin canyons off southeastern Australia. Marine Ecology Progress Series **340**: 73–88.

Schnitker, D., D. F. Belknap, T. S. Bacchus, J. K. Friez, B. A. Lusardi, and D. M. Popek. 2001. Deglaciation of the Gulf of Maine. In: Weddle, T.K., and M.J. Retelle [eds]. Deglacial History and Relative Sea-Level Changes, Northern New England and Adjacent Canada. Geological Society of America Special Papers 351. pp. 9–34.

Schulz, M., M. Bergmann, K. von Juterzenka, and T. Soltwedel. 2010. Colonisation of hard substrata along a channel system in the deep Greenland Sea. Polar Biology **33**: 1359–1369.

Sebens, K. P. 1991. Habitat structure and community dynamics in marine benthic systems, p. 211–234. In S.S. Bell, E.D. McCoy, and H.R. Mushinsky [eds.], Habitat Structure: The physical arrangement of objects in space. Chapman & Hall.

Seiler, J., A. Friedman, D. Steinberg, N. Barrett, A. Williams, and N. J. Holbrook. 2012. Image-based continental shelf habitat mapping using novel automated data extraction techniques. Continental Shelf Research **45**: 87–97.

Shapiro, I., R. Colony, and T. Vinje. 2003. April sea ice extent in the Barents Sea, 1850–2001. Polar Research **22(1)**: 5-10.

Sharma, G., W. Wu, and E. N. Dalal. 2005. The CIEDE2000 color-difference formula: implementation notes, supplementary test data, and mathematical observations. Color Research Applications **30**: 21–30.

Shaw, J., D. J. W. Piper, G. B. J. Fader, E. L. King, B. J. Todd, T. Bell, M. J. Batterson, and D. G. E. Liverman. 2006. A conceptual model of the deglaciation of Atlantic Canada. Quaterly Science Review **25**: 2059–2081.

Shchepetkin, A.F., and J.C. McWilliams. 2005. The regional oceanic modeling system (ROMS): a split-explicit, free-surface, topography-following-coordinate oceanic model. Ocean Modelling **9**: 347–404.

Schneider, D.C., J.-M. Gagnon, and K.D. Gilkinson. 1987. Patchiness of epibenthic megafauna on the outer Grand Banks of Newfoundland. Marine Ecology Progress Series **39**: 1–13.

Sherwood, O.A., R.E. Jamieson, E.N. Edinger, and V.E. Wareham. 2008. Stable C and N isotopic composition of cold-water corals from the Newfoundland and Labrador continental slope: Examination of trophic, depth and spatial effects. Deep-Sea Research I **55**: 1392–1402.

Skagseth, Ø., K.F. Drinkwater, and E. Terrile. 2011. Wind- and buoyancy-induced transport of the Norwegian Coastal Current in the Barents Sea. Journal of Geophysical Research **116**: C08007.

Smith, P.C. 1983. The mean seasonal circulation off southwest Nova Scotia. Journal of Physical Oceanography **13**: 1034-1054.

Smith, C. R., P.A. Jumars, and D.J. DeMaster. 1986. *In situ* studies of megafaunal mounds indicate rapid sediment turnover and community response at the deep-sea floor. Nature **323**: 251–253.

Smith, C.R., and A.R. Baco. 2003. Ecology of whale falls at the deep-sea floor. In: Gibson, R.N., and R.J.A. Atkinson [eds]. Oceanography and Marine Biology: An Annual Review Volume 41. CRC Press. pp. 311–354.

Smith, K. L., R.S. Kaufmann, and R.J. Baldwin. 1994. Coupling of near-bottom pelagic and benthic processes at abyssal depths in the eastern North Pacific Ocean. Limnology and Oceanography **39**: 1101–1118.

Smith, K.L., H. Ruhl, B. Bett, D.S.M. Billett, R.S. Lampitt, and R.S. Kaufmann. 2009. Climate, carbon cycling, and deep-ocean ecosystems. Proceedings of the National Academy of Sciences of the United States of America **106**: 19211–19218.

Snelgrove, P.V.R., and C.A. Butman. 1994. Animal sediment relationships revisited - cause versus effect. Oceanography and Marine Biology: an Annual Review **32**: 111 – 177.

Snelgrove, P.V.R., J.F. Grassle, and R.F. Petrecca. 1994. Macrofaunal response to artificial enrichments and depressions in a deep-sea habitat. Journal of Marine Research **52**: 345–369.

Soltwedel, T., N. Jaeckisch, N. Ritter, C. Hasemann, M. Bergmann, and M. Klages. 2009. Bathymetric patterns of megafaunal assemblages from the arctic deep-sea observatory HAUSGARTEN. Deep-Sea Research Part I: Oceanographic Research Papers **56**: 1856–1872.

Somero, G.N. 2012. The physiology of global change: linking patterns to mechanisms. Annual Review of Marine Science **4**: 39–61.

Spalding, M. D., H.E. Fox, G.R. Allen, N. Davidson, Z.A. Ferdaña, M. Finlayson, B.S. Halpern, M.A. Jorge, A. Lombana, S.A. Lourie, K.D. Martin, E. McManus, J. Molnar, C.A. Recchia, and J. Robertson. 2007. Marine Ecoregions of the World: A Bioregionalization of Coastal and Shelf Areas. BioScience **57**: 573-583.

Stephens, D., and M. Diesing. 2014. A comparison of supervised classification methods for the prediction of substrate type using multibeam acoustic and legacy grain-size data. PLoS ONE **9**: e93950.

Strayer, D. L., M. E. Power, W. F. Fagan, S. T. A. Pickett, and J. Belnap. 2003. A classification of ecological boundaries. Bioscience **53**:723–729.

Sumida, P.Y.G., C.R. Smith, A.F. Bernardino, P.S. Polito, and D.R. Vieira. 2014. Seasonal dynamics of epibenthic megafauna on the deep West Antarctic Peninsula in response to variable phytodetrital influx. Royal Society Open Science **1**: 140294.

Sun, Z., J.-F. Hamel, E.N. Edinger, and A. Mercier. 2010. Reproductive biology of the deep-sea octocoral *Drifa glomerata* in the Northwest Atlantic. Marine Biology **157**: 863–873.

Syvitski, J. P. M. 1991. Towards an understanding of sediment deposition on glaciated continental shelves. Continental Shelf Research **11**: 897–937.

Taylor, P.D., and M.A. Wilson. 2003. Palaeoecology and evolution of marine hard substrate communities. Earth-Science Reviews **62**: 1–103.

Tecchio, S., E. Ramírez-Llodra, F. Sardà, J.B. Company, I. Palomera, A. Mechó, R. Pedrosa-Pàmies, and A. Sanchez-Vidal. 2011. Drivers of deep Mediterranean megabenthos communities along longitudinal and bathymetric gradients. Marine Ecology Progress Series **439**: 181–192.

Teixidó, N., A. Albajes-Eizagirre, D. Bolbo, E. Le Hir, M. Demestre, J. Garrabou, L. Guigues, J. Gili, J. Piera, T. Prelot, and a Soria-Frisch. 2011. Hierarchical segmentation-based software for cover classification analyses of seabed images (Seascape). Marine Ecology Progress Series **431**: 45–53.

Tett, P. 1981. Modelling phytoplankton production at shelf-sea fronts. Philosophical Transactions of the Royal Society London A **302**: 605–615.

Thresher, R.E., J. Adkins, and N. Thiagarajan. 2011. Modal analysis of the deep-water solitary scleractinian, *Desmophyllum dianthus*, on SW Pacific seamounts: inferred recruitment periodicity, growth, and mortality rates. Coral Reefs **30**: 1063–1070.

Tittensor, D. P., A.R. Baco, P.E. Brewin, M.R. Clark, M. Consalvey, J. Hall-Spencer, A.A. Rowden, T. Schlacher, K.I. Stocks, A.D. Rogers. 2009. Predicting global habitat suitability for stony corals on seamounts. Journal of Biogeography **36**: 1111–1128.

Todd, B. J., and V. E. Kostylev. 2011. Surficial geology and benthic habitat of the German Bank seabed, Scotian Shelf, Canada. Continental Shelf Research **31**: S54–S68.

Tong, R., A. Purser, V. Unnithan, and J. Guinan. 2012. Multivariate statistical analysis of distribution of deep-water gorgonian corals in relation to seabed topography on the Norwegian margin. PLoS ONE **7**: e43534.

Tong, R., A. Purser, J. Guinan, V. Unnithan, J. Yu, and C. Zhang. 2016. Quantifying relationships between abundances of cold-water coral *Lophelia pertusa* and terrain features: A case study on the Norwegian margin. Continental Shelf Research **116**: 13–26.

Twoney, E.R., and R.P. Signell. 2013. Construction of a 3-arcsecond digital elevation model for the Gulf of Maine: U.S. Geological Survey Open-File Report 2011-1127, 24 p.

van Aken, H.M., D. Quadfasel, and A. Warpakowski. 1991. The Arctic Front in the Greenland Sea during February 1989: hydrographic and biological observations. Journal of Geophysical Research **96**: 4739–4750.

Vermeij, M.J.A., and S.A. Sandin. 2008. Density-dependent settlement and mortality structure the earliest life phases of a coral population. Ecology **89**: 1994–2004.

Vetter, E.W., and P.K. Dayton. 1999. Organic enrichment by macrophyte detritus, and abundance patterns of megafaunal populations in submarine canyons. Marine Ecology Progress Series **186**: 137–148.

Vincent, L., and P. Soille. 1991. Watersheds in digital spaces: an efficient algorithm based on immersion simulations. IEEE Transactions on Pattern Analysis and Machine Intelligence **13**: 583–598.

Waller, R.G. 2005. Deep Water Scleractinians: Current knowledge of reproductive processes. In: Freiwald, A., and J.M. Roberts [eds]. Cold-water Corals and Ecosystems. Berlin Heidelberg: Springer-Verlag. pp. 691–700.

Walters, L. J., and D. S. Wethey. 1996. Settlement and early post-settlement survival of sessile marine invertebrates on topographically complex surfaces:the importance of refuge dimensions and adult morphology. Marine Ecology Progress Series **137**: 161–171.

Wareham, V.E., and E.N. Edinger. 2007. Distribution of deep-sea corals in the Newfoundland and Labrador region, Northwest Atlantic Ocean. Bulletin of Marine Science **81**: 289–312.

Wassmann, P., I. Andreassen, M. Reigstad, and D. Slagstad. 1996. Pelagic-Benthic Coupling in the Nordic Seas: The Role of Episodic Events. Marine Ecology **17**: 447–471.

Watanabe, S., A. Metaxas, J. Sameoto, and P. Lawton. 2009. Patterns in abundance and size of two deep-water gorgonian octocorals, in relation to depth and substrate features off Nova Scotia. Deep-Sea Research I **56**: 2235–2248.

Watling, L., and E.A. Norse. 2008. Disturbance of the seabed by mobile fishing gear: A comparison to forest clearcutting. Conservation Biology **12**: 1180–1197.

Webb, T. J., E. Vanden Berghe, and R. O'Dor. 2010. Biodiversity's big wet secret: the global distribution of marine biological records reveals chronic under-exploration of the deep pelagic ocean. PLoS ONE **5**: e10223.

Wei, C.-L., G.T. Rowe, G.F. Hubbard, A.H. Scheltema, G.D.F. Wilson, I. Petrescu, J.M. Foster, M.K. Wicksten, M. Chen, R. Davenport, Y. Soliman, and Y. Wang. 2010. Bathymetric zonation of deep-sea macrofauna in relation to export of surface phytoplankton production. Marine Ecology Progress Series **399**: 1–14.

Wentworth, C. K. 1922. A scale of grade and class terms for clastic sediments. Journal of Geology **30**:377–392.

White, M. 2007. Benthic dynamics at the carbonate mound regions of the Porcupine Sea Bight continental margin. International Journal of Earth Sciences **96**: 1–9.

Wiens, J. A. 1989. Spatial scaling in ecology. Functional Ecology **3**: 385–397.

Williams, A., F. Althaus, P.K. Dunstan, G.C.B. Poore, N.J. Bax, R.J. Kloser, and F.R. McEnnulty. 2010. Scales of habitat heterogeneity and megabenthos biodiversity on an extensive Australian continental margin (100-1100m depths). Marine Ecology **31**: 222–236.

Williams, A., F. Althaus, and T.A. Schlacher. 2015. Towed camera imagery and benthic sled catches provide different views of seamount benthic diversity. Limnology and Oceanography: Methods **13**: 62–73.

Wilson, M.F.J., B. O'Connell, C. Brown, J.C. Guinan, and A.J. Grehan. 2007. Multiscale Terrain Analysis of Multibeam Bathymetry Data for Habitat Mapping on the Continental Slope, Marine Geodesy **30**: 3-35.

Woelfle, M., P. Olliaro, and M.H. Todd. 2011. Open science is a research accelerator. Nature Chemistry **3**:745-748.

Wolff, T. 1977. Diversity and faunal composition of the deep-sea benthos. Nature **267**: 780–785.

Wright, D. J., and M. F. Goodchild. 1997. Data from the deep: implications for the GIS community. International Journal of Geographical Information Science **11**: 523–528.

Wright, D.J., M. Pendleton, J. Boulware, S. Walbridge, B. Gerlt, D. Eslinger, D. Sampson, and E. Huntley. 2012. ArcGIS Benthic Terrain Modeler (BTM), v. 3.0, Environmental Systems Research Institute, NOAA Coastal Services Center, Massachusetts Office of Coastal Zone Management.

Wynn, R. B., V. A. I. Huvenne, T. P. Le Bas, B. J. Murton, D. P. Connelly, B. J. Bett, H. A. Ruhl, K. J. Morris, J. Peakall, D. R. Parsons, E. J. Sumner, S. E. Darby, R. M. Dorrell, and J. E. Hunt. 2014. Autonomous Underwater Vehicles (AUVs): Their past, present and future contributions to the advancement of marine geoscience. Marine Geology **352**:451–468.

Xue, H., F. Chai, and N.R. Pettigrew. 2000. A model study of the seasonal circulation in the Gulf of Maine. Journal of Physical Oceanography **30**:1111–1135.

Yearsley, J. M., and J.D. Sigwart. 2011. Larval transport modeling of deep-sea invertebrates can aid the search for undiscovered populations. PLoS ONE **6**: e23063.

Yesson, C., P. Simon, I. Chemshirova, T. Gorham, C.J. Turner, N. Hammeken Arboe, M.E. Blicher, and K.M. Kemp. 2015. Community composition of epibenthic megafauna on the West Greenland Shelf. Polar Biology **38**: 2085-2096.

Young, C.M. 2003. Reproduction, development and life-history traits. In: Tyler, P.A. [ed]. Ecosystems of the Deep Oceans: Ecosystems of the World. Amsterdam: Elsevier Science B.V. pp. 381–426.

Young, C.M. 2009. Communities on deep-sea hard bottoms. In Wahl, M. [ed.]. Marine Hard Bottom Communities, Ecological Studies 206. Springer-Verlag, Berlin Heidelberg, pp. 39-60.

Appendix I:
Calculations for derivations of oceanographic variables from the ocean circulation model (Chapter 6)

Water column structure

1) Brunt-Väisälä frequency (N^2 ; s^{-2})

$$N^2 = -\frac{g}{\rho_0} \cdot \frac{\partial \rho}{\partial z}$$

g = gravitational constant (9.8 $m \cdot s^{-2}$)
ρ = water density ($kg \cdot m^{-3}$)
z = depth (m)
ρ_0 = reference density (average density; $kg \cdot m^{-3}$)

$N^2 = 0$ → Neutral stability
$N^2 > 0$ → Stability (higher N^2 indicates stronger stratification; resistance to mixing)
$N^2 < 0$ → Instability, will lead to convection or overturning

2) Richardson number (dimensionless)

Ratio of buoyancy frequency (N^2) to flow gradient (vertical gradient of currents)

$$Ri = \frac{N^2}{\left(\frac{\partial u}{\partial z}\right)^2}$$

N^2 = Brunt-Vaisala frequency (see above; s^{-2})
u = current speed ($m \cdot s^{-1}$)

When Ri < 0.25, fluid is turbulent, mixing rates are high.

Temporal variability in oceanographic variables

1) Sample autocorrelation coefficient

Pearson's correlation (-1, 1) between observations in a time series *x* at a given lag *k*

$$r_k = \frac{\sum_{t=1}^{n-k}(x_{t+k} - \bar{x})(x_t - \bar{x})}{\sum_{t=1}^{n}(x_t - \bar{x})^2}$$

2) Measures of entropy

(i) Shannon entropy (base 2): Uncertainty associated with a set of observations. Entropy increases with increased unpredictability in the observations, therefore higher values random series.

$$H = -\sum_{i=1}^{N} p_i * log_2 p_i$$

N = set of unique observations
p = proportion of total observations

(ii) Permutation entropy (see Bandt and Pompe 2002):

Consider a time series $\{x_t\}_{t=1...T}$

To calculate permutation entropy of order 3 (i.e., across 3 consecutive months):

1) Consider all groups of 3 consecutive values (akin to a moving window)
2) Establish the relative order of the values in this group. In our study, we allowed tied values based on precision of the values outlined in Table 1).
   Examples:
   Permutation '012' indicates $x_t < x_{t+1} < x_{t+2}$
   Permutation '011' indicates $x_t < x_{t+1} = x_{t+2}$

3) Determine the relative frequency of each permutation.
4) Calculate Shannon entropy using the relative frequencies of each permutation.

Appendix II: List of taxa in epibenthic trawling surveys (Chapter 6)

List of taxa in the benthic trawling surveys (Aug – Sep 2011) in the western Barents Sea (139 sites) presented by phylum (number of occurrences are indicated in parentheses).

Annelida

Ampharetidae (3)
Aphrodita sp. (3)
Brada spp (67)
Eunicida (8)
Euphrosine sp. (6)
Glycera sp. (2)
Hamingia arctica (13)
Lumbrineris sp. (3)
Maldane sp. (7)
Nephtyidae (11)
Nereididae (2)
Pectinaria sp. (20)
Phyllodocidae (1)
Polychaeta (18)
Polynoidae (76)
Sabellidae (9)
Scalibregmatidae (3)
Terebellidae (27)

Arthropoda

Acanthostepheia malmgreni (14)
Aega sp. (8)
Ampelisca eschrichtii (4)
Amphipoda (6)
Anonyx sp. (43)
Arrhis phyllonyx (3)
Atylidae g. sp. (2)
Balanus sp. (6)
Boreonymphon sp. (42)
Calathura brachiata (1)
Chionoecetes opilio (12)
Colossendeis sp. (6)
Cordylochele sp. (9)
Cumacea (4)
Epimeria loricata (45)
Eualus sp. (5)
Gammarus wilkitzkii (5)
Haploops spp (1)
Hyas araneus (36)
Isopoda (1)
Lebbeus polaris (44)
Munida spp (20)
Nymphon elegans (2)
Nymphon hirtipes (35)
Nymphon hirtum (21)
Nymphon sp. (4)
Nymphon stroemi (39)

Arthropoda (continued)

Pagurus sp. (31)
Pandalus montagui (8)
Paralithodes camtschaticus (1)
Paramphithoe hystrix (18)
Pardalisca sp. (1)
Paroediceros lynceus (1)
Pontophilus norvegicus (44)
Pycnogonida (3)
Rhachotropis sp. (19)
Sabinea septemcarinata (82)
Sabinea sp. (13)
Saduria sp. (25)
Scalpellum sp. (3)
Sclerocrangon boreas (5)
Sclerocrangon ferox (44)
Spirontocaris sp. (28)
Stegocephalus sp. (34)
Tmetonyx cicada (7)

Brachiopoda

Brachiopoda (1)
Hemithiris psittacea (8)
Macandrevia cranium (11)
Terebratulina sp. (14)

Bryozoa

Alcyonidium sp. (42)
Bryozoa (6)
Cellepora sp. (8)
Diplosolen intricarius (2)
Eucratea loricata (12)
Flustra sp. (27)
Hornera lichenoides (13)
Infundibulipora lucernaria (2)
Myriapora sp. (1)
Myriozoella sp. (1)
Parasmittina jeffreysii (2)
Porella sp. (4)
Reteporella sp. (4)
Reteporella grimaldii (6)

Chordata (Ascidacea)

Ascidia prunum (34)
Ascidiacea (16)
Botryllus schlosseri (17)
Ciona intestinalis (5)
Didemnidae (1)
Microcosmus glacialis (2)
Styela sp. (2)

Cnidaria

Abietinaria abietina (16)
Actinaria (25)
Actinostola sp. (1)
Caryophyllia smithii (3)
Cerianthus lloydii (1)
Haleciidae (16)
Hormathia digitata (84)
Hydroidolina (30)
Metridium dianthus (1)
Nephtheidae (69)
Sertularella sp. (4)
Symplectoscyphus tricuspidatus (9)
Thuiaria sp. (6)
Tubularia sp. (1)
Urticina felina (18)
Zoantharia (18)

Echinodermata

Asterias rubens (1)
Brisaster fragilis (17)
Ceramaster granularis (18)
Crossaster papposus (27)
Ctenodiscus crispatus (95)
Echinus sp. (12)
Ekmania barthii (2)
Gorgonocephalus arcticus (27)
Gorgonocephalus eucnemis (14)
Gorgonocephalus sp. (7)
Heliometra glacialis (26)
Henricia sp. (54)
Hippasteria phrygiana (11)
Holothuroidea (1)
Hymenaster pellucidus (12)
Icasterias panopla (40)
Korethraster hispidus (1)
Leptasterias sp. (8)
Leptychaster sp. (16)

Echinodermata (continued)

Lophaster furcifer (13)
Molpadia borealis (59)
Myriotrochus sp. (26)
Ophiacantha bidentata (68)
Ophiocten sericeum (2)
Ophiopholis aculeate (83)
Ophiopleura borealis (20)
Ophioscolex glacialis (54)
Ophiura sarsii (63)
Ophiuroidea (1)
Parastichopus tremulus (11)
Poliometra prolixa (4)
Pontaster tenuispinus (95)
Poraniomorpha hispida (16)
Poraniomorpha sp. (1)
Poraniomorpha tumida (11)
Pseudarchaster parelii (4)
Psolus sp. (8)
Pteraster militaris (23)
Pteraster obscurus (6)
Pteraster pulvillus (30)
Solaster endeca (11)
Solaster sp. (8)
Spatangus purpureus (1)
Strongylocentrotus sp. (65)
Urasterias lincki (36)

Mollusca

Admete sp. (1)
Anomalisipho altus (1)
Aplachophora (6)
Astarte sp. (57)
Bathyarca glacialis (36)
Bathypolypus arcticus (6)
Benthoctopus sp. (2)
Beringius sp. (9)
Bivalvia (3)
Boreotrophon sp. (1)
Buccinidae (3)
Buccinum scalariforme (2)
Buccinum finmarkianum (4)
Buccinum fragile (15)
Buccinum glaciale (1)
Buccinum hydrophanum (31)
Buccinum micropoma (2)
Bulbus smithi (13)
Cadlina laevis (1)
Chlamys islandica (26)
Chlamys sp. (7)
Ciliatocardium ciliatum (23)
Colus holboelli (9)

Mollusca (continued)

Colus islandicus (9)
Colus pubescens (2)
Colus sabini (47)
Colus sp. (1)
Colus turgidulus (4)
Cryptonatica affinis (13)
Cuspidaria arctica (11)
Dendronotus sp. (8)
Euspira sp. (13)
Gastropoda (3)
Gonatus fabricii (20)
Hanleya spp (5)
Hiatella arctica (19)
Limneria undata (5)
Macoma calcarea (2)
Margarites sp. (14)
Modiolus modiolus (1)
Musculus sp. (3)
Mya sp. (3)
Naticidae (1)
Neptunea denselirata (5)
Neptunea despecta (13)
Neptunea sp. (1)
Nudibranchia (19)
Onchidiidae (12)
Philine sp. (25)
Piliscus commodus (4)
Polyplacophora (2)
Pseudamussium peslutrae (11)
Rossia sp. (14)
Scaphander punctostriatus (3)
Similipecten greenlandicus (23)
Turrisipho sp. (13)
Velutina sp. (3)
Volutopsius norwegicus (7)
Yoldia hyperborea (3)
Yoldiella sp. (1)

Porifera

Asbestopluma pennatula (1)
Chondrocladia gigantea (1)
Forcepia sp. (1)
Geodia barretti (13)
Geodia macandrewii (15)
Geodia sp. (6)
Haliclona sp. (3)
Mycale sp. (12)
Myxilla sp. (1)
Phakellia sp. (10)
Polymastia sp. (16)
Porifera (72)
Radiella sp. (44)
Radiella hemisphaerica (20)
Sphaerotylus sp. (2)
Stylocordyla borealis (2)
Suberites sp. (7)
Tentorium semisuberites (19)
Tethya sp. (6)
Tetilla sp. (31)
Thenea muricata (34)

Worms (Sipuncula, Nemertea, Platyhelminthes, Cephalorhyncha)

Golfingia sp. (3)
Nemertea (14)
Phascolion sp. (15)
Platyhelminthes (6)
Priapulidae (1)
Priapulopsis bicaudatus (1)
Priapulus caudatus (3)
Sipunculidea (6)

Appendix III: Calculations of the confusion index (Chapter 6)

1) Calculate membership value (μ) of each observation (*i*) to each cluster *k* (1 to *n*):

$$\mu_{ik} = \frac{1}{d_{ik}^2} \cdot \frac{1}{\sum_{k=1}^{n} \frac{1}{d_{ik}^2}}$$

where *d* is the Euclidean distance of each observation to the centroid of the cluster *k*.

2) Calculate a confusion index (CI) for each observation *i*:

$$CI = \frac{\mu_{(max-1)_i}}{\mu_{max_i}}$$

Appendix IV: PCA loadings (Chapter 6)

PCA: Correlation between rotated principal components and oceanographic variables. Indicated in bold are correlation coefficients > |0.7|. 'PC' = principal component.

Oceanographic variables related to temperature

Oceanographic variables	PC1	PC2	PC3	PC4	PC5
Bottom Temperature [mean]	**-0.955**	0.174	0.042	0.069	0.111
Surface Temperature [mean]	**-0.893**	0.155	-0.142	-0.068	0.359
Bottom Temperature [stdev]	-0.300	**0.744**	0.113	-0.245	0.134
Surface Temperature [stdev]	-0.154	-0.018	-0.061	-0.409	**0.860**
Bottom Temperature [max]	**-0.839**	0.129	-0.163	-0.095	0.450
Surface Temperature [max]	**-0.902**	0.347	0.110	-0.010	0.122
Bottom Temperature [min]	**-0.930**	0.150	-0.071	0.185	0.205
Surface Temperature [min]	**-0.960**	-0.050	0.067	0.132	0.093
Bottom Temperature [SAC; 3 months]	-0.074	-0.431	**-0.833**	-0.018	0.089
Bottom Temperature [SAC; 6 months]	-0.030	-0.341	**-0.903**	-0.065	0.013
Bottom Temperature [SAC; 12 months]	0.030	-0.460	0.557	-0.188	0.364
Bottom Temperature [SAC; 60 months]	0.150	0.215	**0.924**	0.051	0.059
Surface Temperature [SAC; 3 months]	0.294	-0.007	0.188	**-0.755**	-0.212
Surface Temperature [SAC; 6 months]	0.360	0.170	-0.181	-0.286	**-0.780**
Surface Temperature [SAC; 12 months]	-0.323	-0.220	0.122	0.557	0.643
Surface Temperature [SAC; 60 months]	-0.220	-0.285	0.234	0.414	0.692
Bottom Temperature [Annual amplitude; mean]	-0.179	**0.761**	0.565	-0.168	-0.020
Bottom Temperature [Annual amplitude; stdev]	-0.081	**0.863**	0.126	0.050	-0.079
Bottom Temperature [Entropy; Perm.; 3 months]	0.098	**-0.715**	-0.087	0.162	0.156
Bottom Temperature [Entropy; 10 years]	-0.145	**0.862**	0.116	-0.204	-0.172
Surface Temperature [Annual amplitude; mean]	-0.274	0.024	-0.035	-0.328	**0.878**
Surface Temperature [Annual amplitude; stdev]	0.178	0.155	-0.501	-0.157	-0.106
Surface Temperature [Entropy; Perm.; 3 months]	0.056	-0.093	0.089	0.544	-0.097
Surface Temperature [Entropy; 10 years]	0.023	0.307	-0.167	**-0.802**	0.204
Bottom water masses [Entropy; 10 years]	0.501	0.435	-0.300	-0.064	0.248

Oceanographic variables related to bottom currents

Oceanographic variables	PC1	PC2	PC3	PC4	PC5
Bottom current speed [mean]	**0.818**	0.061	0.014	-0.494	0.116
Bottom current speed [stdev]	**0.951**	0.146	0.005	-0.184	0.066
Bottom current speed [max]	**0.937**	0.124	-0.024	-0.080	-0.061
Bottom current speed [SAC; 3 months]	-0.058	-0.182	0.034	-0.292	-0.580
Bottom current speed [SAC; 6 months]	-0.056	**-0.883**	0.034	0.082	-0.008
Bottom current speed [SAC; 12 months]	0.009	**0.827**	-0.110	-0.260	-0.096
Bottom current speed [SAC; 60 months]	0.032	**0.837**	-0.094	0.029	0.089
Bottom current speed [Annual amplitude; mean]	**0.938**	0.149	0.010	-0.214	0.099
Bottom current speed [Annual amplitude; stdev]	**0.765**	0.081	-0.037	0.240	-0.198
Bottom current speed [Entropy; Perm.; 3 months]	**-0.758**	0.116	-0.047	0.179	-0.187
Bottom current speed [Entropy; 10 years]	**0.926**	-0.059	0.044	-0.176	0.154
Bottom current direction [NS component; mean]	0.112	-0.181	0.011	-0.280	0.394
Bottom current direction [EW component; mean]	0.105	0.158	0.042	-0.048	0.096
Bottom current direction [circular stdev]	-0.196	-0.247	-0.027	**0.863**	0.016
Bottom current direction [SAC; 3 months]	-0.008	-0.041	0.023	0.027	-0.641
Bottom current direction [SAC; 6 months]	0.011	0.015	**0.728**	-0.067	-0.103
Bottom current direction [SAC; 12 months]	-0.011	0.062	**-0.763**	0.039	-0.119
Bottom current direction [SAC; 60 months]	-0.004	0.086	**-0.721**	-0.048	0.043
Bottom current direction [Entropy; 10 years]	-0.384	-0.214	-0.048	**0.818**	0.052

Oceanographic variables related to water column structure

Oceanographic variables	PC1	PC2	PC3	PC4	PC5	PC6	PC7	PC8	PC9
Vertical velocity gradient [mean]	**-0.752**	-0.300	0.355	0.226	0.118	0.066	-0.042	-0.122	0.195
Vertical velocity gradient [stdev]	**-0.781**	-0.154	0.417	0.286	0.040	0.083	0.004	-0.112	0.190
Vertical velocity gradient [SAC; 3 months]	-0.079	-0.090	-0.464	-0.096	-0.003	-0.013	0.006	0.219	-0.080
Vertical velocity gradient [SAC; 6 months]	0.066	-0.053	**-0.823**	0.134	-0.079	-0.100	0.066	-0.129	0.092
Vertical velocity gradient [SAC; 12 months]	-0.293	-0.196	0.650	-0.071	-0.102	-0.011	-0.285	0.106	-0.152
Vertical velocity gradient [SAC: 60 months]	0.019	0.319	**0.713**	-0.272	0.077	0.100	0.208	-0.007	0.116
Vertical velocity gradient [Annual amplitude; mean]	**-0.760**	-0.130	0.473	0.264	0.060	0.099	0.021	-0.116	0.196
Vertical velocity gradient [Annual amplitude; stdev]	**-0.714**	-0.075	0.203	0.386	0.057	0.072	0.043	-0.100	0.192
Vertical velocity gradient [Entropy; Perm.; 3 months]	-0.620	-0.191	0.328	0.298	0.048	0.057	0.129	-0.136	0.202
Vertical velocity gradient [Entropy; 10 years]	**-0.759**	-0.122	0.358	0.312	0.067	0.087	0.062	-0.156	0.244
Vertical direction gradient [mean]	-0.330	-0.033	-0.068	**0.866**	-0.031	0.109	-0.145	0.080	-0.026
Vertical direction gradient [stdev]	-0.454	-0.064	-0.033	**0.849**	-0.035	0.124	-0.122	0.066	-0.009
Vertical direction gradient [SAC; 3 months]	-0.001	-0.117	-0.033	0.079	0.076	-0.147	-0.009	**0.789**	0.092
Vertical direction gradient [SAC; 6 months]	0.044	-0.071	-0.022	-0.006	0.042	**-0.754**	-0.094	0.119	-0.012
Vertical direction gradient [SAC; 12 months]	-0.235	-0.073	0.113	0.142	0.122	0.656	-0.102	0.220	0.070
Vertical direction gradient [SAC; 60 months]	-0.076	0.120	0.067	0.078	0.016	0.735	-0.027	-0.146	0.015
Vertical direction gradient [Annual amplitude; mean]	-0.425	-0.034	-0.035	**0.865**	-0.046	0.147	-0.107	0.027	-0.013
Vertical direction gradient [Annual amplitude; stdev]	-0.526	0.007	0.026	0.551	0.028	-0.021	-0.092	0.078	0.036
Vertical direction gradient [Entropy; Perm.; 3 months]	0.380	0.067	0.053	-0.385	0.002	0.153	0.147	0.195	-0.034
Vertical direction gradient [Entropy; 10 years]	-0.369	-0.037	-0.068	**0.884**	-0.073	0.025	-0.095	0.003	-0.031
Vertical portion with neg. N^2 [mean]	-0.026	**0.965**	0.027	-0.029	0.112	0.042	0.049	-0.028	0.002
Vertical portion with neg. N^2 [stdev]	-0.062	**0.960**	0.028	0.015	-0.120	0.048	0.019	-0.020	-0.016
Vertical portion with neg. N^2 [SAC; 3 months]	0.003	-0.305	-0.339	-0.069	0.009	-0.077	-0.376	-0.297	-0.063
Vertical portion with neg. N^2 [SAC; 6 months]	-0.077	-0.684	-0.011	0.210	-0.591	-0.017	-0.123	0.110	-0.027

Oceanographic variables related to water column structure (*continued*)

Vertical portion with neg. N^2 [SAC; 12 months]	0.125	**0.723**	0.226	-0.190	0.356	-0.033	0.107	-0.112	0.040
Vertical portion with neg. N^2 [SAC; 60 months]	0.044	**0.730**	0.104	-0.161	0.475	0.080	0.161	0.026	0.009
Vertical portion with neg. N^2 [Annual amplitude; mean]	-0.046	**0.969**	0.031	0.010	-0.106	0.048	0.054	0.001	-0.022
Vertical portion with neg. N^2 [Annual amplitude; stdev]	-0.076	0.259	-0.033	-0.005	**-0.856**	-0.049	0.014	-0.123	-0.013
Vertical portion with neg. N^2 [Entropy; Perm.; 3 months]	0.023	**-0.806**	0.036	-0.054	0.303	-0.017	-0.062	-0.010	0.004
Vertical portion with neg. N^2 [Entropy; 10 years]	-0.057	**0.871**	-0.047	0.010	-0.348	0.024	0.099	-0.025	-0.028
Vertical Portion Ri [0 - 0.25] [mean]	**-0.850**	-0.014	-0.139	0.255	-0.092	0.082	-0.314	0.094	-0.070
Vertical Portion Ri [0 - 0.25] [stdev]	**-0.906**	0.130	-0.099	0.191	-0.076	0.084	-0.213	0.084	-0.097
Vertical Portion Ri [0 - 0.25] [SAC; 3 months]	-0.025	-0.041	0.024	0.047	0.006	-0.052	0.042	-0.063	**-0.822**
Vertical Portion Ri [0 - 0.25] [SAC; 6 months]	0.234	0.158	-0.023	-0.126	0.099	0.026	0.652	0.050	0.134
Vertical Portion Ri [0 - 0.25] [SAC; 12 months]	-0.145	-0.109	0.024	0.230	0.006	0.016	**-0.717**	0.012	0.128
Vertical Portion Ri [0 - 0.25] [SAC; 60 months]	-0.154	-0.098	0.143	0.092	0.092	0.045	-0.489	0.135	0.389
Vertical Portion Ri [0 - 0.25] [Annual amplitude; mean]	**-0.888**	0.122	-0.107	0.201	-0.079	0.086	-0.267	0.089	-0.072
Vertical Portion Ri [0 - 0.25] [Annual amplitude; stdev]	**-0.801**	0.237	-0.045	0.072	-0.077	0.077	0.043	0.034	-0.141
Vertical Portion Ri [0 - 0.25] [Entropy; Perm.; 3 months]	-0.628	0.080	-0.129	0.154	-0.105	-0.022	-0.179	0.133	-0.220
Vertical Portion Ri [0 - 0.25] [Entropy; 10 years]	**-0.899**	0.110	-0.116	0.203	-0.082	0.083	-0.165	0.080	-0.071

Appendix V: Copyright Permissions

JOHN WILEY AND SONS LICENSE TERMS AND CONDITIONS

This Agreement between Myriam Lacharite ("You") and John Wiley and Sons ("John Wiley and Sons") consists of your license details and the terms and conditions provided by John Wiley and Sons and Copyright Clearance Center.

License Number	3880220839657
License date	Jun 01, 2016
Licensed Content Publisher	John Wiley and Sons
Licensed Content Publication	Limnology and Oceanography: Methods
Licensed Content Title	Using object-based image analysis to determine seafloor fine-scale features and complexity
Licensed Content Author	Myriam Lacharité, Anna Metaxas, Peter Lawton
Licensed Content Date	Jun 19, 2015
Licensed Content Pages	15
Type of use	Dissertation/Thesis
Requestor type	Author of this Wiley article
Format	Print and electronic
Portion	Full article
Will you be translating?	No
Title of your thesis / dissertation	Factors influencing the abundance, composition and diversity of deep-water benthic megafaunal communities
Expected completion date	Aug 2016
Expected size (number of pages)	210
Requestor Location	Myriam Lacharite Dept of Oceanography Dalhousie University 1355 Oxford Street Halifax, NS B3H 4R2 Canada Attn: Myriam Lacharite
Publisher Tax ID	EU826007151
Billing Type	Invoice
Billing Address	Myriam Lacharite Dept of Oceanography Dalhousie University 1355 Oxford Street Halifax, NS B3H 4R2 Canada Attn: Myriam Lacharite
Total	0.00 USD

ELSEVIER LICENSE
TERMS AND CONDITIONS

This Agreement between Myriam Lacharite ("You") and Elsevier ("Elsevier") consists of your license details and the terms and conditions provided by Elsevier and Copyright Clearance Center.

License Number	3930240497460
License date	Aug 15, 2016
Licensed Content Publisher	Elsevier
Licensed Content Publication	Progress in Oceanography
Licensed Content Title	Delimiting oceanographic provinces to determine drivers of mesoscale patterns in benthic megafauna: A case study in the Barents Sea
Licensed Content Author	Myriam Lacharité, Lis Lindal Jørgensen, Anna Metaxas, Vidar S. Lien, Hein Rune Skjoldal
Licensed Content Date	August 2016
Licensed Content Volume Number	146
Licensed Content Issue Number	n/a
Licensed Content Pages	12
Start Page	187
End Page	198
Type of Use	reuse in a thesis/dissertation
Portion	full article
Format	both print and electronic
Are you the author of this Elsevier article?	Yes
Will you be translating?	No
Order reference number	
Title of your thesis/dissertation	Factors influencing the abundance, composition and diversity of deep-water benthic megafaunal communities
Expected completion date	Aug 2016
Estimated size (number of pages)	210
Elsevier VAT number	GB 494 6272 12
Requestor Location	Myriam Lacharite Dept of Oceanography Dalhousie University 1355 Oxford Street Halifax, NS B3H 4R2 Canada Attn: Myriam Lacharite
Total	0.00 USD